

**APPLICATIONS OF HYDROGENATION AND DEHYDROGENATION  
ON NOBLE METAL CATALYSTS**

A Dissertation

by

BO WANG

Submitted to the Office of Graduate Studies of  
Texas A&M University  
in partial fulfillment of the requirements for the degree of

DOCTOR OF PHILOSOPHY

August 2007

Major Subject: Chemical Engineering

**APPLICATIONS OF HYDROGENATION AND DEHYDROGENATION  
ON NOBLE METAL CATALYSTS**

A Dissertation

by

BO WANG

Submitted to the Office of Graduate Studies of  
Texas A&M University  
in partial fulfillment of the requirements for the degree of

DOCTOR OF PHILOSOPHY

Approved by:

Co-Chairs of Committee,	Gilbert F. Froment D. Wayne Goodman
Committee Members,	Rayford G. Anthony Kenneth R. Hall
Head of Department,	N.K. Anand

August 2007

Major Subject: Chemical Engineering

**ABSTRACT**

Applications of Hydrogenation and Dehydrogenation  
on Noble Metal Catalysts. (August 2007)

Bo Wang, B.S., Dalian University of Technology;

M.S., Dalian University of Technology;

Ph.D., Dalian University of Technology

Co-Chairs of Advisory Committee: Dr. Gilbert. F. Froment  
Dr. D. Wayne Goodman

Hydrogenation and dehydrogenation on Pd- and Pt- catalysts are encountered in many industrial hydrocarbon processes. The present work considers the development of catalysts and their kinetic modeling along a general and rigorous approach. The first part deals with the kinetics of selective hydrogenation, more particularly of the C<sub>3</sub> cut of a thermal cracking unit for olefins production. The kinetics of the gas phase selective hydrogenation of methyl-acetylene (MA) and propadiene (PD) over a Pd/ $\gamma$ -alumina catalyst were investigated in a fixed bed tubular reactor at temperatures 60 - 80 °C and a pressure of 20 bara. Hougen-Watson type kinetic equations were derived. The formation of higher oligomers slowly deactivated the catalyst. The effect of the deactivating agent on the rates of the main reactions as well as on the deactivating agent formation itself was expressed in terms of a deactivation function multiplying the corresponding rates at zero deactivation. Then, the kinetic model was plugged into the reactor model to

simulate an industrial adiabatic reactor. In the second part the production of hydrogen from hydrocarbons was investigated. In both cyclohexane and decalin dehydrogenations, conversions higher than 98% could be obtained over Pt/ $\gamma$ -alumina catalyst at temperature of 320 and 340 °C, respectively, with no apparent deactivation for 30 h and with co-feed of H<sub>2</sub> in the feed. Except for H<sub>2</sub> and trace amounts of side cracking products, less than 0.01%, benzene was the only dehydrogenated product in cyclohexane dehydrogenation. In the case of decalin dehydrogenation, partially dehydrogenated product, tetralin, was also formed with selectivity lower than 5%, depending on operating conditions. A rigorous Hougen-Watson type kinetic model was derived, which accounted for both the dehydrogenation of cis- and trans- decalin in the feed and also the isomerization of the two isomers. Jet A is the logic fuel in the battlefields. The dehydrogenation of Jet A can produce H<sub>2</sub> for military fuel cell application. Although the H<sub>2</sub> production is lower than that of steam/autothermal reforming, it eliminates the needs of high temperature and product separation operation.

## ACKNOWLEDGEMENTS

I would like to express my deep gratitude and appreciation to Dr. Gilbert F. Froment and Dr. D. Wayne Goodman, the chairmen of my graduate advisory committee, for their encouragement, support and guidance.

I am very thankful to Dr. Jack H. Lunsford for representing Dr. D. Wayne Goodman at my final oral defense. I am very thankful to Dr. Rayford G. Anthony and Dr. Kenneth R. Hall for serving on the committee and for their helpful comments and suggestions. I thank Dr. Rayford G. Anthony for the advice in the course of the selective hydrogenation project.

Thanks also go to Amy Liu and Towanna Hubacek for their secretarial help and friendship. The technical assistance of Randy Marek in the mechanical shop of CHEN is greatly appreciated.

I also wish to thank all the group members for their cooperation and help. Specifically, I would like to thank Dr. Xiancun Wu, Dr. C.V. Philip, Dr. Wahabi Saeed, Dr. Won-Jae Lee, Dr. Rogelio Sotelo-Boyas, Dr. Hans Kumar Gupta, Hemendra Khakhan, Dr. Mingsu Chen, Dr. Patrick Han, Matthew Lundwall, Stephanus Axnanda, Fang Yang, Yun Cai, Zhen Yan and Kerrie Gath for making my graduate years enjoyable and memorable.

Last but not least, my deep gratitude and appreciation go to my family for their continuous support and encouragement that made this work a success.

## TABLE OF CONTENTS

	Page
ABSTRACT .....	iii
ACKNOWLEDGEMENTS .....	v
TABLE OF CONTENTS .....	vi
LIST OF FIGURES.....	ix
LIST OF TABLES .....	xiii
 CHAPTER	
I INTRODUCTION .....	1
II SELECTIVE HYDROGENATION OF C <sub>3</sub> CUT FROM A THERMAL CRACKING UNIT .....	5
II.1 Literature Review .....	5
II.1.1 Propylene Production .....	6
II.1.2 The Process of C <sub>3</sub> Cut Selective Hydrogenation .....	8
II.1.2.1 Gas Phase Hydrogenation.....	9
II.1.2.2 Liquid Phase Hydrogenation .....	11
II.1.3 Catalysts Development .....	13
II.1.4 Green Oil Formation.....	15
II.1.5 The Role of Added CO .....	18
II.1.6 Control of the Selectivity.....	20
II.2 Experimental.....	24
II.2.1 Feed Mixtures .....	24
II.2.2 Catalyst .....	24
II.2.3 Reactor Unit.....	27
II.2.4 Gas Chromatography .....	27
II.3 Results and Discussion .....	28
II.3.1 Definition of Conversions and Selectivities .....	28
II.3.2 Experimental Results .....	31
II.3.3 Two Aspects of the Kinetic Modeling.....	31
II.3.4 Reaction Scheme .....	33
II.3.5 Kinetic Modeling.....	36

CHAPTER	Page
II.3.5.1	Rate Equations for Hydrogenation and Oligomerization . 36
II.3.5.2	Parameter Estimation..... 38
II.3.6	Catalyst Deactivation..... 39
II.3.6.1	Observations ..... 39
II.3.6.2	Kinetic Modeling of Deactivation ..... 40
II.3.6.3	Estimation of the Deactivation Parameters..... 44
II.3.7	Simulation of an Industrial Hydrogenation Unit ..... 45
III	HYDROGEN PRODUCTION VIA THE DEHYDROGENATION OF HYDROCARBONS..... 49
III.1	Literature Review ..... 49
III.1.1	Working Principle of Fuel Cells..... 50
III.1.2	Types of Fuel Cells ..... 51
III.1.2.1	Proton Exchange Membrane Fuel Cell ..... 51
III.1.2.2	Direct-Methanol Fuel Cell ..... 53
III.1.2.3	Alkaline Fuel Cell ..... 54
III.1.2.4	Phosphoric Acid Fuel Cell ..... 54
III.1.2.5	Molten Carbonate Fuel Cell ..... 55
III.1.2.6	Solid Oxide Fuel Cell..... 55
III.1.3	Onboard Hydrogen Storage..... 56
III.1.3.1	Gaseous and Liquid Hydrogen Storage..... 56
III.1.3.2	Carbon-Based Materials ..... 58
III.1.3.3	Metal Hydrides..... 59
III.1.3.4	Chemical Hydrides..... 59
III.2	Experimental ..... 71
III.2.1	Catalyst Preparation ..... 71
III.2.1.1	Pt/ $\gamma$ -Al <sub>2</sub> O <sub>3</sub> and Pt-Sn/ $\gamma$ -Al <sub>2</sub> O <sub>3</sub> Catalysts..... 71
III.2.1.2	Pt/ $\gamma$ -Al <sub>2</sub> O <sub>3</sub> -ZrO <sub>2</sub> /SO <sub>4</sub> <sup>2-</sup> Hybrid Catalyst ..... 71
III.2.2	UHV Bulb Reactor Setup..... 74
III.2.2.1	Pumping System..... 74
III.2.2.2	Sample Mounting ..... 74
III.2.2.3	Operating Procedure..... 75
III.2.2.4	Volume Calibration ..... 76
III.2.3	Fixed-Bed Reactor Setup ..... 79
III.2.4	Gas Chromatography..... 79
III.3	Results and Discussion..... 80
III.3.1	Test of the UHV Bulb Reactor by CO Oxidation on Pt(111) ..... 80
III.3.2	The Dehydrogenation of Cyclohexane on Pt(111)..... 83
III.3.2.1	The Cycle of Dehydrogenation/Hydrogenation ..... 83
III.3.2.2	The Rate of Cyclohexane Dehydrogenation on Pt(111) .. 88
III.3.3	The Dehydrogenation of Cyclohexane in the Fixed-Bed Reactor .. 91

CHAPTER	Page
III.3.3.1 Effect of Various Supports .....	91
III.3.3.2 Effect of Temperature .....	91
III.3.3.3 The Stability of the Pt/ $\gamma$ -alumina Catalyst.....	94
III.3.3.4 Effect of Pt Loadings and of the Addition of Sn.....	94
III.3.4 The Dehydrogenation of Decalin .....	98
III.3.4.1 Defination of Conversions and Selectivities .....	98
III.3.4.2 Effect of Temperature .....	99
III.3.4.3 Catalyst Stability .....	100
III.3.5 Kinetic Study of the Dehydrogenation of Decalin .....	100
III.3.5.1 Experimental Results.....	100
III.3.5.2 Thermodynamic Aspects of Decalin Dehydrogenation .	106
III.3.5.3 Derivation of the Kinetic Model .....	108
III.3.5.4 Parameter Estimation .....	112
III.3.6 The Dehydrogenation of Jet A .....	114
III.3.6.1 The Dehydrogenation of Jet A Surrogate on Pt/ $\gamma$ -Al <sub>2</sub> O <sub>3</sub> Catalyst.....	114
III.3.6.2 The Dehydrogenation of Jet A on Various Catalysts .....	127
IV CONCLUSIONS.....	134
NOMENCLATURE.....	137
LITERATURE CITED .....	140
VITA .....	149



## LIST OF FIGURES

	Page
Figure II-1. The flow diagram of tail end C <sub>3</sub> cut selective hydrogenation in the gas phase. ....	10
Figure II-2. Hydrotreating of the propylene rich cut in liquid phase. IFP technology employing chamber-type reactors. ....	12
Figure II-3. Pd content in original 2-4mm Pd/Al <sub>2</sub> O <sub>3</sub> sphere catalyst and crushed different size fractions. * original 2-4 mm Pd/Al <sub>2</sub> O <sub>3</sub> sphere catalyst. ....	26
Figure II-4. Experimental setup for the selective hydrogenation of the C <sub>3</sub> cut from a thermal cracking unit. ....	29
Figure II-5. Conversions and catalyst bed temperature as a function of run length at constant oil bath temperature of 55 °C. ....	32
Figure II-6. Evolution of the conversions as a function of run length, expressed as $\Sigma F^{\circ}_{MAPD}/W$ at 70 °C, and $W/F^0_{MAPD} = 8.33$ kg hr/kmol. H <sub>2</sub> /MAPD molar ratio in [A] =1.8; in [B] 1.1. ....	34
Figure II-7. Evolution of the conversions as a function of run length for H <sub>2</sub> /MAPD =1.5 (molar ratio) and $W/F^0_{MAPD} = 4.06$ kg hr/kmol. In [C] at 60 °C and in [D] 80 °C. ....	34
Figure II-8. Comparison of experimental and calculated conversions as a function of space time at 70 °C ( $\Delta$ : EXP; Solid line: CAL). ....	41
Figure II-9. Dependence of content of deactivating agent of the catalyst on conversion, amount of MAPD fed per kg cat (shown inside Figure) and molar ratio H <sub>2</sub> /MAPD at 80 °C. H <sub>2</sub> /MAPD =1.5, except for point at $\Sigma F^{\circ}_{MAPD}/W = 57.4$ for which ratio =1.1 and point at $\Sigma F^{\circ}_{MAPD}/W = 82$ for which ratio =1.8. ....	42

Figure II-10. Conversions of MAPD, selectivities for PP, PN and GO as a function of catalyst bed length in an industrial adiabatic reactor after 6360 hrs (Points: industrial results). Process conditions: PD content of feed (wt%): 0.855%; MA(wt%): 1.319%; H <sub>2</sub> /MAPD (molar ratio): 2.37; T(in): 331.3 K; exit T(simulated): 383.8 K; exit T(ind.): 378 K. ....	48
Figure III-1. Schematic diagram of a PEM fuel cell. ....	51
Figure III-2. Preparation of Pt/ $\gamma$ -Al <sub>2</sub> O <sub>3</sub> and Pt-Sn/ $\gamma$ -Al <sub>2</sub> O <sub>3</sub> catalysts. ....	72
Figure III-3. Preparation of Pt/ $\gamma$ -Al <sub>2</sub> O <sub>3</sub> -ZrO <sub>2</sub> /SO <sub>4</sub> <sup>2-</sup> hybrid catalyst. ....	73
Figure III-4. The UHV bulb reactor setup for the dehydrogenation of cyclohexane over Pt(111). ....	77
Figure III-5. Schematics of the sample holder used in the UHV bulb reactor for the dehydrogenation of cyclohexane over Pt(111). ....	78
Figure III-6. Fixed-bed experimental setup for the dehydrogenation of cyclohexane, decalin, and Jet A to produce H <sub>2</sub> . ....	81
Figure III-7. The total pressure change as a function of reaction time during CO-O <sub>2</sub> reaction on Pt(111). ....	84
Figure III-8. The CO <sub>2</sub> production rate as a function of temperature in Arrhenius plot during CO-O <sub>2</sub> reaction on Pt(111). ....	85
Figure III-9. The cycle of dehydrogenation of cyclohexane and hydrogenation of benzene over Pt(111) in an UHV bulb reactor. P <sup>0</sup> <sub>cyclohexane</sub> = 2 torr, P <sup>0</sup> <sub>H<sub>2</sub></sub> =12 torr. ....	87
Figure III-10. The total pressure change as a function of process time during cyclohexane dehydrogenation on Pt(111). P <sup>0</sup> <sub>cyclohexane</sub> =2 torr, P <sup>0</sup> <sub>H<sub>2</sub></sub> =12 torr. ....	89
Figure III-11. The rate of cyclohexane dehydrogenation on Pt(111) as a function of temperature in Arrhenius form. ....	90
Figure III-12. Cyclohexane dehydrogenation over different supported Pt catalysts. 340 °C, space time=20 kg cat h/kmol, H <sub>2</sub> /cyclohexane=1/2. ....	92

	Page
Figure III-13. Effect of temperature on cyclohexane dehydrogenation. Reaction condition: 0.8 wt% Pt/ $\gamma$ -Al <sub>2</sub> O <sub>3</sub> , space time =30 kg cat h/kmol, H <sub>2</sub> /cyclohexane=3. ....	93
Figure III-14. Catalyst stability in cyclohexane dehydrogenation to produce H <sub>2</sub> . 0.8 wt% Pt/ $\gamma$ -Al <sub>2</sub> O <sub>3</sub> , space time=20 kg cat h/kmol, H <sub>2</sub> /cyclohexane=1/2. ....	95
Figure III-15. Effect of Pt loadings on cyclohexane dehydrogenation. Reaction condition: 320 °C, space time=20 kg cat h/kmol, H <sub>2</sub> /cyclohexane=3. ....	96
Figure III-16. Effect of Sn/Pt molar ratio on cyclohexane dehydrogenation. Reaction condition: 320 °C, space time=20 kg cat h/kmol, H <sub>2</sub> /cyclohexane=3. ....	97
Figure III-17. Effect of temperature on decalin dehydrogenation. Reaction condition: 0.8 wt% Pt/ $\gamma$ -Alumina, space time=60 kg cat h/kmol, H <sub>2</sub> /cyclohexane=1. ....	101
Figure III-18. The stability of catalyst in decalin dehydrogenation at 340 °C and space time=80 kg cat h/kmol. ....	102
Figure III-19. Conversions as a function of space time in the dehydrogenation of decalin at 325 °C and H <sub>2</sub> /decalin molar ratio of 1 to 1. ....	104
Figure III-20. Conversions as a function of H <sub>2</sub> /decalin molar ratio in the dehydrogenation of decalin at 325 °C and space time of 60 kg cat h/kmol. ....	105
Figure III-21. Calculation of the equilibrium constants of the reactions involved in the dehydrogenation of decalin. ....	107
Figure III-22. Arrhenius plot of rate coefficients. ....	117
Figure III-23. Van't Hoff plot of adsorption coefficients. ....	118
Figure III-24. Comparison of experimental and calculated conversions as a function of space time at 345 °C ( $\Delta$ : EXP; Solid line: CAL). ....	119
Figure III-25. Comparison of experimental and calculated conversions as a function of space time at 325 °C ( $\Delta$ : EXP; Solid line: CAL). ....	120

	Page
Figure III-26. Comparison of experimental and calculated conversions as a function of H <sub>2</sub> /decalin molar ratio at 325 °C and space time of 40 kg cat/h/ kmol (Δ: EXP; Solid line: CAL). .....	121
Figure III-27. Comparison of experimental and calculated conversions as a function of space time at 300 °C (Δ: EXP; Solid line: CAL). .....	122
Figure III-28. Comparison of experimental and calculated conversions as a function of H <sub>2</sub> /decalin molar ratio at 300 °C and space time of 60 kg cat/h/ kmol (Δ: EXP; Solid line: CAL). .....	123
Figure III-29. Comparison of experimental and calculated conversions as a function of space time at 275 °C (Δ: EXP; Solid line: CAL). .....	124
Figure III-30. Comparison of experimental and calculated conversions as a function of H <sub>2</sub> /decalin molar ratio at 275 °C and space time of 60 kg cat/h/ kmol (Δ: EXP; Solid line: CAL). .....	125
Figure III-31. The hydrogen production yield as a function of reaction temperature in the dehydrogenation of Jet A surrogate on Pt/γ-alumina catalyst. Feed of Jet A surrogate=10ml/min, H <sub>2</sub> =10ml/min, N <sub>2</sub> =40 ml/min. ....	126
Figure III-32. The hydrogen production yield as a function of reaction temperature in the dehydrogenation of Jet A on Pt/γ-alumina catalyst. Jet A=10ml/min, H <sub>2</sub> =10ml/min, N <sub>2</sub> =40 ml/min. ....	128
Figure III-33. The effect of H <sub>2</sub> /Jet A molar ratio on the dehydrogenation Jet A. Temp.=500 °C, Feed of Jet A surrogate=10ml/min, H <sub>2</sub> =10ml/min, N <sub>2</sub> =40 ml/min. ....	129
Figure III-34. The dehydrogenation of Jet A over different catalysts. Temperature= 425 °C, Jet A=10 ml/min, H <sub>2</sub> =10 ml/min, N <sub>2</sub> =40 m/min. ....	132
Figure III-35. The regeneration of Pt-Sn/γ- Al <sub>2</sub> O <sub>3</sub> -ZrO <sub>2</sub> /SO <sub>4</sub> <sup>2-</sup> hybrid catalysts in the dehydrogenation of Jet A by oxidation in air at different temperatures. Run 1: fresh catalyst; Run 2: oxidation at 500 °C in air, then reduction at 300 °C in H <sub>2</sub> ; Run 3: oxidation at 500 °C in air, then reduction at 300 °C in H <sub>2</sub> . ....	133

**LIST OF TABLES**

	Page
Table II-1. Composition of propylene cuts and commercial propylenes .....	6
Table II-2. Composition of propylene cut for different steam cracking feeds .....	7
Table III-1. The calibration of the volume of each segment in the UHV bulb reactor by gas expansion .....	76
Table III-2. Estimates of frequency factors A, activation energy E & enthalpies of activation $\Delta H$ for the model of case I by the Levenberg-Marquardt algorithm .....	115
Table III-3. Estimates of frequency factors A, activation energy E & enthalpies of activation $\Delta H$ for the model of case II by the Levenberg-Marquardt algorithm .....	116

## CHAPTER I

### INTRODUCTION

Hydrogen has wide applications in petroleum and chemical industry. With the development of hydrogen fuel cell and strict environmental regulation, energy and transportation applications will contribute to the increasing demand of hydrogen in the near future. This research will encompass the application of hydrogen in an important petrochemical process, specifically the hydrorefining of  $C_3$  cut from a thermal cracking unit, as well as its onboard production for vehicular fuel cell application via the dehydrogenations of hydrocarbons.

Propylene is one of the major building blocks of the petrochemical industry. The majority of propylene is produced as a co-product of the steam cracking process. The  $C_3$  cut obtained by the steam cracking of ethane, propane and naphtha typically contains small amount of methyl acetylene (MA) and propadiene (PD), which must be removed. Industrially, MA and PD are removed by selective hydrogenation to propylene, while minimizing the over-hydrogenation to propane. Good control of the selectivity of this process can on the one hand remove the undesired MAPD impurities in  $C_3$  stream, and achieve a gain of propylene on the other. This is a dynamic process due to the deactivation of the Pd/alumina catalyst, which is associated with the green oil formation.

---

This dissertation follows the style and format of *Industrial and Engineering Chemistry Research*.

Adaptation of operating variables is needed to maintain the optimum overall propylene selectivity. The objective of this project is to develop a rigorous kinetic model to guide the industrial hydrogenation process. The model is of the Hougen-Watson type, which accounts for the adsorption and desorption of reactants and products on the heterogeneous catalysts. The work can be formulated as follows:

- 1) Build computer controlled bench scale fixed-bed experimental setup; perform experiments to collect the kinetic data.
- 2) Develop a kinetic model based on the complex reaction network.
- 3) Estimate the kinetic parameters using the experimental data in the absence of deactivation.
- 4) Develop a deactivation model.
  - a) Relate the rate of catalyst deactivation to the rate of formation of deactivating agent on the catalyst rather than run length.
  - b) Estimate the deactivation parameters using the conversion data in the presence of catalyst deactivation and the content of the deactivating agent on the catalyst at the end of the run.
- 4) Plug the kinetic models into the adiabatic reactor model to simulate the industrial adiabatic reactor operation.

Fuel cells are an important enabling technology for the hydrogen economy and have the potential to revolutionize the way to power the world, offering cleaner, more-efficient alternatives to the combustion of gasoline and other fossil fuels. Cars that run on PEMFC with hydrogen fuel still fail to compete with traditional gasoline vehicles.

One of the biggest hurdles remains finding a material capable of storing enough hydrogen onboard for a vehicle to cover over 300 miles on a full tank without adding significant weight or volume relative to a gasoline car. One promising technology to store and transport hydrogen is the utilization of dehydrogenation of high hydrogen-content organic hydrocarbons. Only hydrogen and dehydrogenated hydrocarbons are formed as the main products in this reaction. The absence of any substantial amount of carbon monoxide eliminates the need to purify the hydrogen. So, these hydrocarbons may be used as H<sub>2</sub> carrier to generate H<sub>2</sub> for fuel cell application without purification. In this work hydrogen production via the dehydrogenation of cyclohexane and decalin was investigated. The work can be summarized as follows:

- 1) Develop Pt-catalyst for the dehydrogenation of cyclohexane and optimize the reaction conditions.
- 2) Kinetic modeling of the dehydrogenation of decalin on Pt/ $\gamma$ -Al<sub>2</sub>O<sub>3</sub> catalyst.
  - a) Perform kinetic experiments to collect data.
  - b) Model the dehydrogenation of decalin and estimate the parameters using the Marquardt algorithm.

Jet fuel is available on the battlefields. It is desirable to extract hydrogen from jet fuel for fuel cell application in the military domain. Furthermore, if the extraction of hydrogen is controlled in the range that has minimum compromise on the fuel properties, the fuel can still be used after dehydrogenation. Thus, the hydrogen produced will be an extra gain. For the first time we explored the possibility of dehydrogenation of Jet A to produce hydrogen. The work can be summarized as follows;



- 1) Perform the dehydrogenation of Jet A on Pt-Sn/catalyst. The operating conditions were optimized.
- 2) Prepare zeolite-supported Pt catalyst for the dehydrogenation of Jet A
- 2) Design bi-functional catalysts for the dehydrogenation of Jet A

## CHAPTER II

### SELECTIVE HYDROGENATION OF C<sub>3</sub> CUT FROM A THERMAL CRACKING UNIT\*

#### II.1 Literature Review

Propylene is one of the major building blocks of the petrochemical industry. It is used to produce a wide range of polymers and intermediates. The major derivatives of propylene are polypropylene, acrylonitrile, propylene oxide, oxo chemicals, and cumene, which are used to make packaging, coating, textiles, automobiles, medical products, fibers, and other consumer products. As the needs for these products grows, so will the need for propylene. More than 60% of the world's production of propylene is used to make polypropylene. Since its invention in 1954, polypropylene has grown into one of the most widely used and versatile products of the petrochemical industry.

Propylene is typically obtained via two main routes. The majority of propylene is produced as a co-product of the steam cracking process.<sup>1,2</sup> Second major source of propylene is a co-product of the refinery catalytic cracking process used to make gasoline.<sup>3-5</sup> Only a few percent is produced on-demand through propane dehydrogenation

---

\*Reprinted with the permission from "Kinetic modeling and simulation of the selective hydrogenation of C<sub>3</sub>-cut of a thermal cracking unit" by Wang, B. and Froment, G.F., 2005, *Industrial and Engineering Chemistry Research*, 44(26), 9860-9867, Copyright [2005] by American Chemical Society.

and metathesis.<sup>6,7</sup>

### II.1.1 Propylene Production

The C<sub>3</sub> cut obtained by the steam cracking of ethane, propane and naphtha typically contains more than 90% propylene and up to 4% methyl-acetylene (MA) and propadiene(PD). Table II-1 summarizes the composition of typical feeds available from steam cracking or fluidized bed catalytic cracking (FCC), as well as the standard propylene grades.

Table II-1. Composition of propylene cuts and commercial propylenes

	C <sub>3</sub> cuts		Propylene grade	
	SC <sup>a</sup>	FCC	Chemical grade	Polymerization grade
Propylene (%)	92	65	92-94	95-99.9
MA + PD (%)	4	0.01	20-30 ppm	10 ppm
C <sub>4</sub> + (wt. ppm)	2000	2000	200	50
C <sub>6</sub> + (wt. ppm)			1000	10

<sup>a</sup>From naphtha steam cracking

The MAPD content in the C<sub>3</sub> cut depends mainly on the type of feed cracked, and also varies with the severity of the steam cracking operation and the design of the furnaces, as shown in Table II-2.

Table II-2. Composition of propylene cut for different steam cracking feeds

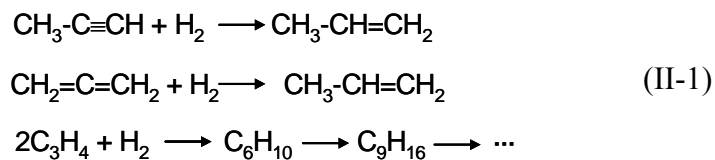
Type of feed	Ethane	Propane	Butane	Naphtha	Gas-oil
Propylene yield (wt%) <sup>a</sup>	2	16	15	13.2	13.1
Composition of C <sub>3</sub> cut					
C <sub>3</sub> H <sub>4</sub> (MAPD)	1.6	3.2	4.2	3.6	
C <sub>3</sub> H <sub>6</sub> (propylene)	64	94	92	93	
C <sub>3</sub> H <sub>8</sub> (propane)	34.4	2.8	3.8	3.4	

<sup>a</sup>On the basis of 100 of feed to the cracking furnaces.

Small quantities of MA and PD impurities in the C<sub>3</sub>-fraction from a thermal cracking unit have a great effect on downstream polyolefin production. MAPD disrupt the chain order and provide a site for cross-linking. Cross-linking increases the chain length and effectively changes the polymer's average molecular weight and may convert it from a thermoplastic to a thermoset. In addition, PD produces rigidity in the chain so that rotation is prohibited. This creates a stronger, but less flexible material. Lastly, MAPD may create unwanted branching of the polymer.

The MAPD in the C<sub>3</sub> cut may be removed by either cryogenic separation and/or selective hydrogenation.<sup>8,9</sup> Energy consumption in cryogenic distillation is high. It is scarcely used. The selective hydrogenation of MAPD to propylene in a catalytic bed can remove MAPD efficiently and at the same time yield more propylene. So, it is more cost effective and is widely employed in industrial production.

The hydrotreating of the C<sub>3</sub> cut involves three hydrogenation reactions and one oligomerization reaction with the formation of green oils of different carbon numbers:



The hydrogenation reactions are very exothermic and result in a reduction in the number of molecules. They are therefore favored thermodynamically by low temperature and high total pressure. The industrial hydrogenations are usually performed in a temperature range 20 ~ 120 °C, 25 bara and H<sub>2</sub> to hydrocarbon molar ratio of 1/17. The isomerization reaction between MA and PD does not take place with the usual catalysts.

Control of the selectivity for propylene is very important as over-hydrogenation will result in the loss of valuable propylene. The propylene yield, for a given feed, increases with decreasing severity of the MAPD specification (within the range of 0 to 5000 ppm of residual MAPD). Hence it is important to avoid hydrogenation levels beyond the quality requirements of commercial propylene.

### II.1.2 The Process of C<sub>3</sub> Cut Selective Hydrogenation

Both gas and liquid phase hydrogenation of MAPD are in use in industry. Liquid phase selective hydrogenation has been developed recently with naphtha steam cracking and the front-end demethanizer scheme.<sup>10,11</sup> It is currently predominant, being more suitable for high MAPD contents in C<sub>3</sub> cut. The dominant process is an adiabatic fixed-bed reactor in liquid phase. Some C<sub>3</sub> liquid phase hydrogenation units have isothermal tubular reactors. Many gas phase C<sub>3</sub> hydrogenation units are still in service. Industrially, the hydrogenation may take place either before (front end) or after (tail end) the

fractionation unit which is used to remove H<sub>2</sub>, CH<sub>4</sub>, CO, and C<sub>2</sub> cut from the C<sub>3</sub> cut. The essential feature of the tail end selective hydrogenation is the relative pure feed and accurate control of feed composition.

### II.1.2.1 Gas Phase Hydrogenation

Figure II-1 shows the typical flow diagram of a tail end gas phase selective hydrogenation of C<sub>3</sub> cut from a thermal cracking unit. The product from the steam cracker is sent to the demethanizer to remove CO, H<sub>2</sub> and CH<sub>4</sub> from the overhead. The bottom is sent to the deethanizer to recover C<sub>2</sub> cut in the overhead, then sent to the C<sub>2</sub> selective hydrogenation reactor. The bottom from the deethanizer is sent to the depropanizer to separate the C<sub>3</sub> cut in the overhead. The C<sub>3</sub> cut is taken as the gas phase from the depropanizer reflux drum. The hydrogen/hydrocarbon mixture is raised to the reaction temperature (about 60 °C) and then selectively hydrogenated in two or three reactors in series, with intercoolers. The effluent from the last reactor is cooled and sent to a washing column, where the green oils are eliminated from the C<sub>3</sub> cut by absorption in a liquid reflux of the C<sub>3</sub> cut itself. The bottom product is sent back to the depropanizer for C<sub>3</sub>/oligomer separation. The C<sub>3</sub> compounds are recycled. The condensed top product from this washing column is sent to a secondary demethanizer to eliminate light fractions such as H<sub>2</sub>, CO and CH<sub>4</sub>. If the MAPD content exceeds 3%, even with good selectivity, the reaction will generate large amounts of heat. It is necessary to increase the number of reactors and intercoolers, or dilute the feed. This dilution is achieved by

increasing the recycling of the bottoms from the washing column, or by adding a recycle of part of the overhead stream of the same column.

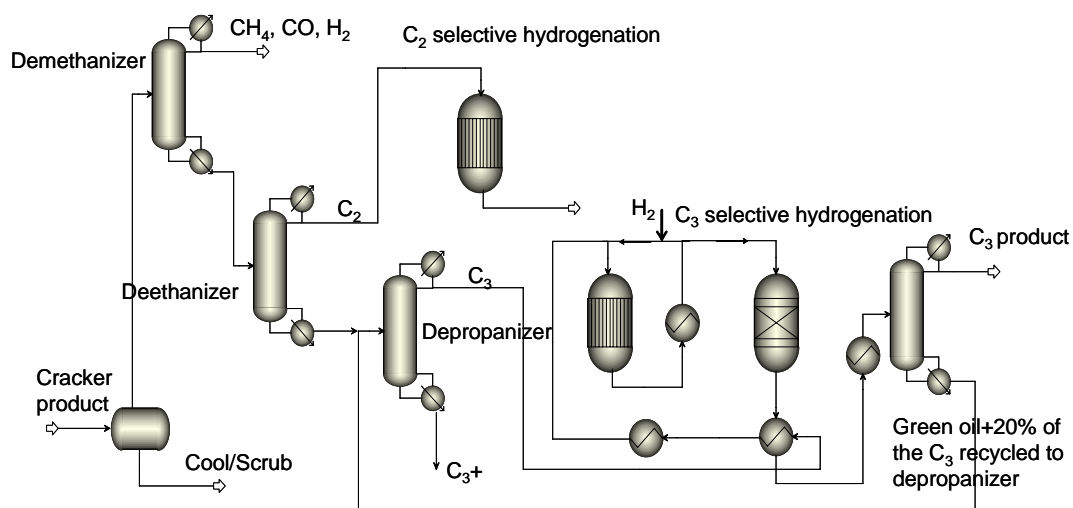


**Figure II-1.** The flow diagram of tail end C<sub>3</sub> cut selective hydrogenation in the gas phase.

### II.1.2.2 Liquid Phase Hydrogenation

The dominant liquid phase  $C_3$  hydrogenation process is licensed by IFP. Typically, this is a two-stage process (Figure II-2). Adiabatic fixed-bed reactors are used. The liquid  $C_3$  cut is taken from the top of the depropanizer. It is diluted by intermediate recycling, mixed with a first hydrogen make up and sent to the top of the first reactor. The reaction heat causes a slight temperature rise and partial vaporization of  $C_3$  mixtures. The reaction is controlled by the hydrogen make up, to reduce MAPD in the first reactor effluent to about 3000 ppm. The reactor effluent is then sent to the separator drum, where the pressure is maintained by a second  $H_2$  make up, avoiding hydrocarbons losses or the need for gas recycling to the cracked gas compressor. The pressure of the first reactor is adjusted by a booster pump, to optimize the operation of the water cooler. The liquid effluent from the separator drum is partly recycled. Part of it is sent to the second reactor. A third  $H_2$  make up is provided before the inlet of this second reactor. The  $H_2/HC$  ratio is used to control the progress of the reaction for any feed composition. The MAPD content in the effluent of the second reactor will be less than 1 ppm. Liquid phase operation may be more economical because the size of the reactors and associated equipment may be smaller than that of the gas phase operation, thus a saving on capital investment and energy may occur.

The primary safety concern with acetylene and  $C_3$  hydrogenation is to prevent situations that lead the reactors to a runaway exothermic reaction. The liquid phase system is inherently safer than the vapor phase system due to the heat sink of the liquid, which can absorb considerable amounts of heat by vaporization. However, the liquid



phase operation introduces another concern over localized hot spots caused by flow maldistribution.

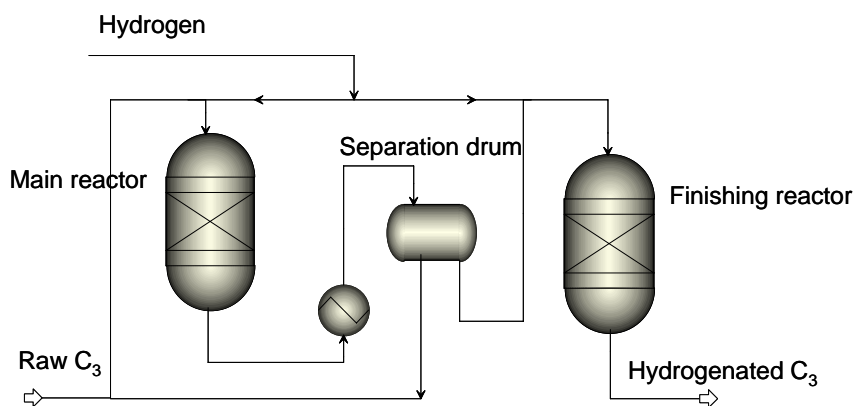


**Figure II-2.** Hydrorefining of the propylene rich cut in liquid phase. IFP technology employing chamber-type reactors.

### II.1.3 Catalysts Development

The selective hydrogenation of alkynes and dienes in olefin streams has been a topic of considerable research over the past several decades. Most of the work has been focused on the selective hydrogenation of C<sub>2</sub> or C<sub>4</sub> olefin streams.<sup>12-18</sup> This is because C<sub>2</sub> and C<sub>4</sub> mixtures are more easily available in a lab setting. Furthermore, the C<sub>2</sub> and C<sub>4</sub> cuts are in gas and liquid phase respectively at the conventional operating pressures of 25 bara. Whereas, the C<sub>3</sub> cut occupies an intermediate position and the phase may vary depending on temperature. This makes it more difficult to control the operation and feed the C<sub>3</sub> cut in the lab condition. However, the selective hydrogenation of olefins from a thermal cracking unit have many common features, i.e. similar catalyst, consecutive reactions, green oil formation, catalyst deactivation, etc. The results from the C<sub>2</sub> and C<sub>4</sub> selective hydrogenation could be a good reference to guide the C<sub>3</sub> hydrogenation. Thus, all the literature concerning hydrorefining of olefin streams from a thermal cracking unit will be introduced. Metals that have a high activity for hydrogenation reactions include Ni, Fe, Rh, Ru, Pd, and Pt, etc.<sup>19</sup> The selective hydrogenation catalysts have undergone considerable evolution over the past several decades. The first generation industrial catalysts in selective hydrogenation were sulfides such as nickel sulfide<sup>20</sup> or nickel-tungsten sulfide.<sup>21</sup> Some copper based catalysts were also used for vapor phase hydrogenation.<sup>22</sup> These catalysts had low catalytic activities and needed to operate in a temperature range from 170 to 230 °C due to low activities. In addition to reducing the selectivity, high operating temperatures decreased the cycle time of the catalyst due to the deactivation caused by green oil formation. Typically, this hydrogenation unit

operated with an ethylene loss. Furthermore, the Ni catalyst must be presulfided to maintain it in a sulfided state via continuous injection of sulfur compounds

Second generation selective hydrogenation catalysts were introduced in the late 1960s.<sup>23, 24</sup> They contained palladium dispersed on porous support and are selective to the hydrogenation of alkyne and diene in alkene rich streams. High selectivity for olefin is not a feature that is unique to palladium. Other metals, especially nickel and copper, can also perform well. It has recently been shown that gold also gives ethylene with total selectivity.<sup>25</sup> Other metals such as platinum and iridium show much lower mechanistic selectivities.<sup>26</sup> Palladium was employed in industry due to its both high activity and selectivity. Supported palladium catalysts containing only very small amounts of palladium could be used at low temperatures.

The third generation of selective hydrogenation catalysts was introduced in the early 1980s. While these catalysts contain palladium, they also include a second metal from group IB (Cu, Ag, Au, etc.). Both supported on a refractory oxide. Presently, all industrial catalysts used in selective hydrogenation are bimetallic catalysts with a palladium active phase supported on alumina and promoted by another metal.

The addition of a second metal, such as Pb,<sup>27, 28</sup> B,<sup>29</sup> or Cu<sup>30, 31</sup> to Pd results in catalysts which are more stable and more ethylene selective. This may be due to geometric isolation of Pd in a matrix of inactive metal which could reduce the production of species requiring multiple adsorption sites,<sup>32</sup> reduce the extent of hydrogen spillover<sup>33</sup>, and/or electronically alter the nature of the adsorbed species<sup>34</sup> or the relative strengths of acetylene and ethylene adsorption.<sup>35</sup> The use of bimetallic or alloy catalysts

appears to represent the best method of increasing catalyst life time and ethylene yields during selective hydrogenation of  $C_2$  cut. Hancock and co-workers<sup>36</sup> from Chevron Phillips reported that the most active and selective catalysis occurred when the alumina core was coated with a layer of 300 microns Pd on the surface. The addition of silver to the Pd layer offered a trade of small loss in catalyst activity for a large increase in selectivity. There was an optimum silver loading. Too much silver, while increasing selectivity reduced the activity to unacceptable low levels. Silver reduced the impact of variability in Pd distribution within the catalyst pellet.

According to literature the rate of hydrogenation of ethylene in an ethylene-hydrogen mixture is 10-100 times faster than the rate of acetylene hydrogenation under identical conditions of temperature, pressure and catalyst. Thus the selectivity of acetylene hydrogenation can only be explained by the preferential adsorption of acetylene molecules on the surface of the palladium. Hence, kinetics is controlled by relative adsorption rates. The preferential adsorption of acetylene over ethylene means that provided there are sufficient acetylene molecules to cover all the active sites then ethylene hydrogenation to ethane is minimized.

#### **II.1.4 Green Oil Formation**

Pd/alumina catalyst is widely used in the selective hydrogenation of alkyne and diene in olefin streams. In addition to the hydrogenation reactions, oligomers, referred to as green oil, are also produced from the oligomerization of unsaturated alkyne, diene

and/or olefin.<sup>37</sup> The catalyst slowly deactivates, because of the accumulation of the deactivating agent, formed by oligomerization side reactions.

The subject of green oil formation is of industrial importance. It was reported that the amount of green oil formation was primarily a function of the conversion of acetylene. Hence, the rate of formation of green oil was higher on the lead bed where higher acetylene concentrations exist. The amount of green oil formed decreased as the hydrogen partial pressure increased. So, catalyst deactivation by green oil became a major problem at low hydrogen to acetylene ratios. Furthermore, the amount of green oil formation has been reported to be related to surface acidity of the support, palladium crystallite size, pore openings, water content in the feed, and operating temperature. The net result of green oil formation is the shortening of the catalyst cycle length and the decrease in the catalyst selectivity.

It was reported in  $C_2$  cut selective hydrogenation that about 10-20 % of the acetylene was converted to  $C_4$  and heavier green oil.<sup>38, 39</sup> A major improvement of the promoted catalysts lies in the suppression of the formation of green oil. Hence, ethylene yield and catalyst cycle length were increased. It was disclosed that green oils formed in the ethylene plants in China were long chained olefinic compounds with a general formula corresponding to  $C_nH_{(1.8-1.9)n}$  where  $n=14-17$ . The quantity of aromatic compounds was negligible and one quarter of the olefins were alpha olefins.

Axens<sup>38</sup> reported at the 1995 Spring AIChE Meeting that addition of Ag to a Pd catalyst reduces green oil formation. Axens compared the formation of green oil on a Pd-only catalyst with a Pd/Ag catalyst. Both catalysts were on an alumina support. The

acetylene in the feed was 2.6 %. Green oil was formed through oligomerization of acetylene. The amount of acetylene converted to ethylene was increased on addition of the silver.

Süd Chemie<sup>40</sup> reported the effect of Ag on green oil formation in its brochure. Addition of Ag reduced the green oil formation. In essence, Ag acted like an atomic spacer to increase the distance between the active palladium sites. This reduced the chance for two molecules of acetylene to combine to form the 1,3-butadiene precursor, leading directly to less potential polymer formation. Süd Chemie has reported laboratory data to illustrate the effect of Ag on reducing the amount of heavy green oil formed during hydrogenation of acetylene. The amount of polymer formation with the promoted catalyst was only about 40% of the amount produced with the Pd-only catalyst.

In industry, to compensate for the loss of catalytic activity, reactor temperature and H<sub>2</sub>/MAPD molar ratio are increased to maintain the optimal selectivity for propylene. When the inlet temperature reaches 393 K, then the catalyst has to be regenerated; this is typically done after a few months of reactor operation. For this reason hydrogenation units consists of two parallel reactors, which allow simultaneous use of one of the reactors for hydrogenation and the other for on-line regeneration of the catalyst to maintain continuous operation. The deactivated catalysts are typically regenerated by a steam/air burn, followed by H<sub>2</sub> reduction.<sup>41-43</sup> The regeneration condition is critical. A well executed regeneration may fully recover the catalyst activity to essentially the same performance as was achieved during the previous cycle. Conversely, an incorrectly executed regeneration/reduction can result in placing back in service a catalyst that

performs worse than it did when it was taken offline. Typically, it is recommended that the catalyst be subjected to temperatures in the range 450 - 480 °C. The burn is controlled by limiting the amount of air in a steam/air mixture. Extreme attention must be paid to the regeneration as the accumulated green oil in the reactor may cause the temperature to exceed the limit and damage the catalyst. Typical vendor guidelines call for maintaining air between 1-5% during the steam/air burn. Regeneration and the subsequent reduction are usually carried out counter current to the process flow. The catalyst service life is about 5 years.

### **II.1.5 The Role of Added CO**

Adsorption phenomena play an important role in heterogeneous catalysis. Reactants must be transported from the bulk fluid to the catalyst surface, and then adsorbed on the catalyst surface for the desired reaction. Relative adsorption strengths, in the absence of diffusion limitations, determine the concentration of each reactant on the catalytic surface, thus affect the reaction rate and selectivity. Additives, both in the fluid phase or on the catalyst, are commonly used to alter adsorption behavior of the reactants on the catalyst.

CO is commonly used to inhibit hydrogenation reactions on group VIII metals. It is added to the C<sub>2</sub> and C<sub>3</sub> cut of a thermal cracking unit in the amount of near 1000 ppm, particularly those with high hydrogen to acetylene ratios (front end mixtures), where the selectivity for mono olefins would be very poor in its absence.<sup>44-47</sup> Investigations on the effects of added CO have shown uniformly high ethylene selectivity.

The role of CO is attributed to its competition with hydrogen, alkynes and dienes for the active sites. Freund and co-workers<sup>48</sup> studied the selective hydrogenation of 1,3-butadiene on Pd(111) and Pd(100) single crystals at atmospheric pressure in the temperature range 298-373 K. In the initial stage of the reaction, butene isomers were the main reaction products. After full 1, 3-butadiene consumption, the selectivity for butene decreased due to the formation of butane. Addition of small amounts of CO drastically changed the selectivity on Pd (110); that is, the hydrogenation to n-butane was completely suppressed, whereas the hydrogenation to butenes were hardly affected. This was rationalized by considering that CO reduced the hydrogen surface concentration to a level that was still sufficient for 1,3-butadiene hydrogenation, but too low for butene hydrogenation. In contrast, on Pd (111), catalytic activity basically vanished in the presence of CO traces.

LeViness et al.<sup>49</sup> observed that the addition of 60 ppm CO to tail-end (low hydrogen/acetylene) mixtures sharply decreased the rate of ethylene hydrogenation to ethane, and amounts above 500 ppm completely terminated it. Under the same conditions the rate of acetylene consumption was only marginally lowered. Weiss<sup>50</sup> reported that the addition of CO reduced the rate of acetylene hydrogenations in both front and tail end hydrogenation mixtures. The effect was attributed to competition between CO and hydrogen. In addition, these authors concluded that the decrease in the rate of ethylene hydrogenation observed at very low CO concentration, where no decrease in the rate of acetylene consumption was observed, was due to CO preventing hydrogen spillover to the support, where it could react with adsorbed ethylene.



The addition of CO is also not without its problems. Sarkany et al.<sup>31</sup> have observed that the selectivity to gas phase oligomers passes through a broad maximum as CO concentration increases. We might expect that the operational lifetime of catalysts used in the presence of CO would be decreased, necessitating more frequent regeneration cycles. The increase in gas phase oligomer concentration may also contribute to the real problems of reactor fouling and plugging.<sup>9</sup>

In summary, the role of CO in the selective hydrogenation of C<sub>3</sub> cut is that it competes with hydrogen for Pd adsorption sites to reduce the surface hydrogen concentration, hence slows down the hydrogenation rate to prevent the over-hydrogenation of propylene. If the hydrogenation of propylene takes place on the support due to activation by hydrogen spillover, then CO also competes with hydrogen and propylene for adsorption sites on the alumina support.

For front-end acetylene hydrogenation units, CO will be in the reactor feed at a level of about 200-2000 ppm. For tail-end units, trace amounts of CO (0.1-5 ppm) can be injected into the reactor feed. Usually, this CO comes from bypassing a small stream of untreated hydrogen around the PSA unit or methanator.

### **II.1.6 Control of the Selectivity**

The selective hydrogenation process is very sensitive to a number of operating variables such as temperature, space velocity, H<sub>2</sub>/HC molar ratio and alkyne and diene concentration in olefin stream. Control of the selectivity in MAPD selective hydrogenation is very important because propylene can be consecutively hydrogenated

to form propane if operating variables such as  $H_2$ /MAPD molar ratio or temperature are not controlled properly. In this case the overall propylene selectivity may be negative, meaning a loss of valuable propylene. The reactions are strongly exothermic. The excessive heat production can lead to a run away situation.

Many attempts have been made to improve this process through fundamental studies of catalysts and the development of novel approaches. One approach is to use a membrane.<sup>51</sup> The driving forces behind the interest in this topic continue to be the use of membranes to catalyze reactions and also to carry out important separations. Currently, there are three popular approaches with regard to the membrane: 1) use inorganic oxide membranes (that are size selective) to contain a catalyst, and 2) deposit a catalytic material on these inorganic oxide membranes in order to provide catalysis at the surface where separation occurs. The third alternative 3) is to use a material that preferentially allows only one gas to permeate through a permselective metal. Some studies on hydrogenation in Pd membrane reactors have shown that the permeate hydrogen, being atomic form, is more reactive than molecular hydrogen. Gryzanov et al.<sup>52</sup> studied  $C_2H_2$  hydrogenation using Pd-Ni membrane as catalyst at 180 °C with the aid of mass spectral analysis. They found that molecular hydrogen on the surface of the membrane did not react with ethylene, whereas hydrogen atoms coming from the membrane participated in the hydrogenation of ethylene. Sathe et al.<sup>53</sup> studied the selective hydrogenation of acetylene over Pt and Pd alloy membrane reactors. Two different ways of supplying hydrogen, premixed and permeation modes, were compared. It was concluded that the permeation of hydrogen through the palladium-based membranes was preferable to

premix due to the elimination of the mass transfer steps. In the premixed mode, the ethylene yield increased with the hydrogen flow rate in the case of Pd-Ag, Pd-Ni, and Pd-Ru membrane. However, to achieve higher selectivity for ethylene in the permeate mode, the membranes needed to operate at low flow rates of hydrogen to avoid the consecutive hydrogenation of ethylene.

The control of the selectivity in the hydrotreating of the olefin streams from a thermal cracking unit is a very hard task in industrial production. While the usage of Pd-based hydrotreating catalyst significantly improves the process performance, there are still many problems to be addressed in regard to the operating variables. In light of the huge capacity of this process in petrochemical industry, the slight improvement on the olefin yield amounts to a large profit.

The selective hydrogenation of a C<sub>3</sub>-cut is very exothermic and CO is added to the feed when the catalyst is fresh, in order to moderate its activity. The catalyst slowly deactivates, because of a deactivating agent, formed by oligomerization side reactions. So, this is a dynamic process. The deactivation of the catalyst with time imposes a continuous adaptation of the operating conditions to maintain the optimal selectivity. The deactivated catalyst needs to be periodically regenerated. Operating variables must be optimized taking into account selectivity, run length and regeneration cost in order to obtain a maximum profit. The lack of a valid model for this process make the adjustment of operating variables based mainly in an empirical way and upon the knowledge of the catalyst. The unadapted adjustment of operating variables caused the negative overall

selectivity for propylene, meaning a loss of valuable propylene. Our approach is to develop a rigorous kinetic model for the process to guide the operation.<sup>54</sup>

Relatively little work has been performed on the kinetics of the selective hydrogenation of the C<sub>3</sub> cut. Villora et al. reported the kinetics of gas phase selective hydrogenation of a C<sub>3</sub>-cut as well as the C<sub>2</sub>-C<sub>3</sub> mixture at atmospheric pressure.<sup>55,56</sup> The kinetics were expressed in terms of empirical power law models. Green oil formation was not reported. Uygur et al. investigated the kinetics of liquid phase selective hydrogenation of a C<sub>3</sub>-cut.<sup>57</sup> A Hougen-Watson model was used to model the reaction kinetics. The experiments were performed in the presence of internal and external mass transfer resistance, but these limitations were accounted for in the derivation of the rate equation.

Kinetic equations for the hydrogenation as well as for the green oil formation are valuable tools for the improvement of the process performance. So far no work has been done to determine the kinetics of green oil formation and the catalyst deactivation. The purpose of this work was to develop a kinetic model for this process. The operating conditions were similar to an industrial tail end gas phase hydrogenation process. The kinetic model was of the Hougen-Watson type, i.e., accounting for the adsorption of propylene, MA, PD and green oil. The deactivation of the catalyst is accounted for by linking the activity to the content of the deactivating agent.<sup>58-60</sup>

## II.2 Experimental

### II.2.1 Feed Mixtures

The C<sub>3</sub> mixture, similar in composition to that of the industrial C<sub>3</sub> cut, was purchased from Scott Specialty Gases. The composition of the C<sub>3</sub> mixture is as follows: 1% PD, 2% MA, 96.8% C<sub>3</sub>H<sub>6</sub>, 0.17% C<sub>3</sub>H<sub>8</sub> and 0.03% CH<sub>4</sub>. The purity of the H<sub>2</sub> and N<sub>2</sub> gas is 99.99%.

### II.2.2 Catalyst

The catalyst used was C31-1 supplied by SÜD-CHEMIE. C31-1 is a Pd-based hydrogenation catalyst. It contains 0.03 wt % Pd with < 0.1wt % other heavy metals as promoter, coated as a 200 µm layer on the 2-4 mm γ-Al<sub>2</sub>O<sub>3</sub> core. Prior to reaction, the catalyst was activated by removing water from the catalyst and subsequent reduction of palladium oxide on the support to palladium black. The removal of water was carried out by purging nitrogen through the reactor at 150 °C for 2 hrs. The reduction was conducted by feeding a quantity of hydrogen diluted with nine volumes of nitrogen at 150 °C for 2 hrs. After reduction the catalyst bed was cooled to ambient temperature by continuing the nitrogen purging to ensure a hydrogen-free atmosphere in the reactor prior to start-up of the reaction.

For fixed bed catalytic reactors, the ratio of tube to particle diameter,  $d_t/d_p$ , should be at least 10 to approximate plug flow. The commercial C31-1 catalyst is a sphere with

diameter between 2-4 mm, and the reactor ID is limited to 0.45" for reasons of heat transfer area per weight of catalyst. The ratio requirement is not satisfied. Therefore, the eggshell catalyst was crushed and sieved to different size fractions. The samples were digested in concentrated HF and HCl mixture solutions, and then analyzed by Inductively Coupled Plasma Spectrometer (ICP). It was shown in Figure II-3 that the Pd content of the various sieve fractions was not identical. To come to particles representative for the commercial catalyst, but also satisfying the requirements of a kinetic study in bench scale equipment, the different sieve fractions were mixed and repelletized again, evidently to a size much smaller than the original. The hydrogenation was then tested with catalyst pellets of this type but having different sizes. It was found that internal mass and heat transfer resistance were negligible for particle sizes smaller than 0.20 mm and these were retained for the kinetic study. Also, the operating conditions were chosen by calculation to avoid external mass and heat transfer resistance.<sup>57</sup>

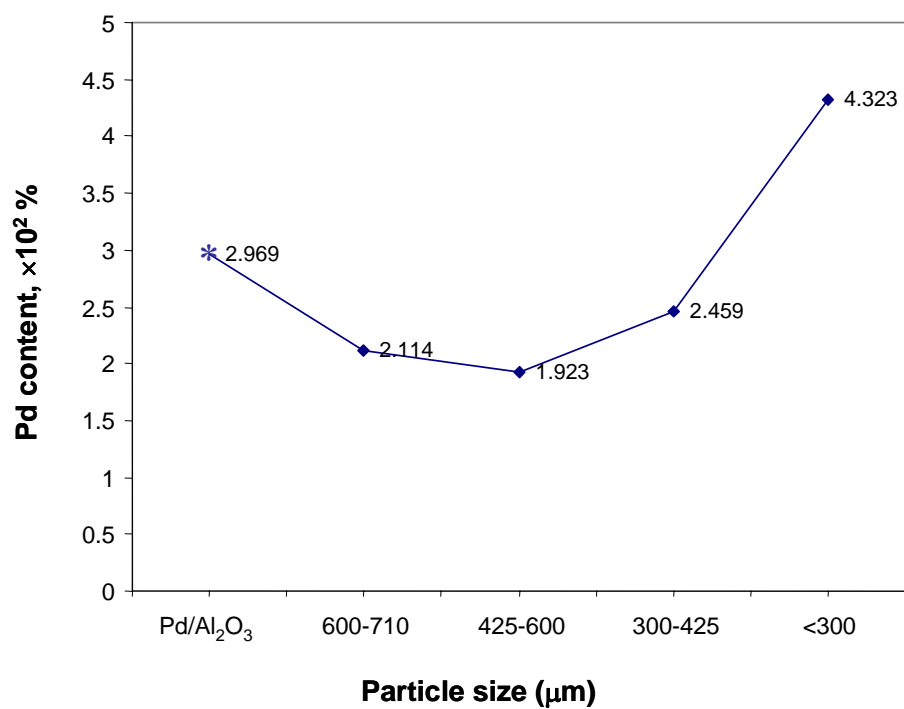


**Fig II-3.** Pd content in original 2-4mm Pd/Al<sub>2</sub>O<sub>3</sub> sphere catalyst and crushed different size fractions. \* Original 2-4 mm Pd/Al<sub>2</sub>O<sub>3</sub> sphere catalyst.

### II.2.3 Reactor Unit

The kinetics of the selective hydrogenation of MA and PD was investigated in a bench scale fixed bed reactor, as shown in Figure II-4. A PC, equipped with Labview software and Fieldpoint modules, was used to monitor and control process variables such as feed flow rate, total pressure and temperature. The reactor feed consisted of four streams, i.e., H<sub>2</sub>, C<sub>2</sub>H<sub>6</sub>, the C<sub>3</sub> mixture and N<sub>2</sub>. Ethane was used as internal standard. The flow rates of H<sub>2</sub>, N<sub>2</sub> and C<sub>2</sub>H<sub>6</sub> were controlled by gas mass flow controllers. The flow rate of the pressurized C<sub>3</sub> mixture was controlled by a liquid mass flow controller. The C<sub>3</sub> mixture was vaporized in the mixing chamber, then mixed with other gas streams inside this chamber before flowing to the reactor. The reactor was heated by an oil bath. The reactor temperature profile was monitored by a sliding thermocouple, mounted inside the reactor along the reactor axis. The reactor pressure was controlled at the exit by a back pressure regulator. In the kinetic study, the temperature and pressure were varied in the range of 60 ~ 90 °C and 16 ~ 20 bara, respectively. At these operating conditions, the C<sub>3</sub> mixture was gaseous. The reactor effluent was analyzed by two on-line GCs which were also controlled by a computer. As the different compounds elute the column, they are detected by a detector. The PeakSimple chromatography software was used to integrate the peaks in the chromatogram.

### II.2.4 Gas Chromatography

The Chromatographic separation involves the use of a stationary phase and a mobile phase. The components of a gas mixture carried out by the mobile phase in the column



elute the column at different rates depending on their separation factor, determined by their chemical and physical properties and their interaction with a specific column filling, called the stationary phase. Different columns were used to achieve the necessary chromatographic separation. An FID GC with HP PLOT/Alumina capillary column was used to analyze C<sub>3</sub> and green oil (up to C<sub>12</sub>). The TCD GC was equipped with 5A and 13X packed column to analyze H<sub>2</sub>. Ar was used as the carrier gas in the TCD GC. The flow rate was maintained at 30 ml/min. N<sub>2</sub> was added into the feed stream as an internal standard to calibrate H<sub>2</sub>.

## II.3 Results and Discussion

### II.3.1 Definition of Conversions and Selectivities

Conversion of MA

$$X_{MA} = \frac{\text{moles of MA in} - \text{moles of MA out}}{\text{moles of MA in}} \times 100$$

Conversion of PD

$$X_{PD} = \frac{\text{moles of PD in} - \text{moles of PD out}}{\text{moles of PD in}} \times 100$$

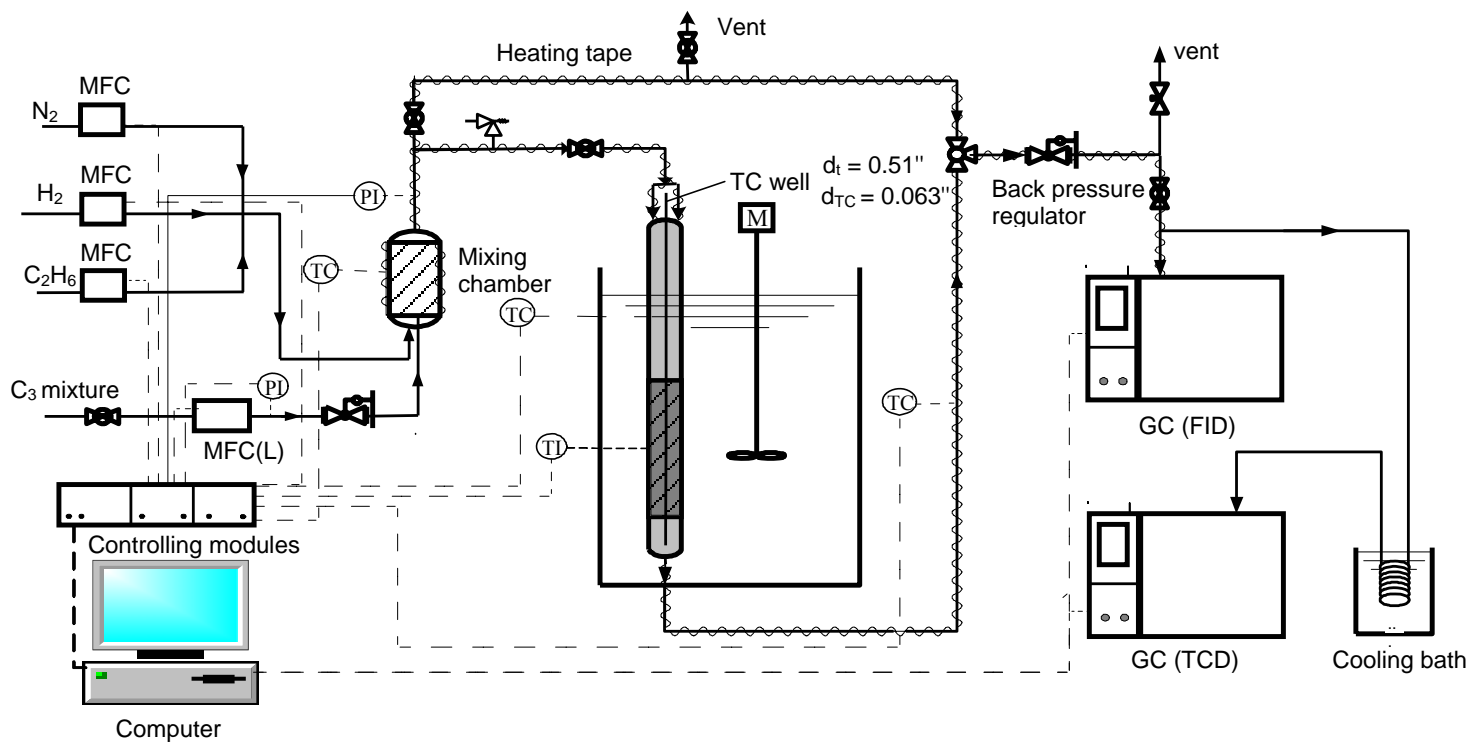


**Figure II-4.** Experimental setup for the selective hydrogenation of the C<sub>3</sub>-cut from a thermal cracking unit.

Conversion of MA and PD into propylene

$$X_{PP} = \frac{\text{moles of PP out} - \text{moles of PP in}}{\text{moles of MAPD in}} \times 100$$

(II-2)

Conversion of MA and PD into propane

$$X_{PN} = \frac{\text{moles of PN out} - \text{moles of PN in (impurity in C}_3\text{)}}{\text{moles of MAPD in}} \times 100$$

Conversion of MA and PD into green oil

$$X_{GO} = \frac{\text{moles of GO out}}{\text{moles of MAPD in}} \times 100$$

Selectivity for products

$$\text{Selectivity} = \frac{\text{moles of product i formed}}{\text{moles of MAPD converted}} \times 100 \quad \text{i refers to PP, PN or GO}$$

### II.3.2 Experimental Results

Figure II-5 shows the conversions and catalyst bed temperature as a function of run length at oil bath temperature of 55 °C. The MA and PD conversions declined from the start of the run onwards due to catalyst deactivation. The green oil formation rate also slowly decreases with the loss of catalyst activity. Holding the oil bath temperature constant at 55 °C, the catalyst bed temperature decreases from 69 °C at start of the run to 64 °C after 10 hr. Hydrogenations are highly exothermic reactions. The heat generated during the reaction increased the temperature of the catalyst bed by over 10 °C. With the loss of catalyst activity, the reaction generates less heat, thus the temperature difference between catalyst bed and oil bath decreases.

### II.3.3 Two Aspects of the Kinetic Modeling

Due to the deactivation of the catalyst, the kinetic modeling of the process therefore involved two aspects: the kinetics of the main reactions and the kinetics of deactivation. It was decided to partition the problem and to use the initial data for the first aspect and the complete data set collected in a run, as shown in Figure II-6, for the second. Each run was carried out with fresh catalyst to avoid having to deal with different dispersion of the metal compound of the catalyst caused by regeneration. A rigorously standardized catalyst pretreatment produced samples with identical initial activity. To study the deactivation under sufficiently varied conditions the run length was chosen to cover a 10%-20% decrease in conversion. The reactor effluent was analyzed at time intervals of one hour. Each run lasted for 10 to 20 hr, depending upon the operating condition, i.e.

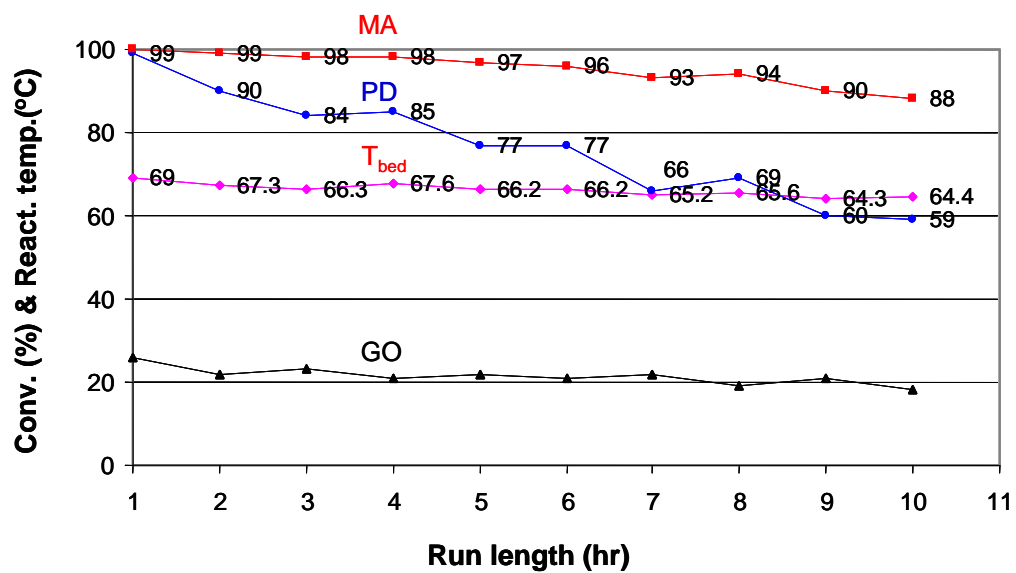


**Figure II-5.** Conversions and catalyst bed temperature as a function of time run length at constant oil bath temperature of 55 °C.

upon the deactivation rate of the catalyst. The amount of deactivating agent was determined at the end of the run by combustion. Each conversion measured at the exit was used in the parameter estimation. The catalyst deactivation significantly changed the amount of heat generated. In order to maintain a constant temperature profile during the run, the oil bath temperature needed to be adjusted frequently. A set of 21 runs were performed, covering a wide range of temperature,  $H_2$ /MAPD molar ratio and also covering a wide range of run length, so as to gather information on the deactivation. Typical examples illustrating the effects of temperature, space time,  $W/F^\circ_{MAPD}$  and the molar ratio of  $H_2$ /MAPD are given in Fig II-6 and Figure II-7. The run length is expressed in terms of the total amount of MAPD fed per kg of catalyst,  $\Sigma F^0_{MAPD}/W$ .

### II.3.4 Reaction Scheme

In the hydrogenation process over  $Pd/\gamma-Al_2O_3$  catalyst, two kinds of active sites, i.e. metal sites and acid sites, are involved. The metal sites catalyze hydrogenation reactions, but the acidity of the alumina catalyzes oligomerization of the olefins, thus producing the so-called green oil. Three possible reaction schemes, which differ only in the mechanism of green oil formation with carbon number below 12, were derived. In Scheme II-1, green oil is formed out of MA and PD, and hydrogenated afterwards. In Scheme II-2 green oil is formed out of propylene only. In Scheme II-3 green oil is formed not only out of MA and PD but also out of propylene.

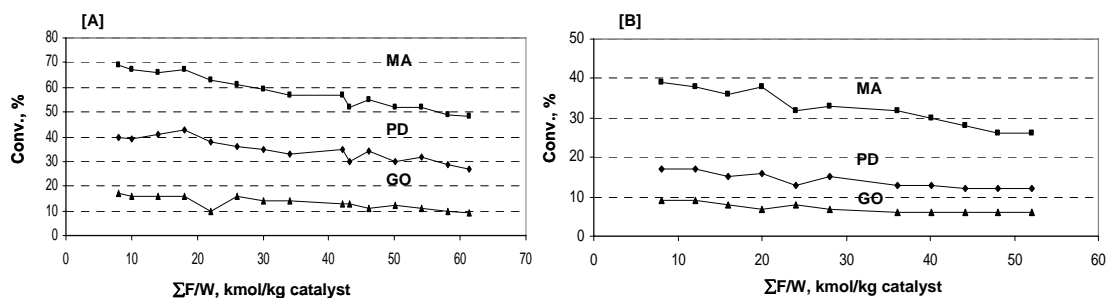


**Figure II-6.** Evolution of the conversions as a function of run length, expressed as  $\Sigma F_{\text{MAPD}}^0/W$ , at 70 °C, and  $W/F_{\text{MAPD}}^0 = 8.33$  kg hr/kmol. H<sub>2</sub>/MAPD molar ratio in [A] =1.8; in [B] 1.1.

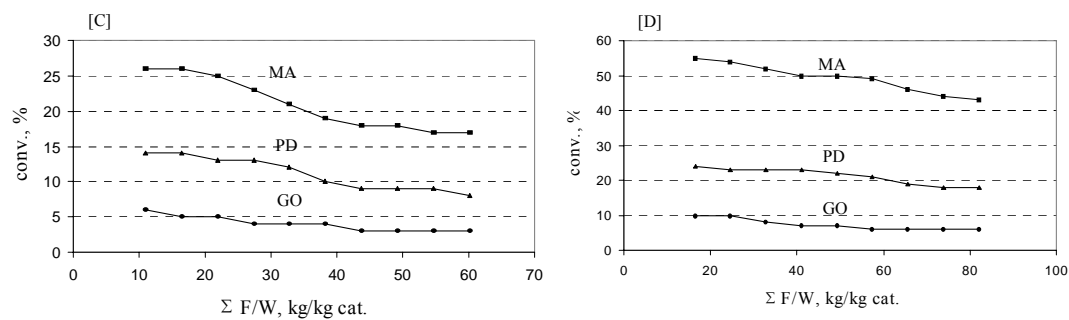
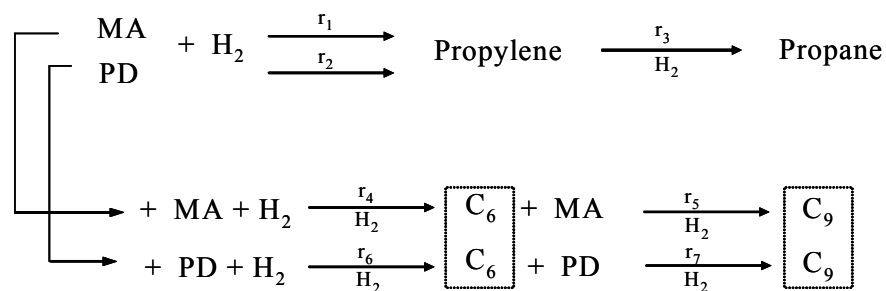
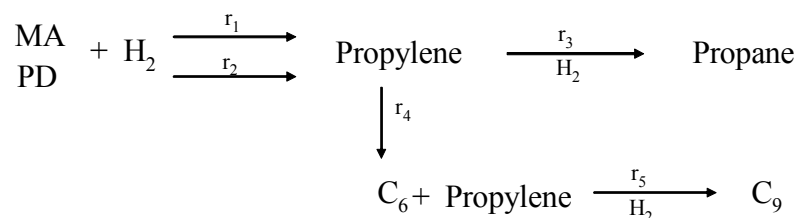


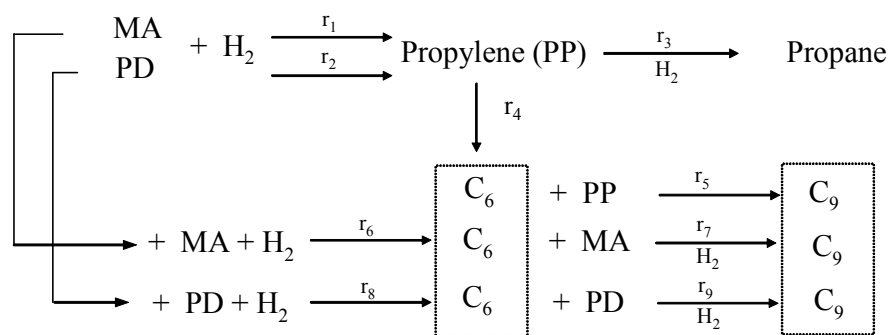
**Figure II-7.** Evolution of the conversions as a function of run length for H<sub>2</sub>/MAPD =1.5 (molar ratio),  $W/F_{\text{MAPD}}^0 = 4.06$  kg hr/kmol. In [C] at 60 °C and in [D] 80 °C.



Scheme II-1. Reaction scheme with formation of oligomers out of MA and PD.



Scheme II-2. Reaction scheme with formation of oligomers out of propylene.



Scheme II-3. Reaction scheme with formation of oligomers out of MA, PD and propylene.



### II.3.5 Kinetic Modeling

#### II.3.5.1 Rate Equations for Hydrogenation and Oligomerization

In all three schemes, MA and PD are hydrogenated over Pd active sites to form propylene, which is subsequently hydrogenated to form propane. When the surface reaction between dissociatively adsorbed H<sub>2</sub> and MA or PD is the rate determining step, the hydrogenation rates on Pd can be written, in the absence of deactivation:

$$\begin{aligned} r_1^0 &= k_{MA}^0 K_{MA} K_{H_2} (P_{MA} P_{H_2} - P_{PP} / K_1) / \Delta \\ r_2^0 &= k_{PD}^0 K_{PD} K_{H_2} (P_{PD} P_{H_2} - P_{PP} / K_2) / \Delta \\ r_3^0 &= k_{PP}^0 K_{PP} K_{H_2} (P_{PP} P_{H_2} - P_{PN} / K_3) / \Delta \end{aligned} \quad (II-3)$$

The denominator  $\Delta$  appearing in the reaction rates  $r_1^0$ ,  $r_2^0$  and  $r_3^0$  is

$$[1 + (K_{H_2} P_{H_2})^{1/2} + K_{MA} P_{MA} + K_{PD} P_{PD} + K_{PP} P_{PP} + K_{PN} P_{PN}]^3 \quad (II-4)$$

Acid sites are responsible for the formation of green oil. The reaction rates for the formation of green oil from MA and PD in Scheme 1 are as follows:

$$\begin{aligned} r_{MA-C6}^0 &= k_{MA-C6}^0 P_{MA}^2 P_{H_2}^2 / \Delta \\ r_{MA-C9}^0 &= k_{MA-C9}^0 P_{MA} P_{C6} P_{H_2} / \Delta \\ r_{PD-C6}^0 &= k_{PD-C6}^0 P_{PD}^2 P_{H_2}^2 / \Delta \\ r_{PD-C9}^0 &= k_{PD-C9}^0 P_{PD} P_{C6} P_{H_2} / \Delta \end{aligned} \quad (II-5)$$

The denominator  $\Delta$  in the above reaction rates is

$$[1 + (K_{H_2} P_{H_2})^{1/2} + K_{MA} P_{MA} + K_{PD} P_{PD} + K_{C6} P_{C6} + K_{C9} P_{C9}]^3 \quad (II-6)$$

The reaction rates of green oil formation from propylene in Scheme 2 are written

$$r_{PP-C6}^0 = k_{PP-C6}^0 K_{PP}^2 P_{PP}^2 / \Delta \quad (II-7)$$

$$r_{PP-C9}^0 = k_{PP-C9}^0 K_{C6} K_{PP} P_{C6} P_{PP} / \Delta$$

$$\text{with } \Delta = [1 + K_{PP} P_{PP} + K_{C6} P_{C6} + K_{C9} P_{C9}]^2 \quad (II-8)$$

In Scheme 1, the equations defining the net rate of formation for the various components are

$$R_{MA} = r_1 + 2r_4 + r_5$$

$$R_{PD} = r_2 + 2r_6 + r_7$$

$$R_{PP} = r_1 + r_2 - r_3 \quad (II-9)$$

$$R_{PN} = r_3$$

$$R_{C6} = r_4 + r_6 - r_5 - r_7$$

$$R_{C9} = r_5 + r_7$$

In Scheme 2, the equations defining the net rate of formation for the various components are

$$R_{MA} = r_1$$

$$R_{PD} = r_2$$

$$R_{PP} = r_1 + r_2 - r_3 - 2r_4 - r_5 \quad (II-10)$$

$$R_{PN} = r_3$$

$$R_{C6} = r_4 - r_5$$

$$R_{C9} = r_5$$

Scheme 3 is actually the combination of Scheme 1 and Scheme 2. In Scheme 3, the equations defining the net rate of formation for the various components are

$$\begin{aligned}
 R_{MA} &= r_1 + 2r_6 + r_7 \\
 R_{PD} &= r_2 + 2r_8 + r_9 \\
 R_{PP} &= r_1 + r_2 - r_3 - 2r_4 - r_5 & \text{(II-11)} \\
 R_{PN} &= r_3 \\
 R_{C6} &= r_4 + r_6 + r_8 - r_5 - r_7 - r_9 \\
 R_{C9} &= r_5 + r_7 + r_9
 \end{aligned}$$

### II.3.5.2 Parameter Estimation

In the absence of deactivation the set of steady state continuity equations for the components in a plug flow reactor can be written

$$\frac{dX_i}{dW/F^0_{MAPD}} = R_i \quad i = 1, 2, \dots, 6 \quad \text{(II-12)}$$

The integral method was used for the kinetic analysis. The above set of differential equations was numerically integrated by a fourth-order-Runge-Kutta method. The parameter estimation was based on the Marquardt algorithm for multiple responses, minimizing the objective function  $\sum(X_{iexp} - X_i)^2$ . The numbers of parameters in the above three models amount to 28, 24 and 38, respectively. The parameter estimation was performed on all initial data simultaneously at all temperatures by directly substituting the temperature dependence of all the parameters into the corresponding continuity

equations. To facilitate the parameter estimation the following re-parameterization was carried out, where  $T_m$  was the average temperature of the experiments.

$$k = A \exp\left(\frac{-E}{RT}\right) = A^* \exp\left[\frac{-E}{R} \left(\frac{1}{T} - \frac{1}{T_m}\right)\right]$$

$$K = A \exp\left(\frac{H}{RT}\right) = A^* \exp\left[\frac{H}{R} \left(\frac{1}{T} - \frac{1}{T_m}\right)\right]$$
(II-13)

The discrimination between rival models was based on the requirement for all parameters to be positive and significant, and on the residual sum of squares as a test for the fit of the data. The model based on Scheme 1 fits the data best. The sums of squares of residues for the three models are 0.08, 0.13 and 0.12, respectively, so that model 1 was retained for the main reactions in the absence of deactivation. Figure II-8 compares the experimental conversions obtained at 70 °C with the values simulated using model 1.

### II.3.6 Catalyst Deactivation

#### II.3.6.1 Observations

Due to catalyst deactivation, the conversion at the outlet decreased with run length. The catalyst deactivated faster when the content in the exit flow of oligomers, called “green oil”, was high. The deactivation rate declined with run length. Each run covered at least a 10 - 20% decrease of conversion of MA and PD so as to permit an accurate modeling of the deactivation. Each run lasted for 10-20 hr, depending on the operating conditions, therefore on the deactivation rate of the catalyst. The reactor effluent was

analyzed at intervals of one hour. The deactivating agent content was determined at the end of the run by combustion. Typical results at 80 °C are shown in Figure II-9.

The formation of deactivating agent is affected by such factors as conversion, process time, expressed as  $\Sigma F_{\text{MAPD}}/W$  and the  $\text{H}_2/\text{MAPD}$  molar ratio. The higher the conversion and the longer the process time, the higher the content of deactivating agent. Moreover, as seen in Figure II-9, the deactivating agent content at a  $\text{H}_2/\text{MAPD}$  molar ratio of 1.1 is higher than that at 1.8, even at shorter process time. A high  $\text{H}_2/\text{MAPD}$  molar ratio reduces the formation of deactivating agent.

### II.3.6.2 Kinetic Modeling of Deactivation

The GC analysis detected green oil up to  $\text{C}_{12}$  in the reactor effluent. Therefore, the deactivation was ascribed to even heavier oligomers, with carbon number exceeding 12 and represented here by C. These higher oligomers would not elute from the reactor under the operating conditions of this study, in other words, would be irreversibly adsorbed on the catalyst sites and act as deactivating agent.

A  $\text{C}_{15}$  oligomer can be formed in various ways out of lower oligomers and propylene:



The initial rate of formation of the deactivating agent can be written

$$r_{\text{C}}^0 = k_1 P_{\text{C}_6} P_{\text{PP}}^3 + k_2 P_{\text{C}_9} P_{\text{PP}}^2 + k_3 P_{\text{C}_{12}} P_{\text{PP}} \quad (\text{II-15})$$

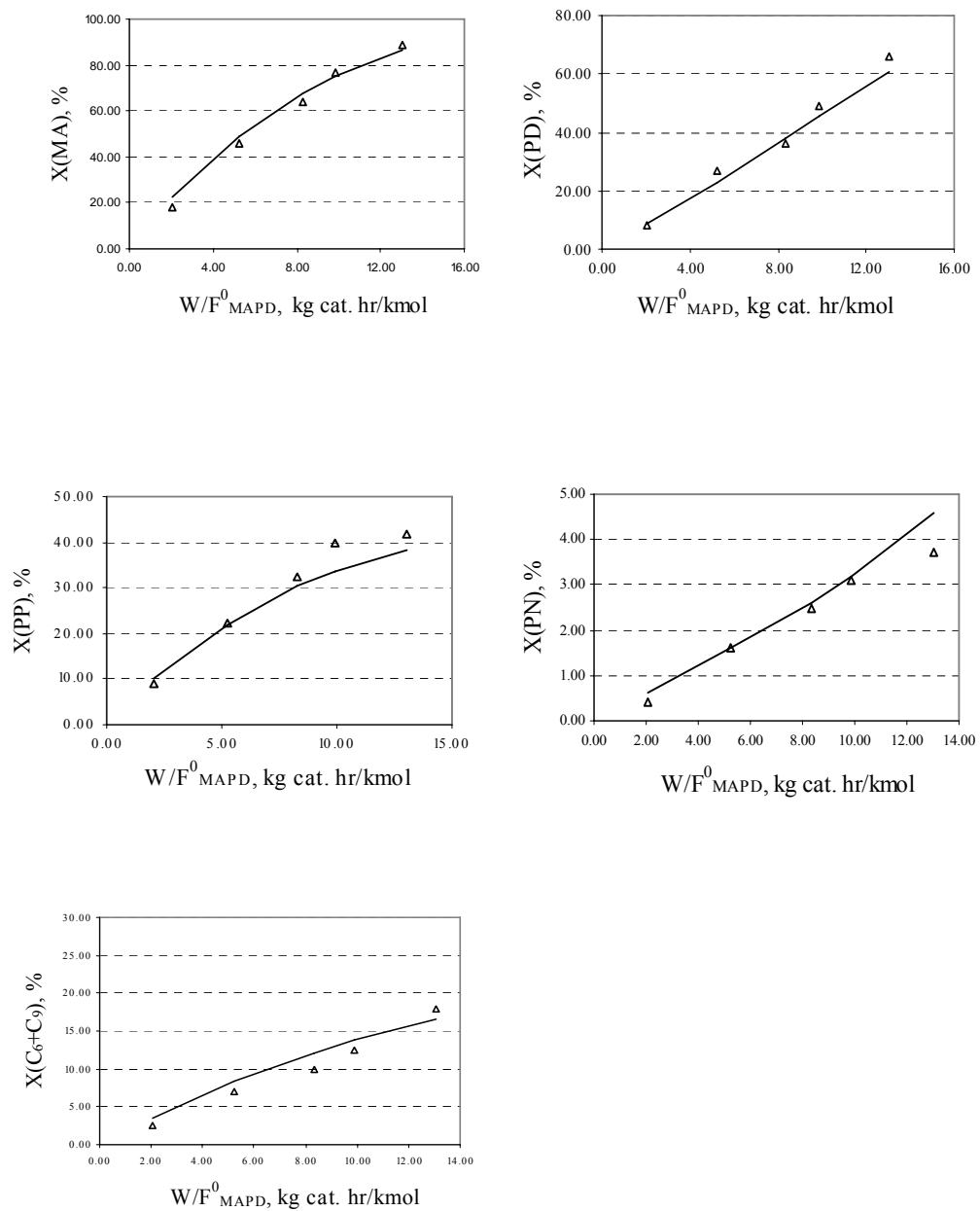


**Figure II-8.** Comparison of experimental and simulated conversions as a function of space time at 70 °C. ( $\Delta$ : EXP; Solid line: CAL).

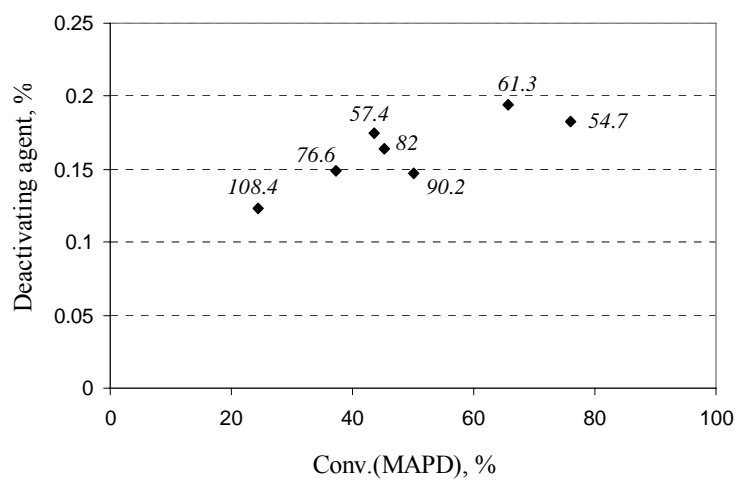


**Figure II-9.** Dependence of content of deactivating agent of the catalyst on conversion, moles of MAPD fed per kg cat (shown inside Fig) and molar ratio  $H_2/$ MAPD at 80 °C.  $H_2/$ MAPD = 1.5, except for point at  $\Sigma F^\circ_{MAPD}/W = 57.4$  for which ratio = 1.1 and point at  $\Sigma F^\circ_{MAPD}/W = 82$  for which ratio = 1.8.

Because the amount of  $C_9$  and  $C_{12}$  is so small,  $r_C^0$  was reduced to  $k_1 P_{C_6} P_{PP}^3$ . The effect of the deactivating agent on the main reaction as well as on its own formation was expressed in terms of a deactivation function,  $\Phi_i$ , multiplying the corresponding rates at zero deactivation. Froment studied the kinetics of catalyst deactivation in hydrocarbon transformation reactions and justified the use of an exponential deactivation function. An exponential function in terms of the content of the real deactivating agent,  $C$ , not of time, was used. That establishes a link between the deactivation and the operating conditions, but requires a rate equation for the formation of the deactivating agent.

Referring to Scheme 1 the rate equations for the main reaction can be written in the presence of deactivation

$$r_i = r_i^0 \Phi_i = r_i^0 \exp(-\alpha_i C_C) \quad i=1,2 \dots 7 \quad (\text{II-16})$$

The rate of formation of the deactivating agent (II-15) becomes

$$r_C = r_C^0 \exp(-\alpha_C C_C) = A_C \exp(-E_C/RT) P_{C_6} P_{PP}^3 \exp(-\alpha_C C_C) \quad (\text{II-17})$$

In the above equation  $C_C$  is written in terms of the amount of carbon per unit weight of catalyst. The amount of deactivating agent was determined by combustion at the end of the run, as if it were coke.

When the catalyst deactivates in a point in the reactor, the conversion in that point is affected. Consequently, the conversion profile is modified with time and the reactor is operating in non-steady state conditions. The continuity equations for component  $i$  and the evolution with time of the content of deactivating agent of the catalyst,  $C_C$ , can be written



$$\left\{ \begin{array}{l} \frac{\partial F_i}{\partial t} + \frac{F_t M_m}{\varepsilon \rho_g \Omega} \frac{\partial F_i}{\partial Z} = \frac{F_t M_m \rho_B R_i}{\varepsilon \rho_g} \\ \frac{\partial C_C}{\partial t} = r_C \end{array} \right. \quad (\text{II-18})$$

If the deactivation is not too fast the term  $\frac{\partial F_i}{\partial t}$  can be neglected.

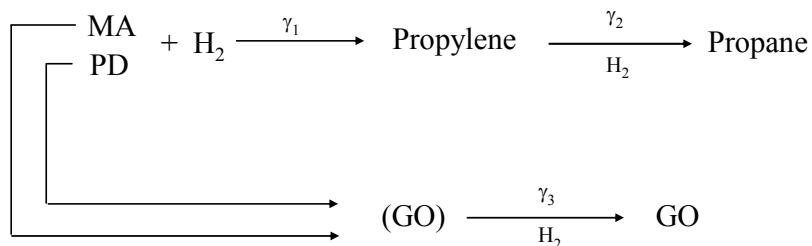
### II.3.6.3 Estimation of the Deactivation Parameters

It follows from Scheme 1 that accounting for the deactivation introduces 10 deactivation parameters for the hydrogenations and oligomerizations: the  $\alpha_i$  ( $i=1, 2, \dots, 7$ ) in (II-16) and  $\alpha_C$  in (II-17) as well as the frequency factor  $A_C$  and the activation energy  $E_C$  in the rate equation for the formation of the deactivating agent. The content of the deactivating agent is available at the end of run so that the objective function not only includes the residual sum of squares of each component-response during the run but also that of the deactivating agent at the end of each run. The number of runs used for the estimation of the deactivation parameters amounts to 21 with each response MA, PD, PP, PN,  $C_6$ ,  $C_9$  taken every hour and  $C$  at the end of the run (Figure II-9). The values of the kinetic parameters derived from the estimation based upon the initial rate data were fixed in the present estimation. The plots of the experimental and simulated values as a function of space time at different temperatures accounting for the deactivation are similar to those of Figure II-8 and are not shown here. The model provides a good fit of the experimental data.

### II.3.7 Simulation of an Industrial Hydrogenation Unit

The selective hydrogenation process to be simulated operates in the gas phase and is carried out in a fixed bed adiabatic reactor. The reaction is very exothermic and CO is added industrially to the feed when the catalyst is fresh, in order to moderate its activity. The catalyst is slowly deactivated in this process, due to oligomer formation with  $n_C > 12$ . To compensate for the loss of catalyst activity and maintain satisfactory yields, the reactor temperature needs to be increased correspondingly, and sometimes  $H_2$ /MAPD and space time also need to be adjusted during the run. When the catalyst has lost too much of its activity, it needs to be regenerated by careful combustion to avoid excessive temperature that could damage the catalyst.

The effect of addition of CO at the start of the run was accounted for by multiplying the rate equations for the hydrogenation by a factor  $\exp(-\gamma_{CO}P_{CO})$ . The  $\gamma_{CO}$  is different for the various reactions so that there are three different  $\gamma_{CO}$ , i.e.,  $\gamma_1$ ,  $\gamma_2$  and  $\gamma_3$ , which correspond to MAPD hydrogenation, propylene hydrogenation and GO formation reaction, respectively.



Scheme II-4. Definition of parameters expressing the effect of CO on the various reactions.

Because internal diffusion limitations are negligible with the egg-shell catalyst a pseudo- homogeneous model with plug flow was used to simulate the industrial adiabatic reactor. An energy equation needed to be added to (II-23)

$$\frac{\sum_{i=1}^N F_i c_{pi}}{\Omega} \frac{\partial T}{\partial Z} + \varepsilon \sum_{i=1}^N C_i c_{pi} \frac{\partial T}{\partial t} = [\sum_{j=1}^R r_j (-\Delta H) \Phi_j] \rho_B \quad (\text{II-19})$$

with initial and boundary conditions:

$$C_C = 0, \text{ at } t=0, \text{ all } Z$$

$$F_i = F_i^0 \text{ and } T = T_0, \text{ at } Z=0, \text{ all } t, i = 1, 2, \dots, 6$$

The continuity equations and the energy equation were integrated simultaneously with respect to  $t$  (run length) and  $Z$  (reactor length). The history of the unit over 6360 hr

was accounted for in the calculation of the amount of deactivating agent,  $C_C$ , using the rate equation for its formation and accounting for its deactivation.

The calculated conversions and selectivities are plotted in Figure II-10 as a function of bed length. The agreement with the industrial exit conversions is excellent. It can be seen that MA and PD are completely converted after 10% of the total bed length already. The industrial reactor is oversized in order to compensate for catalyst deactivation. It is also observed that the conversion into propylene reaches a maximum at about 10% of bed length, beyond which it decreases because of hydrogenation into propane. The oversizing significantly penalizes the propylene production of the hydrogenation process.

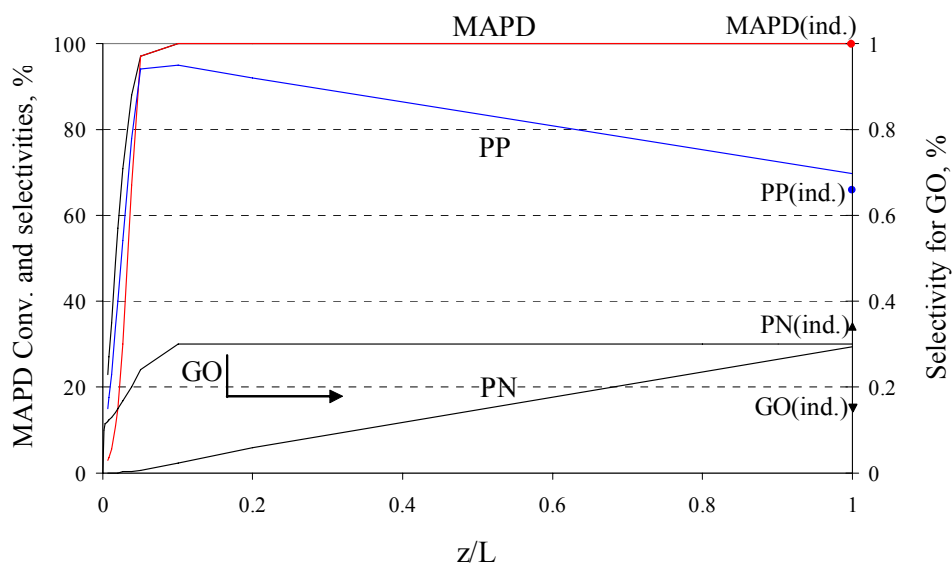


**Figure II-10.** Conversions of MAPD, selectivities for PP, PN and GO as a function of catalyst bed length in an industrial adiabatic reactor after 6360 hrs (Points: industrial results). Process conditions: PD-content of feed (wt%): 0.855%; MA(wt%): 1.319%;  $H_2$ /MAPD(molar ratio): 2.37;  $T(\text{in})$ : 331.3 K; exit  $T(\text{simulated})$ : 383.8 K; exit  $T(\text{ind.})$ : 378 K.

## **CHAPTER III**

### **HYDROGEN PRODUCTION VIA THE DEHYDROGENATION OF HYDROCARBONS**

#### **III.1 Literature Review**

A hydrogen economy is proposed to solve the ill effects of using hydrocarbon fuels in transportation, and other end-use applications where the carbon is released to the atmosphere.<sup>61, 62</sup> In the current economy, the transportation of people and goods is fueled primarily by petroleum, refined into gasoline, jet fuel, and diesel. However, the burning of these hydrocarbon fuels causes the emission of greenhouse gases and other pollutants. Furthermore, the supply of hydrocarbon resources in the world is limited, and the demand for hydrocarbon fuels is increasing, particularly in China, India and other developing countries.

In a hydrogen economy, hydrogen fuel would be manufactured from some primary energy sources and used as a replacement for hydrocarbon-based fuels for transportation. The hydrogen would be utilized either by direct combustion in internal combustion engines or as fuel in proton exchange membrane fuel cells. The primary energy source can then become a stationary hydrogen plant which can use renewable, nuclear or coal fired energy sources, easing the pressure on finite liquid and gas hydrocarbon resources. There is no carbon dioxide emission at the point of use. With suitable primary energy

sources and emission control technology at the centralized hydrogen production plant, the emissions of greenhouse gases and other pollutants can be reduced or eliminated.

Fuel cells are an important enabling technology for the hydrogen economy and have the potential to revolutionize the way to power the world, offering cleaner, more-efficient alternatives to the combustion of gasoline and other fossil fuels.<sup>63-71</sup> Fuel cells have the potential to replace the internal combustion engine in vehicles and provide power in stationary and portable power applications because they are energy-efficient, clean, and fuel-flexible. Currently, fuel cells are more expensive to produce than common internal combustion engines, but are becoming cheaper as new technologies and production systems are developed.

### **III.1.1 Working Principle of Fuel Cells**

A fuel cell is an electrochemical energy conversion device, which combines a fuel, e.g. hydrogen, methanol, etc., and oxygen to produce a direct current. The typical design is based on: an anode, to which the fuel is supplied, a cathode, to which the oxidant is supplied, and an electrolyte, which allows the flow of ions, but not electrons and reactants, from the anode to the cathode. The net chemical reaction is exactly the same as if the fuel were burnt, but by spatially separating the reactants, the fuel cell intercepts flow of electrons from the anode to the cathode and diverts it for uses in an external circuit. Figure III-1 illustrates how a standard Fuel Cell works.

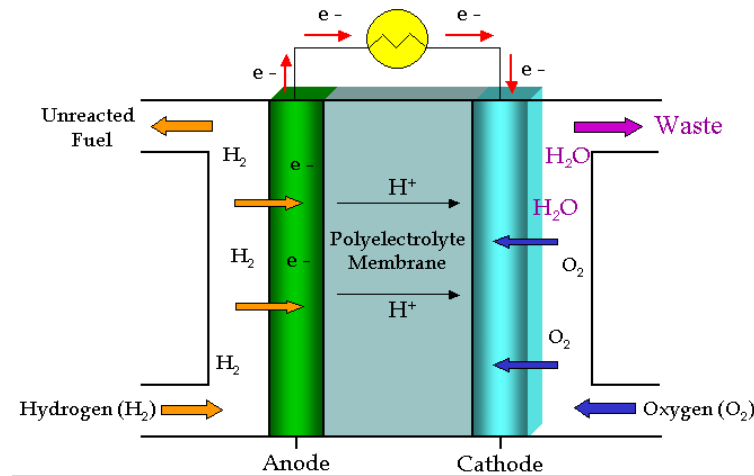


Figure III-1 Schematic diagram of a PEM fuel cell.

### III.1.2 Types of Fuel Cells

There are several different types of fuel cells, each using a different chemistry. Fuel cells are usually classified by their operating temperature and the type of electrolyte they use. Some types of fuel cells work well for use in stationary power generation plants. Others may be useful for small portable applications or for powering cars. The main types of fuel cells include:

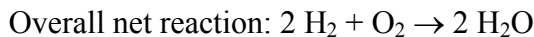
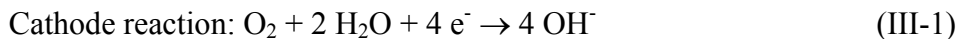
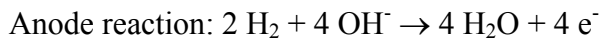
#### III.1.2.1 Proton Exchange Membrane Fuel Cell

Proton Exchange Membrane Fuel Cells (PEMFC) are believed to be the best type of fuel cell as the vehicular power source to eventually replace the gasoline and diesel internal combustion engines. PEM fuel cells use a solid polymer membrane as the



electrolyte. This polymer is permeable to protons when it is saturated with water, but it does not conduct electrons.

The fuel for the PEMFC is hydrogen and the charge carrier is the hydrogen ion. At the anode, the hydrogen molecule is split into protons and electrons. The protons permeate across the electrolyte to the cathode while the electrons flow through an external circuit and produce electric power. Oxygen, usually in the form of air, is supplied to the cathode and combines with the electrons and the protons to produce water. The reactions at the electrodes are as follows:



The PEMFC has a high power density and a relatively low operating temperature. The low operating temperature means that it does not take very long for the fuel cell to warm up and begin generating electricity. These characteristics make the PEMFC the top candidate for automotive power applications.

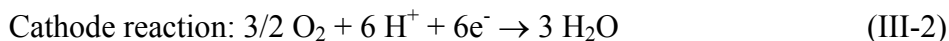
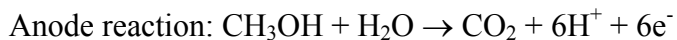
Other advantages result from the electrolyte being a solid material, compared to a liquid. The sealing of the anode and cathode gases is simple with a solid electrolyte, and therefore, less expensive to manufacture. The solid electrolyte is also more immune to difficulties with orientation and has less problem with corrosion, compared to many of the other electrolytes, thus leading to a longer cell and stack life.

One of the disadvantages of the PEMFC for some applications is that the operating temperature is low. Temperatures near 100°C are not high enough to perform useful

cogeneration. Also, since the electrolyte is required to be saturated with water to operate optimally, careful control of the moisture of the anode and cathode streams is important.

### III.1.2.2 Direct-Methanol Fuel Cell

The direct-methanol fuel cell (DMFC) is similar to the PEMFC in that the electrolyte is a polymer and the charge carrier is the hydrogen ion (proton). However, the liquid methanol is oxidized in the presence of water at the anode generating CO<sub>2</sub>, hydrogen ions and the electrons that travel through the external circuit as the electric output of the fuel cell. The hydrogen ions travel through the electrolyte and react with oxygen from the air and the electrons from the external circuit to form water at the cathode completing the circuit.



These cells have been tested in a temperature range from about 50°C-120°C. This low operating temperature and no requirement for a fuel reformer make the DMFC an excellent candidate for very small to mid-sized applications, such as cellular phones and other consumer products, up to automobile power plants. One of the drawbacks of the DMFC is that the low-temperature oxidation of methanol to hydrogen ions and carbon dioxide requires a more active catalyst, which typically means a larger quantity of expensive platinum catalyst is required than in conventional PEMFCs.

One other concern driving the development of alcohol-based fuel cells is the fact that methanol is toxic. Therefore, some companies have embarked on developing a Direct Ethanol Fuel Cell (DEFC). The performance of the DEFC is currently about half that of the DMFC, but this gap is expected to narrow with further development.

### **III.1.2.3 Alkaline Fuel Cell**

Alkaline fuel cells (AFC) use an electrolyte that is an aqueous solution of potassium hydroxide (KOH) retained in a porous stabilized matrix. The concentration of KOH can be varied with the fuel cell operating temperature, which ranges from 65°C to 220°C. The charge carrier for an AFC is the hydroxyl ion that migrates from the cathode to the anode where it reacts with hydrogen to produce water and electrons. Water formed at the anode migrates back to the cathode to regenerate hydroxyl ions. Therefore, the chemical reactions at the anode and cathode in an AFC are the same as that of PEMC

One characteristic of AFCs is that they are very sensitive to CO<sub>2</sub> that may be present in the fuel or air. The CO<sub>2</sub> reacts with the electrolyte, poisoning it rapidly, and severely degrading the fuel cell performance. Therefore, AFCs are limited to closed environments, such as space and undersea vehicles, and must be run on pure hydrogen and oxygen.

### **III.1.2.4 Phosphoric Acid Fuel Cell**

The Phosphoric Acid Fuel Cell (PAFC) uses an electrolyte that is phosphoric acid (H<sub>3</sub>PO<sub>4</sub>). The ionic conductivity of phosphoric acid is low at low temperatures, so PAFCs are operated at the upper end of the range 150°C–220°C. The charge carrier in

this type of fuel cell is the hydrogen ion. The set of reactions in the fuel cell are the same as that of PEMFC. The PAFC operates at greater than 40% efficiency in generating electricity. In addition, CO<sub>2</sub> does not affect the electrolyte of cell performance and can therefore be easily operated with reformed fossil fuel. These advantages make PAFC a good candidate for stationary applications. Typical installations include buildings, hotels, hospitals, and electric utilities.

#### **III.1.2.5 Molten Carbonate Fuel Cell**

Molten Carbonate Fuel Cells (MCFC) operate at very high temperature of 650 °C. At these high operating temperatures the fuel cell acts as its own reformer. The electrolyte here is molten carbonate salt. These fuel cells require carbon dioxide in the oxidant stream to regenerate the carbonate. The main application areas of these fuel cells are large scale and stationary electricity production for utility power generation. These cannot be used for transportation purposes because of their bulk, thermal cycling, difficult start-up and complex control requirements.

#### **III.1.2.6 Solid Oxide Fuel Cell**

The electrolyte in Solid Oxide Fuel Cell (SOFC) is a thin, solid ceramic material (solid oxide) that is conductive to oxygen ions (O<sup>2-</sup>). The charge carrier in the SOFC is the oxygen ion (O<sup>2-</sup>). Operating temperature is around 1000 °C. Internal reforming is one of the main advantages of using SOFC. High operating temperature causes slow start up

and also start up/shut down cycles are stressful to cell integrity. SOFC use nickel as a catalyst and have a very narrow operating temperature range.

### **III.1.3 Onboard Hydrogen Storage**

Cars that run on PEMFC with hydrogen fuel still fail to compete with traditional gasoline vehicles. One of the biggest hurdles remains finding a material capable of storing enough hydrogen onboard for a vehicle to drive over 300 miles on a full tank without adding significant weight or volume relative to a petrol car. Specifically, 5-13 kg H<sub>2</sub> is required to propel a highly fuel efficient automobile for 300 miles and must fit into a space comparable to a conventional gasoline tank. Hence, there is a lot of ongoing research on developing novel methods for hydrogen storage. Hydrogen can be produced from hydrogen rich fuels at plants and then distributed to the local fueling stations. In such a scenario we need to develop an onboard hydrogen storage system which supplies the hydrogen.<sup>72-73</sup> Otherwise we can miniaturize the hydrogen plant on a vehicle to produce hydrogen through *in situ* generation and then supply this hydrogen when it is needed.

#### **III.1.3.1 Gaseous and Liquid Hydrogen Storage**

Although molecular hydrogen has excellent energy density on a mass basis, as a gas at ambient conditions it has poor energy density by volume due to its low molecular weight. As a result, if it is to be stored and used as fuel onboard the vehicle, hydrogen must be pressurized or liquefied to provide sufficient driving range. The energy density

of gaseous hydrogen can be improved by storing hydrogen at high pressures. This requires material and design improvements in order to ensure tank integrity. Achieving higher pressures necessitates greater use of external energy to power the compression. Volumetric capacity, high pressure and cost are thus key challenges for compressed hydrogen tanks.

The energy density of hydrogen can be improved by storing hydrogen in the liquid state.<sup>74</sup> Liquid hydrogen is widely used today for storing and transporting hydrogen. Liquid hydrogen tanks can store more hydrogen in a given volume than compressed gas tanks. The volumetric capacity of liquid hydrogen is 0.070 kg/L, compared to 0.030 kg/L for 10,000 psi gas tanks. However, the issues with liquid hydrogen tanks are hydrogen boil-off, the energy required for hydrogen liquefaction and tank cost. The liquefaction process, involving pressurizing and cooling steps, is energy intensive. Storage tanks must also be well insulated to minimize boil off. Insulation for liquid hydrogen tanks is usually expensive and delicate. It also reduces system gravimetric and volumetric capacity.

Storing hydrogen onboard in compressed gas cylinders has been investigated by many automobile manufacturers. Unfortunately, neither highly compressed hydrogen gas nor liquefied hydrogen is likely to be capable of sufficient volumetric density to meet the mileage target. The limitation is due to specifically the very weak intermolecular interactions between hydrogen molecules. Small quadrupole and low polarizability of hydrogen do not provide significant binding through electrostatic, induction or dispersion interactions. Consequently, the van der Waals forces between

two hydrogen molecules are negligible compared with the strength of a hydrogen bond or a chemical bond. Because of the weak intermolecular interactions, the volumetric capacities of both compressed H<sub>2</sub> (40 g l<sup>-1</sup> at 700 bar) and liquid H<sub>2</sub> (70 g l<sup>-1</sup> at 20K) fall far short of the automotive industry's volumetric target.

### **III.1.3.2 Carbon-Based Materials**

Hydrogen can be adsorbed onto certain materials like nanotubes and the adsorbed gas can be released reversibly.<sup>75-76</sup> Single-walled carbon nanotubes were reported as hydrogen storage materials with hydrogen gravimetric capacities in the range of 3-10 wt% at room temperature. However, there has been controversy due to difficulty in reproducing these results. Recent results at NREL show that while no hydrogen storage was observed in pure single-walled carbon nanotubes, roughly 3 wt% was measured in metal-doped nanotubes at room temperature. The room temperature gravimetric capacity measured in carbon nanotubes is below the 2010 hydrogen system target of 6.0 wt% and further improvements must be made. In addition, low cost, high volume manufacturing processes must be developed for single-walled carbon nanotubes in order for them to be economically viable in vehicular applications.

### **III.1.3.3 Metal Hydrides**

One way to overcome the volumetric density challenge is chemical hydrogen storage. This covers a broad range of materials but is defined as a process that releases hydrogen

by a chemical reaction. The spent material can then be reprocessed or regenerated off-board.

Metal hydrides have the potential for reversible onboard hydrogen storage. Group A I, II, and III elements, (e.g. Li, Mg, B and Al) form a large variety of metal-hydrogen complexes.  $\text{NaAlH}_4$ <sup>77</sup> and  $\text{LiBH}_4$ <sup>78</sup> can reversibly absorb/desorb hydrogen at moderate temperatures. Recently, a new complex hydride system based on lithium amide has been developed.<sup>79</sup> For this system, the following reversible displacement reaction takes place at 285°C and 1 atm



In this reaction, 6.5 wt% hydrogen can be reversibly stored.

#### **III.1.3.4 Chemical Hydrides**

Chemical hydrides can be used as hydrogen media to generate hydrogen through chemical reactions. The hydrolysis, reforming and dehydrogenation are the most widely employed reactions to extract hydrogen from hydrogen-rich fuel. The spent fuel and byproducts must be removed from the vehicle and regenerated off-board.



### III.1.3.4.1 Hydrolysis Reactions

Hydrolysis reactions involve the oxidation reaction of chemical hydrides with water to produce hydrogen.<sup>80</sup> The reaction of sodium borohydride has been the most studied to date. This reaction is:



The hydride is sensitive to moisture and needs to be stored and transported in an inert stabilizing liquid. The reaction can be carried out on a catalyst in an aqueous medium. The borohydride regeneration reaction must take place off-board. Millennium Cell has reported that their NaBH<sub>4</sub> based hydrogen on demand system possessed a system gravimetric capacity of about 4 wt%.<sup>81</sup> Problems concerning the real application include system volume, weight, and cost.

Another hydrolysis reaction that is being investigated is the reaction of MgH<sub>2</sub> with water to generate H<sub>2</sub>.<sup>82</sup> In this case, particles of MgH<sub>2</sub> are stored in a non-aqueous slurry. However, similar to the sodium borohydride approach, water must also be carried on-board the vehicle and the Mg(OH)<sub>2</sub> must be regenerated off-board.

### **III.1.3.4.2 Reforming of Hydrocarbons**

#### **III.1.3.4.2.1 Steam Reforming (SR)**

Steam reforming of hydrocarbons for hydrogen production has been studied for several decades, mainly for applications in ammonia synthesis, methanol synthesis and for substitute for natural gas applications. Worldwide industrial hydrogen is currently produced at over 41 million tons/yr with 80% of production coming from the steam reforming of natural gas.<sup>83-85</sup> In steam reforming of methane (SMR), the feedstock is first desulfurized to reduce the sulfur levels to below 2 ppmv to protect the SMR catalyst. This desulfurization step is performed at 360 to 400 °C with a Co-Mo or ZnO hydrogenation catalyst to convert the sulfur into H<sub>2</sub>S, which is later removed from the gas via a downstream adsorption step. After desulfurization, steam methane reforming is then carried out at 780 to 900 °C and 25 to 35 atm using an alkali-promoted Ni catalyst supported on alumina. The reaction is



This reaction is highly endothermic and hence requires a substantial energy input. SMR produces the greatest number of hydrogen molecules per molecule of methane. Some of the needed energy can be obtained from combustion of recycled product gases, CO and H<sub>2</sub>, and unconverted CH<sub>4</sub>.

#### **III.1.3.4.2.2 Partial Oxidation Reforming (POX)**

In partial oxidation reforming the feed consists of methane and oxygen.<sup>86-87</sup> Methane can be partially oxidized to syngas with or without a catalyst. When a catalyst is not used

the reaction is usually carried out at temperatures 1300 to 1400 °C and pressures 55 to 80 atm. The reactions that occur include:



The H<sub>2</sub> to CO ratio in the product is usually in the range 1.6 to 1.8. This process takes advantage of the heat generated by reactions (III-6), (III-7), and (III-8). Reaction (III-9) is environmentally attractive as it uses CO<sub>2</sub> as the reactant. It produces, however, the smallest number of hydrogen molecules per molecule of methane. For the catalytic partial oxidation process, the flame temperature is lower, i.e., between 780 and 900 °C, and the pressure is reduced to between 25 and 35 atm. The catalyst is generally similar to or the same as the SMR catalyst, being comprised of nickel. One advantage of POX process is that it does not require a desulfurization step.

#### **III.1.3.4.2.3 Autothermal Reforming (ATR)**

This method is a combination of both the POX and SR methods.<sup>88</sup> When steam and oxygen are mixed with methane and fed to a reactor, the process is generally referred to as autothermal reforming (ATR). POX takes place in the first zone of the reactor. The heat generated by the combustion is used to supply the heat needed for the SMR reaction

in the second zone. Since no external heat source is required, it is called an autothermal reformer.

SMR is more common for industrial hydrogen production and maintains an economic edge over ATR and POX, except for very large installations where ATR becomes more cost effective. However, POX, and to a lesser extent ATR, are more effective for handling diverse hydrogen feedstocks, such as naphtha.

Depending on the application, a water gas shift reactor (WGS) may be needed downstream of the reformer to decrease the CO concentration in the reformer and to improve H<sub>2</sub> production and purity. After the WGS reactors, the CO concentration can be reduced to around 0.5 vol%. Both high temperature (HT) and low temperature (LT) WGS reactions are commercially practiced. The HT WGS reaction uses iron/chrome oxide catalyst and operates in the range of 350 to 500 °C. The LT WGS reaction uses a copper/zinc oxide catalyst and operates in the range of 180 to 250 °C. The WGS reaction proceeds as



#### **III.1.3.4.2.4 H<sub>2</sub> Purification**

The reforming of hydrocarbons produces CO as a by-product and its presence poisons the Pt-based electro-catalysts used in PEM fuel cells. Hydrogen must be purified to be used for PEM fuel cells. Three different hydrogen purification technologies are widely practiced in industry. These include 1) adsorption, both physical and chemical, 2) membranes and 3) cryogenic separation.

Prior to 1980,<sup>89</sup> the CH<sub>4</sub> reforming step was followed by a shift process to convert CO to H<sub>2</sub>. Wet scrubbing, with a weak base such as potassium carbonate or an amine, was then used to remove CO<sub>2</sub>. The remaining CO and CO<sub>2</sub> are sent to a methanation reactor to reduce the carbon oxides to around 50 ppmv. Later on new hydrogen plants were built with PSA units as the main H<sub>2</sub> purification process.<sup>90-91</sup> This eliminated the CO shift reactor and the CO<sub>2</sub> scrubber. PSA units for H<sub>2</sub> purification use layered beds containing 3 to 4 adsorbents to adsorb the impurities in the H<sub>2</sub> stream. Modern Polybed PSA units offer advantages of improved product purity (99-99.99 vol% H<sub>2</sub>) with capital and operating costs comparable to those of wet scrubbing. Cryogenic separation processes are generally used in the production of high purity CO and moderately pure H<sub>2</sub> from syngas.<sup>92</sup> This process is also used to adjust the composition of the syngas for a chemical feedstock unit, especially in the production of ammonia.

While reforming of hydrocarbons are mostly used for large scale industrial production, a detailed understanding of these commercial processes provide an essential basis for guiding further R&D to minimize the reformer for onboard hydrogen production.

#### **III.1.3.4.3 Dehydrogenation of Hydrocarbons**

Another promising technology to store and transport hydrogen is the utilization of dehydrogenation of high hydrogen content organic hydrocarbons. Only hydrogen and dehydrogenated hydrocarbons are formed as the main products in this reaction. The absence of any substantial amount of carbon monoxide eliminates the need to further

purify the hydrogen. So, these hydrocarbons may be used as a H<sub>2</sub> carrier to generate H<sub>2</sub> for fuel cell application without purification. Another advantage of using these liquid hydrocarbons as H<sub>2</sub> storage media is that the present infrastructures such as oil tankers and gas station could also be used for the storage and transportation of the liquid hydrocarbon. The dehydrogenation of cycloalkane is a reversible process. The products, benzene, toluene, naphthalene, etc., can be hydrogenated back to cycloalkanes in specialized gas stations.

#### **III.1.3.4.3.1 Catalysts in the Dehydrogenation of Hydrocarbons**

Different supported metal catalysts have been reported in the literature for the dehydrogenation of cycloalkane to produce hydrogen. The fundamental study on the single crystal catalysts with specific crystal structures can lend us more insights into the design of new catalysts. Somorjai studied the dehydrogenation of cyclohexane over single crystal Sn/Pt(111) and Pt(111)/Sn/K in a vacuum chamber at 573K.<sup>93</sup> The adsorption of tin on Pt(111) decreased the tendency of the surface to deactivate by coke deposition. This was verified directly by the decrease of carbon buildup after reaction with cyclohexane. These results pointed that Sn titrated the high activity, coke-forming defect sites present on Pt(111) or inhibited the formation of highly unsaturated molecules by making the presence of large ensembles of Pt unavailable. In the presence of both tin and potassium the CO TPD suggested an interaction between K and Sn with the formation of a “surface alloy”. Adsorbed potassium decreased the turnover rate of cyclohexane dehydrogenation on Pt and Pt/Sn samples with a monotonic decrease in

activity with increasing potassium coverage. Potassium could possibly decrease the rate of deactivation by site coverage, especially because K has a large ionic radius.

Ichikawa et al. investigated the dehydrogenation of cyclohexane, methylcyclohexane and decalin over activated carbon supported Ni, Pt and Ni-Pt catalysts using a spray pulse mode reactor operating at 287-375 °C.<sup>94, 95</sup> The maximum rate of hydrogen evolution using monometallic Ni catalysts was 8.5 mmol g<sup>-1</sup>cat min<sup>-1</sup> for Ni loading of 20% by weight. A synergistic effect was observed when a small amount of Pt (0.5% wt%) was added to the Ni based catalysts. The hydrogen production was enhanced by 1.5 times as compared to the 20 wt% Ni only catalyst. The dehydrogenation conversions were in the range 25-35% with the hydrogen selectivity above 98.8%. As compared to 0.5 wt% monometallic Pt catalyst, the 20 wt% Ni-0.5 wt% Pt bimetallic catalyst exhibited 60 times higher hydrogen production rates. Selectivity towards dehydrogenation was enhanced by addition of Pt into a Ni/ACC catalyst.

Saito et al. performed dehydrogenation of decalin at 210 °C with carbon supported Pt catalysts in a batch reactor.<sup>96</sup> Hydrogen was removed from the reactor through the condenser. Under liquid film conditions, hydrogen was evolved from decalin much more efficiently than the suspended ones due to the superheated states of dehydrogenation catalyst. The conversions after 2.5 h were in the range 25.4-35.8%. Okada et al. also reported their results for alumina supported Pt-based catalysts in methylcyclohexane dehydrogenation in a fixed bed reactor.<sup>97</sup> This catalyst could generate hydrogen from methylcyclohexane with a conversion of 95% and toluene selectivity above 99.9% at 320 °C.

Recently, Huffman used stacked-cone carbon nanotubes (SC-CNT) as support medium to prepare Pt and Pd catalysts for the dehydrogenation of cyclohexane and methylcyclohexane to produce pure hydrogen.<sup>98</sup> The catalysts exhibited 100% selectivity for conversion of cyclohexane to hydrogen and benzene and methylcyclohexane to hydrogen and toluene. It was reported that a 0.25 wt % Pt/SC-CNT catalyst had approximately the same activity as a commercial 1wt % Pt/Al<sub>2</sub>O<sub>3</sub> catalyst. Transmission electron microscopy showed that the dispersion of the Pt catalyst particles on the SC-CNT support was quite high after 6.5 h of reaction, with particle sizes of 1.5-2 nm. However, the regeneration of the deactivated catalyst with carbon material as a support is a problem, which limited its application.

#### **III.1.3.4.3.2 Reactor Aspect**

The dehydrogenation of cycloalkane is an equilibrium restricted reaction at low temperature. The separation of the products from the reactants allows equilibrium limited reactions to proceed toward completion. Membrane and chromatographic reactors can be useful to achieve such a separation.

Anderson and co-workers investigated the dehydrogenation of cyclohexane on Pt/SiO<sub>2</sub> in a pure membrane reactor, a conventional packed bed reactor, and hybrid membrane reactors consisting of a packed bed reactor segment followed by a membrane reactor segment in the temperature range 190-220 °C.<sup>99</sup> Commercially available alumina membranes were employed for the membrane reactor segment of the hybrid reactor. In this temperature range the dehydrogenation of cyclohexane is



equilibrium restricted. Because of the increase in the number of moles which accompanies the dehydrogenation reaction, dilution of the reactant has the effect of driving the reaction to higher conversions. Dilution is caused by the transport of inert sweep gas from the permeate side of the membrane reactor segment to the retentate stream in counterdiffusion to the product and reactant species leaving the retentate stream. The experimental results reflect the fact that for this application, the dilution effect is much more significant than the effect of product removal through the membrane.

Takeda et al investigated the dehydrogenation of cyclohexane in three kinds of membrane reactor, porous Vycor glass, ceramic sol-gel, and palladium-silver membrane.<sup>100</sup> A double cylindrical-type reactor was used in this study. The inner tube, whose outer diameter was 14 mm, was the membrane, while the outer tube, whose inner diameter was 28 mm, was pyrex glass. The 0.5 wt% Pt/Al<sub>2</sub>O<sub>3</sub> pellet catalyst was packed in the space between the membrane and glass. It was observed that the conversions have exceeded the equilibrium one, 6.4%. Among the membranes used, Pd-Ag is the most selective to remove hydrogen, enabling the Pd-Ag membrane to have better performance. In a membrane reactor, pressure difference significantly affects the conversion. A pseudo equilibrium model was proposed to predict the conversion achieved in the reactor.

The yields of useful products from conventional flow reactors may be limited either by the value of the equilibrium constant or by the consumption of primary products by secondary reactions. By combining in one reactor both catalytic and chromatographic functions and by pulsing the reactants both of these limitations can be removed. The

reverse reaction can be minimized by chromatographically separating the products from each other, while secondary reactions may be reduced by retaining the primary product on the column relative to the reactant pulse. The catalytic dehydrogenation of cyclohexane to benzene has been studied in a gas chromatographic reactor.<sup>101</sup> An enhancement of product yield above equilibrium has been observed and direct evidence for equilibrium displacement was obtained by the observation of a maximum yield at an optimum flow rate.

#### **III.1.3.4.3.3 Kinetics of the Dehydrogenation of Cycloalkane**

Froment studied the kinetics of the dehydrogenation of methylcyclohexane in a tubular reactor on commercial Pt/Al<sub>2</sub>O<sub>3</sub> and Pt-Re/Al<sub>2</sub>O<sub>3</sub> reforming catalysts.<sup>102</sup> The partial substitution of Pt by Re caused drastic changes. Pt/Al<sub>2</sub>O<sub>3</sub> was continuously exposed to a H<sub>2</sub>S/H<sub>2</sub>, molar ratio of 10-5, whereas Pt-Re/Al<sub>2</sub>O<sub>3</sub>, was presulfided only. The inlet partial pressures of methylcyclohexane and hydrogen varied from 0.15 to 1.5 bar and from 4 to 20 bar, respectively. The temperature ranged from 582 to 683 K on Pt/Al<sub>2</sub>O<sub>3</sub>, and from 627 to 719 K on Pt-Re/Al<sub>2</sub>O<sub>3</sub>. It was observed that increasing hydrogen partial pressures caused a decrease of the rate of dehydrogenation on Pt/Al<sub>2</sub>O<sub>3</sub>, but had no effect on the rate of dehydrogenation on Pt-Re/Al<sub>2</sub>O<sub>3</sub>. This different behavior was attributed to a shift of the rate determining step in the reaction sequence. Competitive adsorption by toluene was important only with Pt-Re/Al<sub>2</sub>O<sub>3</sub>. The rate of dehydrogenation was higher on Pt/Al<sub>2</sub>O<sub>3</sub> than on Pt-Re/Al<sub>2</sub>O<sub>3</sub>. The apparent activation energy was 60 kJ/mol higher on Pt-Re/Al<sub>2</sub>O<sub>3</sub> than on Pt/Al<sub>2</sub>O<sub>3</sub>.

In the present study cyclohexane and decalin were first investigated for the dehydrogenation to produce H<sub>2</sub>. Catalysts and operating conditions were optimized. The product in decalin dehydrogenation, naphthalene, is environmentally favorable over benzene, and thus is more applicable for onboard hydrogen production. A rigorous kinetic model was proposed and is a valid tool for the scale up of this process and a guide for operation.

Jet fuel is another possible feedstock for the extraction of hydrogen for fuel cell applications. So far few efforts have been reported in the literature on steam/autothermal reforming of jet fuel to produce hydrogen. Sung et al. reported the autothermal reforming of Jet A surrogate for use with solid-oxide fuel cells in aerospace application.<sup>103</sup> Key operating variables such as inlet temperature, operating pressure, steam to carbon ratio and oxygen to carbon ratio were investigated in their research to optimize the reformer performance. Aicher et al. investigated autothermal reforming of Jet A.<sup>104</sup> The performance of the reformer was investigated at different operating conditions. The influence of sulphur compounds in the fuel on reforming behavior, as well as the poisoning effect of formed hydrogen sulphide on the fuel cell, were also addressed. Different desulphurization methods were examined. The selective adsorption for removing sulphur (SARS) process seemed to be promising for mobile application. Again, autothermal reforming of Jet A has CO separation problems like steam/autothermal reforming of natural gas and other fuels. Further, the operation temperature is high in autothermal reforming, which also restricted the mobility of the reformer. If the dehydrogenation of Jet fuel does not compromise fuel properties, the

hydrogen produced will be an extra gain. For the first time we explored the possibility of the dehydrogenation of Jet A to produce hydrogen.

## **III.2 Experimental**

### **III.2.1 Catalyst Preparation**

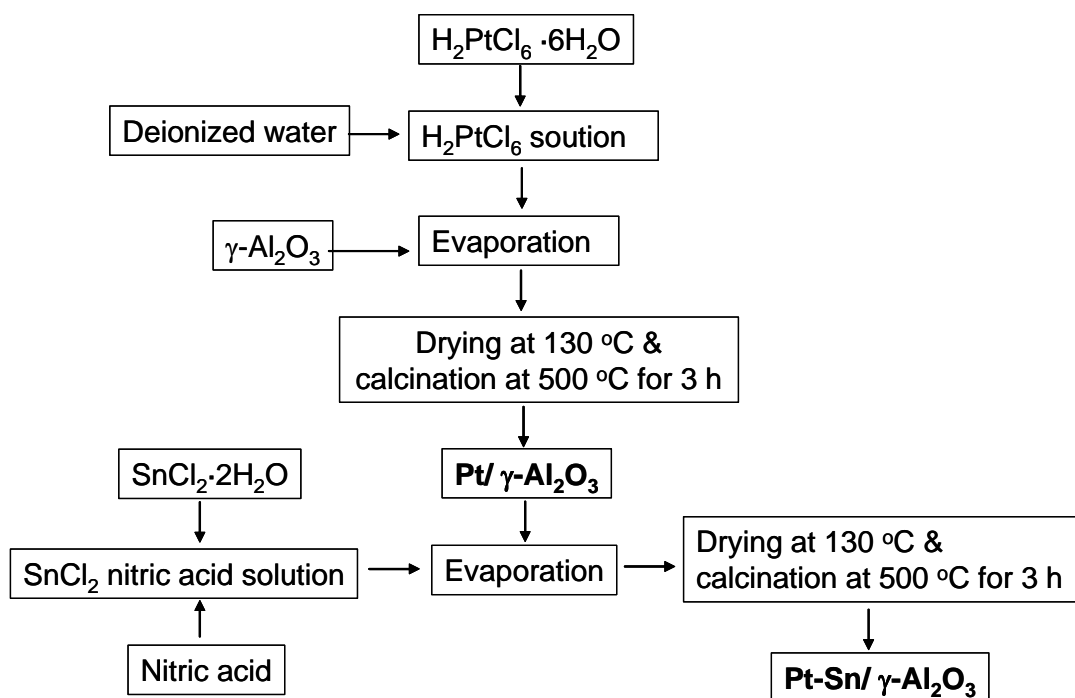
#### **III.2.1.1 Pt/ $\gamma$ -Al<sub>2</sub>O<sub>3</sub> and Pt-Sn/ $\gamma$ -Al<sub>2</sub>O<sub>3</sub> Catalysts**

The catalysts used in the dehydrogenation of cycloalkanes are supported Pt catalysts. Three different kinds of high surface area supports such as  $\gamma$ -alumina, silica and activated carbon were used for the preparation of the catalyst.<sup>105</sup> They were prepared by evaporative impregnation method (Figure III-2). Pt/alumina catalyst was prepared by adding a certain amount of aqueous H<sub>2</sub>PtCl<sub>6</sub> solution to the support, and impregnated at 80 °C for 2 h. The resulting Pt/support catalyst was dried in air at 130 °C, then calcined at 500 °C for 3 h. Sn was added to the supported Pt catalyst by evaporative impregnation of a certain amount of nitric solution of tin chloride at 80 °C for 2h, dried at 130 °C, and then calcined at 500 °C for 3h. Prior to reaction, the catalyst was activated first by removing water at 500 °C for 2 h, followed by reduction at 500 °C with hydrogen.

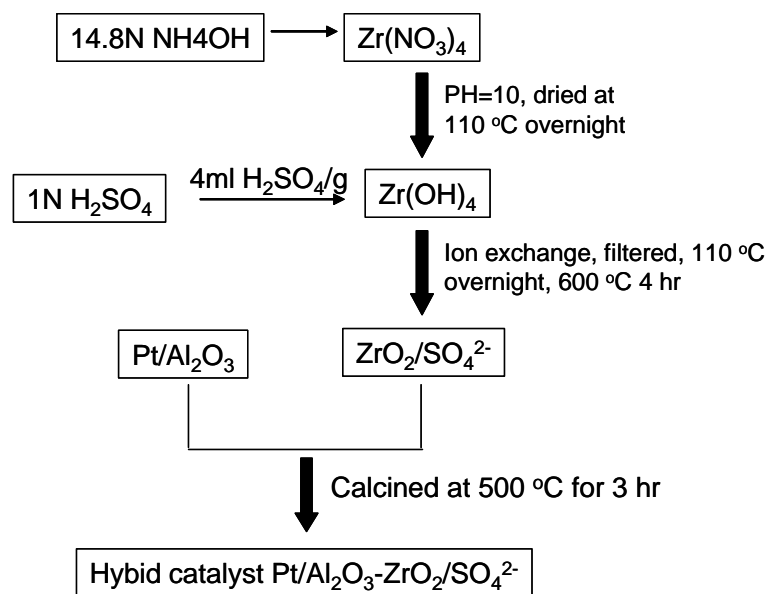
#### **III.2.1.2 Pt/ $\gamma$ -Al<sub>2</sub>O<sub>3</sub> -ZrO<sub>2</sub>/SO<sub>4</sub><sup>2-</sup> Hybrid Catalyst**

Figure III-3 shows the procedure to prepare Pt/ $\gamma$ -Al<sub>2</sub>O<sub>3</sub> -ZrO<sub>2</sub>/SO<sub>4</sub><sup>2-</sup> hybrid Catalyst. The sulfated zirconia was prepared according to the standard protocol.<sup>106</sup> Zirconium nitrate was precipitated with 14 N ammonium nitrate at PH=10. The precipitate was filtered, washed, and then dried overnight at 110 °C. Zirconium hydroxide was then ion

exchanged with 1N sulfuric acid and filtered. The solid was dried overnight at 110 °C and calcined at 600 °C in air for 3 h. The hybrid catalyst was made by physically mixing 0.9 wt% Pt/alumina and sulfated zirconia in mass ratio of 6 to 4, and then pelletized to particle size in the range 0.15-0.5 mm. The catalyst was loaded into the reactor, and activated by calcination in the air at 500 °C for 12 hr and subsequent reduction with hydrogen at 300 °C.



**Figure III-2.** Preparation of  $\text{Pt}/\gamma\text{-Al}_2\text{O}_3$  and  $\text{Pt-Sn}/\gamma\text{-Al}_2\text{O}_3$  catalysts.



**Figure III-3.** Preparation of  $\text{Pt}/\gamma\text{-Al}_2\text{O}_3\text{-ZrO}_2/\text{SO}_4^{2-}$  hybrid catalyst.

## **III.2.2 UHV bulb Reactor Setup**

### **III.2.2.1 Pumping System**

The dehydrogenation of cyclohexane over Pt (111) single crystal was investigated in an ultrahigh vacuum (UHV) bulb reactor, as shown in Figure III-4. The pumping system consists of two pumps which enable reaching a base pressure  $< 1.0 \times 10^{-8}$  Torr in the bulb reactor. The forepump is capable of evacuating the system down into the millitorr pressure range. At that pressure the turbomolecular pump, with a 170L/sec pumping speed can be turned on and pressures as low as  $10^{-8}$  Torr can be achieved.

### **III.2.2.2 Sample Mounting**

The sample was mounted in the UHV bulb reactor as depicted in Figure III-5. The Pt (111) single crystal measured 0.92 cm in diameter by 0.11 cm thick. It was mounted into the bulb reactor by spot welding a tantalum heating wire to the peripheral of the sample, then attached to the copper legs of the sample holder. The sample was heated resistively and the temperature was monitored by a W-5%Re/W-26%Re thermocouple spot welded to the back center of the crystal face. Reference gage I was used to monitor the pressure change during the reaction. Prior to the reaction, the sample was cleaned by CO oxidation at 427 °C for half an hour, and then annealed at 650 °C for 2 h.

### III.2.2.3 Operating Procedure

The operating cycle consists of reactor (un)installation, evacuation and reaction. The followings are highlights of the operation and valve status in each stage.

Stage 1: (Un)install reactor

Operation: close valves V1, V3, V4 and V9, then (un)install reactor.

Valve status:

Open: V5, V7, V8, V12

Close: V1, V2, V3, V4, V6, V9, V10, V11.

Stage 2: Evacuation

Operation: Open V4 first, then open V2 slowly. When the readings of gages (II) and (I) decreased to 0, close V2, then open V1 and V3.

Valve status:

Open: V1, V3, V4, V5, V7, V8, V12

Close: V2, V6, V9, V10, V11

Stage 3: Reaction

Operation: Open V9, close V3 and V7.

Valves status:

Open: V1, V4, V5, V8, V9

Close: V2, V3, V6, V7, V10, V11, V12

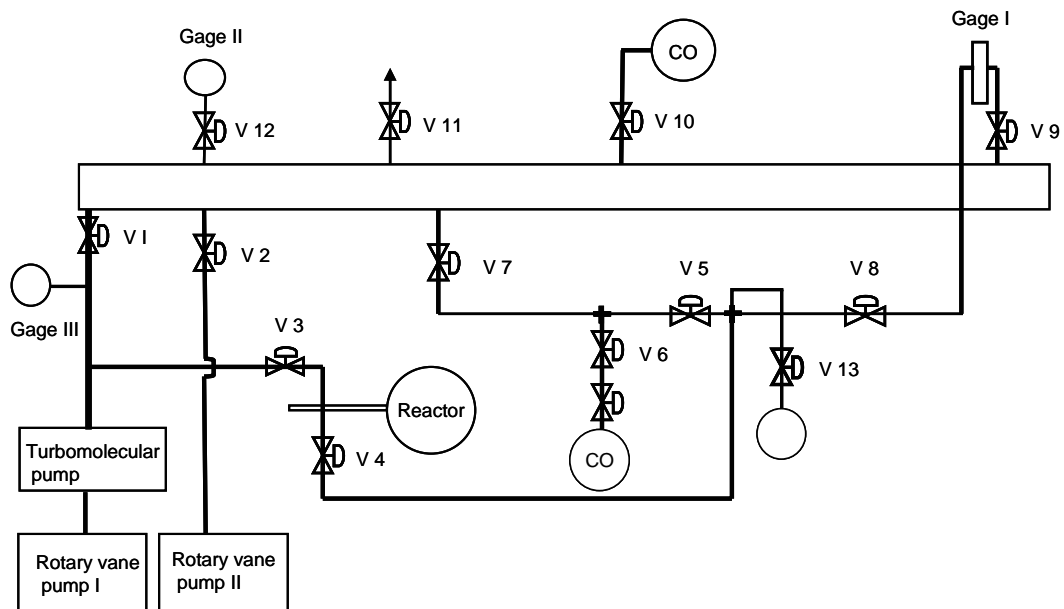


### III.2.2.4 Volume Calibration

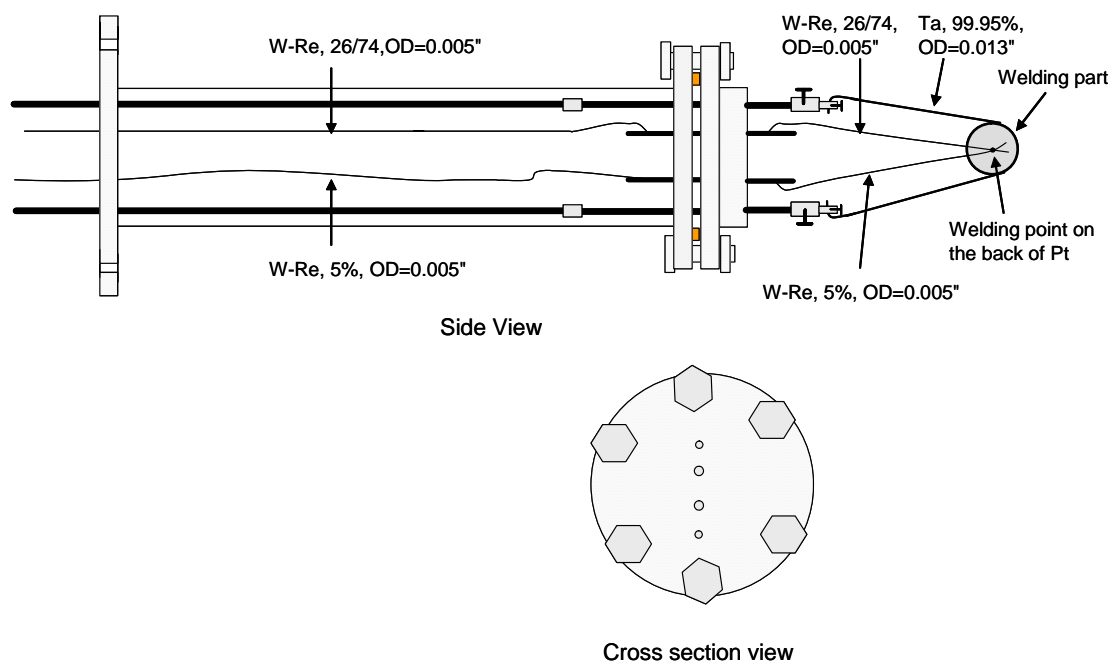
The volume of each segment in the UHV setup was calibrated in Table III-1 below by gas expansion method.

Table III-1. The calibration of the volume of each segment in the UHV bulb reactor by gas expansion

Segment	Volume (ml)
V4-V5	91.2
V4-V7	124.9
V5-V7	33.7
V4-V2	1278.2
V7-V2	1153.2
V2-V3	3668.4
V3-V4	2390.2



**Figure III-4.** The UHV bulb reactor setup for the dehydrogenation of cyclohexane on Pt(111).



**Figure III-5.** Schematics of the sample holder used in the UHV bulb reactor for the dehydrogenation of cyclohexane over Pt(111).

### III.2.3 Fixed-Bed Reactor Setup

The dehydrogenations of cyclohexane and decalin were carried out over supported Pt catalyst in a fixed bed reactor at atmospheric pressure (Figure III-6). Gas feeds, consisting of H<sub>2</sub>, N<sub>2</sub>, and air for regeneration of the deactivated catalyst, were controlled by gas mass flow controllers. The flow rate of the liquid was controlled by a reciprocal pump. The liquid feed was vaporized in the mixing chamber, and mixed with other gas streams before flowing to the reactor. The reactor is 1.2 cm ID stainless steel tube, and is heated by a tube furnace. Like in the selective hydrogenation reactor, the reactor temperature profile was also monitored by a sliding thermocouple, mounted inside the reactor along the reactor axis. The reaction products were analyzed by a HP 5890 online gas chromatography equipped with thermal conductivity (TC)- and flame ionization (FI)- detectors.

### III.2.4 Gas Chromatography

The Chromatographic separation involves the use of a stationary phase and a mobile phase. The components of a gas mixture carried out by the mobile phase in the column pass through the column at different rates depending on their separation factor, determined by various chemical and physical properties and their interaction with a specific column packing, i.e. stationary phase. Columns were used to achieve the necessary chromatographic separation. HP-PLOT/alumina and HP-5 capillary columns with a flame ionization detector were used to analyze hydrocarbon components in the dehydrogenation of cyclohexane and decalin, respectively. The 13X packed column

connected to a thermal conductivity detector was used to detect H<sub>2</sub>. Ar was used as the carrier gas and the flow rate was maintained at 30 ml/min. N<sub>2</sub> was fed into the feed stream as an internal standard to calibrate H<sub>2</sub>. For accurate GC analysis, the transfer line from the reactor exit to the GC and the sampling valve need to be heat insulated to keep the reactor effluent in the gas state. In the dehydrogenation of Jet A, only H<sub>2</sub> was analyzed due to the complex nature of the feed and product.

### **III.3 Results and Discussion**

#### **III.3.1 Test of the UHV Bulb Reactor by CO Oxidation on Pt (111)**

The oxidation of CO by O<sub>2</sub> on group VIII metal catalysts has been the subject of a large body of ultra high vacuum (UHV) surface science and high pressure catalysis work due to its importance in pollution control. The relative simplicity of this reaction makes CO oxidation an ideal model system of a heterogeneous catalytic reaction. Currently, the removal of CO as CO<sub>2</sub> from automobile exhaust is accomplished by catalytic converters which employ a supported Pt, Pd, and Rh catalyst. This has led to numerous studies of the kinetics of this reaction on supported metal catalysts and single crystal catalysts. In this study the CO oxidation was performed on Pt(111) in the bulb reactor.

Research grade CO (99.99%) and O<sub>2</sub> (99.995%) were supplied by Matheson. CO was further purified before use by slowly passing it through a molecular sieve trap at 77 K. The reactor was charged with 49.9 Torr of CO and 24.9 Torr of O<sub>2</sub>. Then the single crystal was quickly heated up to 520 K for the reaction. As two moles of CO react with one mole of O<sub>2</sub> to form two moles of CO<sub>2</sub>, the decrease of the total pressure is used as an

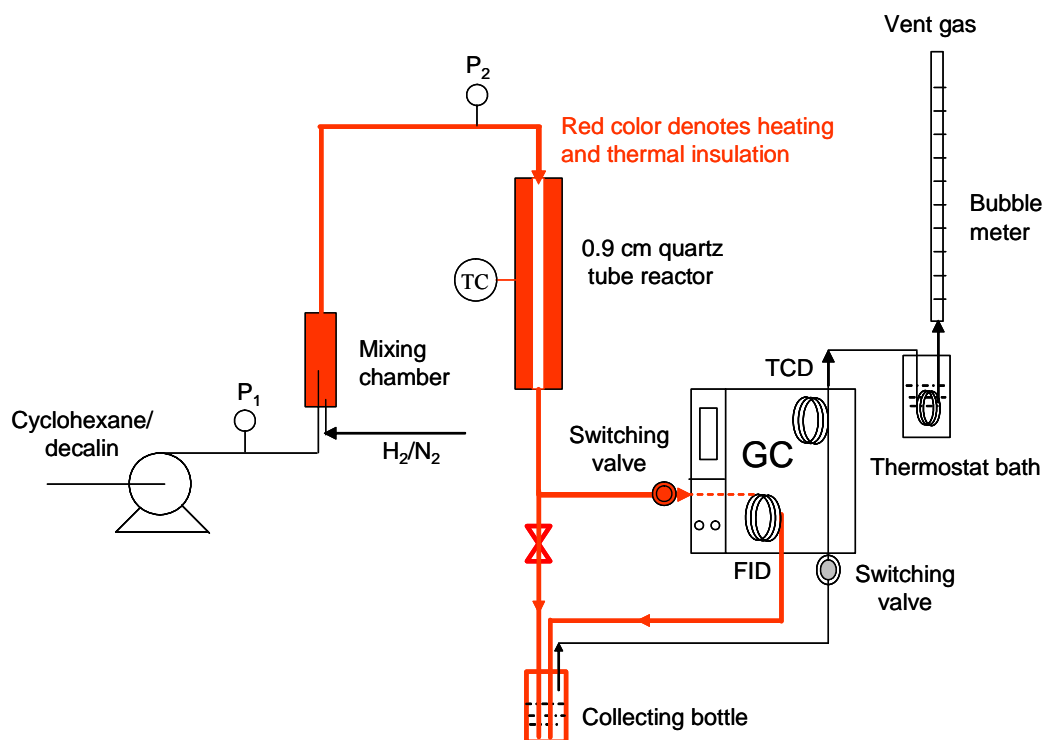


**Figure III-6.** Fixed bed experimental setup for the dehydrogenation of cyclohexane, decalin, and Jet A to produce H<sub>2</sub>.

index of the extent of the reaction. The maximum reaction time at 520 K was set to maintain a differential conversion of the reactant CO. After reaction at 520 K, the temperature of Pt (111) was quickly heated up to 540 K for the reaction. The differential reactions were performed sequentially at 520, 550, 560, 575, 590, 600 and 610 K. The rate of CO oxidation reaction increases with the temperature. To maintain the differential conversion of the reactant CO, the reaction time at high temperature was controlled shorter than that at lower temperature. The changes of total pressure as a function of the reaction time at different temperatures are plotted in Figure III-7.

Rates of reaction, expressed as turnover frequencies (TOF), are defined as the number of CO<sub>2</sub> molecules produced per active metal site per second.

$$r = \frac{1}{n_{\text{Pt}}} \frac{dN_{\text{CO}_2}}{dt} \quad (\text{III-11})$$

$$\frac{dN_{\text{CO}_2}}{dt} = \frac{-2dN_t}{dt} \quad (\text{III-12})$$

Where  $N_t$  is the sum of the moles of CO, O<sub>2</sub> and CO<sub>2</sub>. As  $PV=N_tRT$ , So

$$\frac{dN_t}{dt} = \frac{V}{RT} \frac{dP}{dt} \quad (\text{III-13})$$

The reaction rate can be expressed in terms of the rate of total pressure change in the bulb reactor. The TOF at different temperatures are calculated as

$$r = \frac{1}{n_{\text{Pt}}} \frac{dN_{\text{CO}_2}}{dt} = \frac{-2}{n_{\text{Pt}}} \frac{V}{RT} \frac{dP}{dt} \quad (\text{III-14})$$

The CO<sub>2</sub> production rate can be expressed by a power law type model as

$$r = A \exp(-E/RT) P_{\text{CO}}^m P_{\text{O}_2}^n \quad (\text{III-15})$$

The partial pressure of CO and O<sub>2</sub> may be treated as constant in the differential operating condition. Figure III-8 shows the CO<sub>2</sub> production rate as a function of the sample temperature in Arrhenius form. The activation energy of CO oxidation is calculated as 93.1 kJ/mol. This activation energy is in the same range of the activation energy of CO oxidation over supported Pt catalysts and single crystals reported in the literature.<sup>47</sup>

Next the dehydrogenation of cyclohexane over Pt (111) was investigated in this UHY bulb reactor.

### **III.3.2 The Dehydrogenation of Cyclohexane on Pt (111)**

#### **III.3.2.1 The Cycle of Dehydrogenation/Hydrogenation**

It is well known that supported metal catalysts are good hydrogenation and dehydrogenation catalysts, and they have found a wide range of applications in chemical industry. However, working catalyst systems have complicated structures. The large surface area internal pore structure of the support hides the metal particles and makes it difficult to study their structure, oxidation state, and composition, which determine both activity and selectivity. The metal particle may be viewed as composed of single-crystal surfaces. Each surface has a different reactivity, and the product distribution reflects the chemistry of the different surface sites. The dehydrogenation of cyclohexane was first investigated over single crystal Pt(111) as a model system to examine its reactivity. A



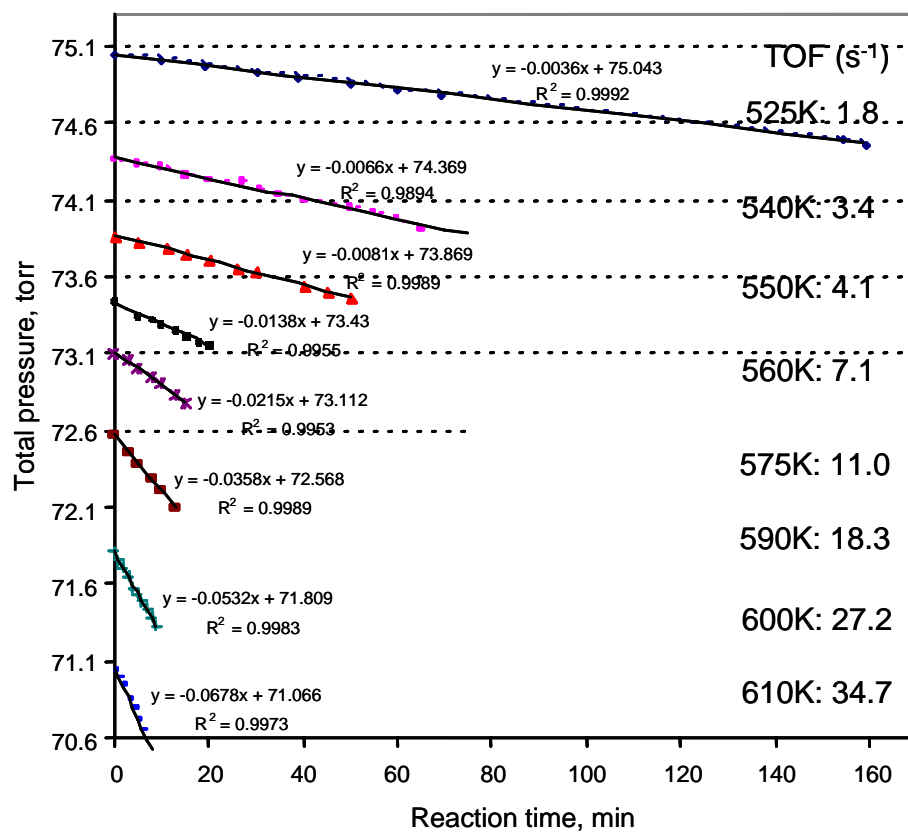


**Figure III-7.** The total pressure change as a function of reaction time during CO-O<sub>2</sub> reaction on Pt (111).

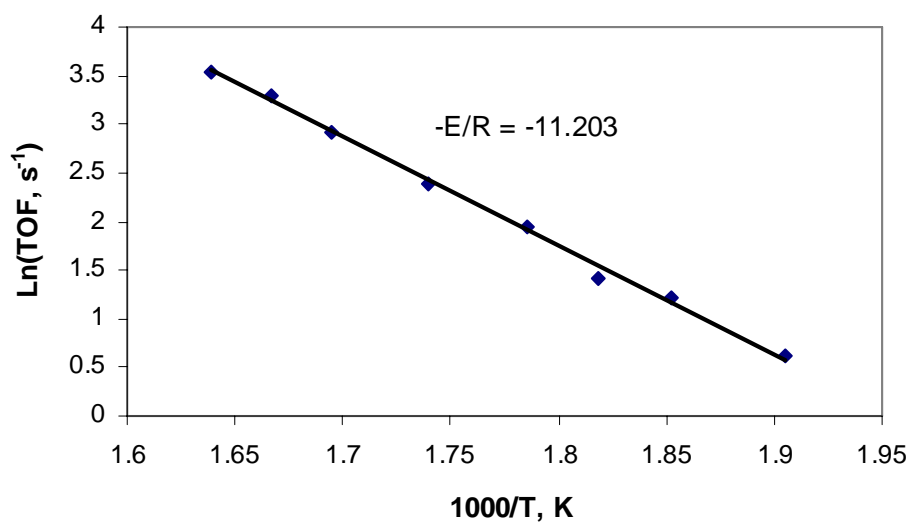


**Figure III-8.** The CO<sub>2</sub> production rate as a function of temperature in an Arrhenius plot during CO-O<sub>2</sub> reaction on Pt(111).

comparison with the supported catalyst in terms of the reaction rate, crystal surface orientation and surface irregularities rewards insights for designing efficient working catalyst systems.

Figure III-9 shows the cycle of dehydrogenation of cyclohexane and hydrogenation of benzene on Pt(111) catalyst. Prior to the reaction, the sample was cleaned by CO oxidation at 700 K for half an hour, and annealed at 900 K for 2 h. Reactant cyclohexane was vacuum distilled three times to remove adsorbed air and water before use. Then, 2 torr of cyclohexane and 12 torr of H<sub>2</sub> were fed into the bulb reactor. As the number of molecules increases in the dehydrogenation reaction, the pressure change is used as an index of the extent of reaction. The reference gauge (Gage I) was used to monitor the pressure change during the reaction. The reaction was firstly carried out at 620 K, and then the temperature was increased to 650 and 700 K for reaction, respectively. At each temperature the reaction was performed over 1 hr until the total pressure was stabilized. The reaction temperature was then decreased to 423 K for backward hydrogenation reaction for over 1 hr, then, was cooled down to room temperature. The conversion increased with temperature, leading to an increase in the pressure change. The black, red and blue curves corresponds to the first, second and third cycles of the reaction, respectively. It was found that the total pressure was completely recovered after the first reaction cycle, but could not be recovered after the second and third cycles due to deactivation of the catalyst. The presence of H<sub>2</sub> in the feed inhibits the deactivation of the catalyst. The UHV bulb reactor is a good tool to study the cycling of the dehydrogenation and hydrogenation reactions.

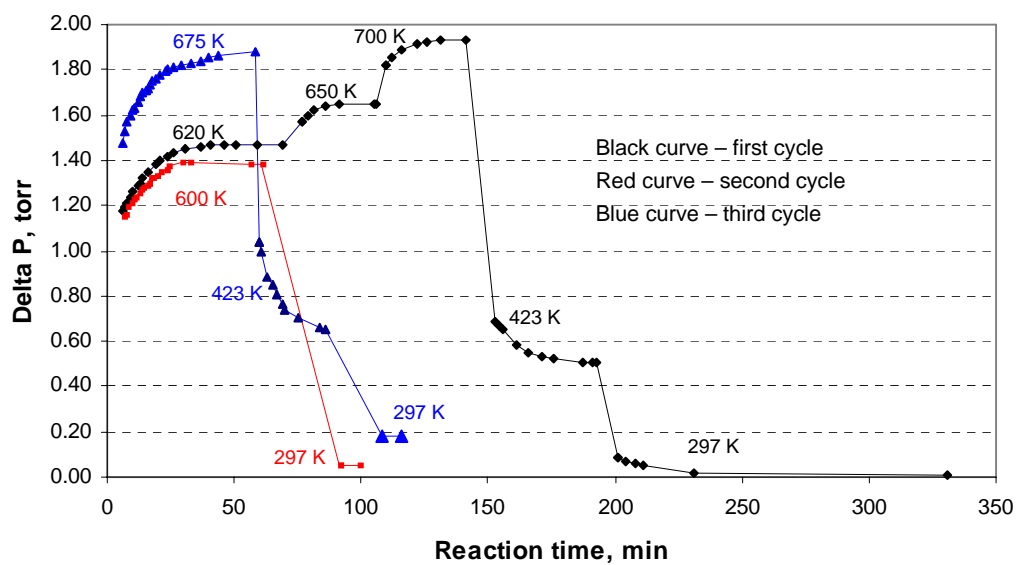


**Figure III-9.** The cycle of dehydrogenation of cyclohexane and hydrogenation of benzene over Pt(111) in an UHV bulb reactor.  $P^0_{\text{cyclohexane}}=2$  torr,  $P^0_{\text{H}_2}=12$  torr.

### III.3.2.2 The Rate of Cyclohexane Dehydrogenation on Pt(111)

The rate of cyclohexane dehydrogenation, expressed in terms of TOF, is defined as the number of cyclohexane converted per metal site per second.

$$r = \frac{-1}{n_{Pt}} \frac{dN_{C_6H_{12}}}{dt} \quad (III-16)$$

$$\text{And } \frac{dN_{C_6H_{12}}}{dt} = \frac{-1}{3} \frac{dN_t}{dt} \quad (III-17)$$

where  $N_t$  is the sum of the moles of  $C_6H_{12}$ ,  $H_2$  and  $C_6H_6$ . As  $PV=N_tRT$ , So

$$\frac{dN_t}{dt} = \frac{V}{RT} \frac{dP}{dt} \quad (III-18)$$

The reaction rate can be expressed in terms of the rate of total pressure change in the bulk reactor. The TOF at different temperatures can be calculated as

$$r = \frac{-1}{n_{Pt}} \frac{dN_{C_6H_{12}}}{dt} = \frac{1}{3} \frac{V}{n_{Pt}RT} \frac{dP}{dt} \quad (III-19)$$

When The rate is expressed by a power law type expression

$$r = A \exp(-E/RT) P_{C_6H_{12}}^m P_{C_6H_6}^n P_{H_2}^l \quad (III-20)$$

The partial pressure of cyclohexane, benzene and hydrogen may be treated as constant in the differential operation condition. Figure III-10 shows the rate of cyclohexane conversion as a function of temperature in Arrhenius form. The activation energy of cyclohexane dehydrogenation, calculated from the slope, is 31.5 kJ/mol (Figure III-11).

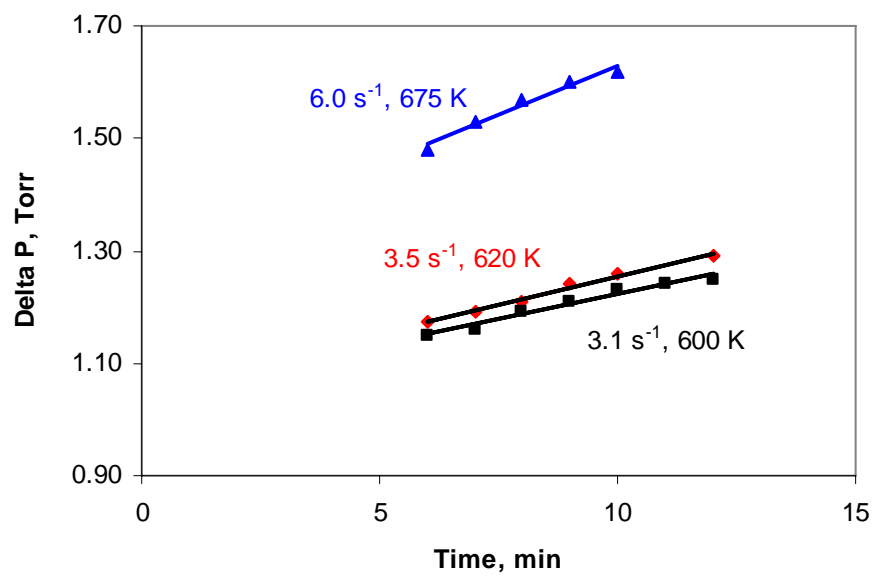


**Figure III-10.** The total pressure change as a function of reaction time during cyclohexane dehydrogenation on Pt(111).  $P^0_{\text{cyclohexane}}=2$  torr,  $P^0_{\text{H}_2}=12$  torr.

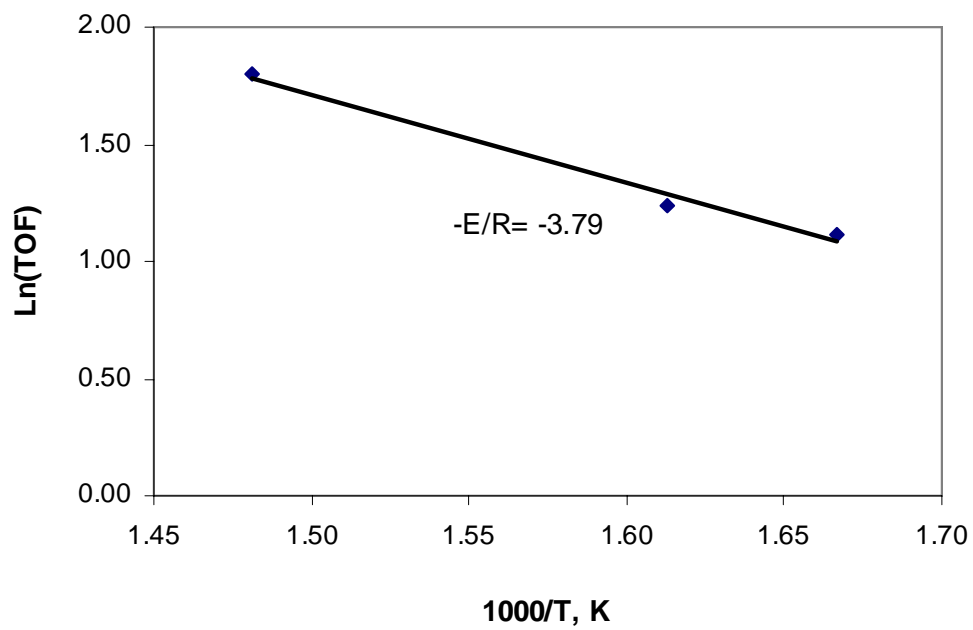


**Figure III-11.** The rate of cyclohexane dehydrogenation on Pt(111) as a function of temperature in Arrhenius form.

### **III.3.3 The Dehydrogenation of Cyclohexane in the Fixed-Bed Reactor**

#### **III.3.3.1 Effect of Various Supports**

Three different kinds of high surface area support such as  $\gamma$ -alumina, silica and activated carbon were used for the preparation of the catalyst. It is found in Figure III-12 that the catalytic activity decreases in the order  $\gamma$ -alumina > silica > activated carbon. The catalyst prepared with a  $\gamma$ -alumina support also shows good stability, with no decrease of cyclohexane conversion at 98.7% after 20 h. Therefore  $\gamma$ -alumina was chosen as the support to prepare supported Pt catalysts for the dehydrogenation of cyclohexane and decalin.

#### **III.3.3.2 Effect of Temperature**

The dehydrogenation of cyclohexane was carried out at 260, 280, 300, 320, 340, 360, 380 and 400 °C, respectively. It is shown in Figure III-13 that the conversions increase from 51.7% at 260 °C to 100% for temperatures above 360 °C. Furthermore, trace amounts of cracking products such as methane and ethane were detected at 380 and 400 °C respectively.



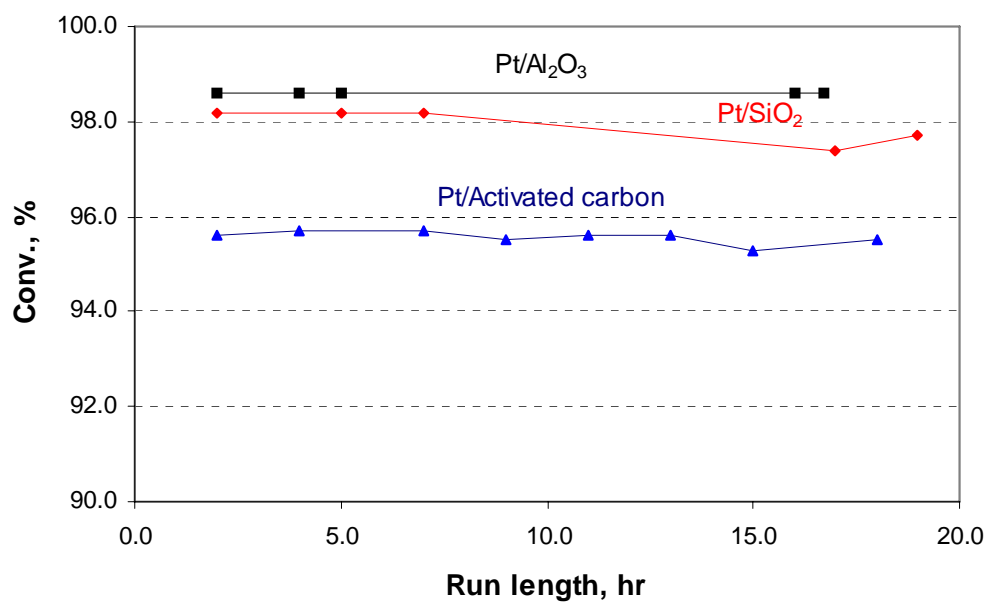


**Figure III-12.** Cyclohexane dehydrogenation over different supported Pt catalysts. 340 °C, space time=20 kg cat h/kmol, H<sub>2</sub>/cyclohexane=1/2.

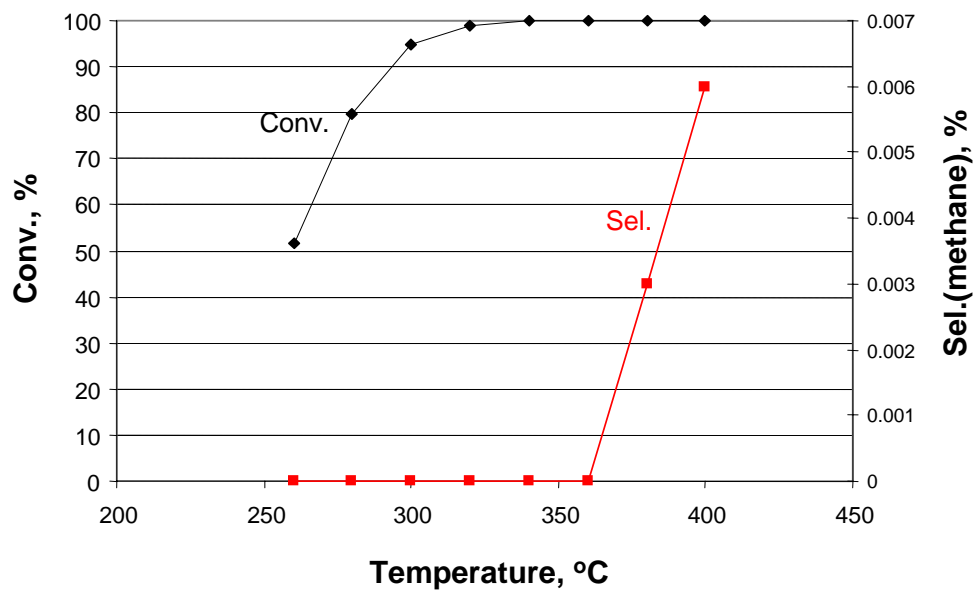


**Figure III-13.** Effect of temperature on cyclohexane dehydrogenation. Reaction condition: 0.8 wt% Pt/ $\gamma$ -Alumina, space time=30 kg cat h/kmol,  $H_2$ /cyclohexane=3.

### **III.3.3.3 The Stability of the Pt/ $\gamma$ -alumina Catalyst**

The dehydrogenation reaction was carried out over 0.8 wt% Pt/ $\gamma$ -alumina catalyst at cyclohexane space time 20 kg cat h/kmol, hydrogen to cyclohexane molar ratio of 1 to 2 and reaction temperatures in the range 320 - 410 °C. As shown in Figure III-14, The conversions of cyclohexane at 320 (10 hrs), 350 (16 hrs) 380 (23 hrs) and 410 °C (22 hrs) are 94.4, 99.5, 99.8, and 99.9%, respectively, and there is no observation of catalyst deactivation.

### **III.3.3.4 Effect of Pt Loading and of the Addition of Sn**

It is shown in Fig III-15 that the conversions of cyclohexane on four Pt/alumina catalysts with 0.3, 0.5, 0.8 and 1.0 wt % of Pt loadings are 45.0, 87.2, 95.0 and 97.2%, respectively. Figure III-16 shows that the addition of Sn into a Pt/alumina catalyst decreases the catalyst activity due to the coverage of the active Pt sites by Sn. However, it was reported in catalytic reforming that the addition of Sn prevented the sintering of Pt cluster and improved catalyst stability against deactivation by coking.

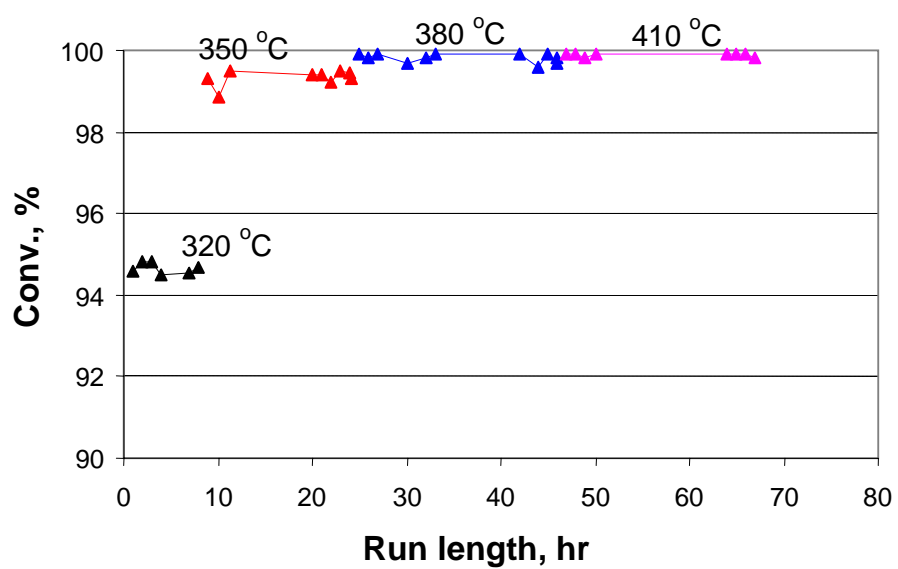


**Figure III-14.** Catalyst stability in cyclohexane dehydrogenation to produce H<sub>2</sub>. 0.8 wt% Pt/ $\gamma$ -Alumina, space time=20 kg cat h/kmol, H<sub>2</sub>/cyclohexane=1/2.

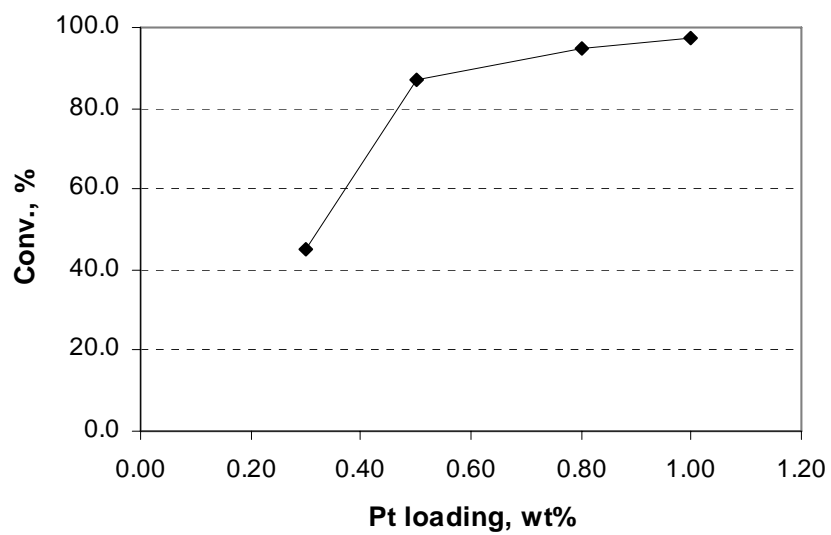


**Figure III-15.** Effect of Pt loadings on cyclohexane dehydrogenation. Reaction condition: 320 °C, space time=20 kg cat h/kmol,  $H_2$ /cyclohexane=3.

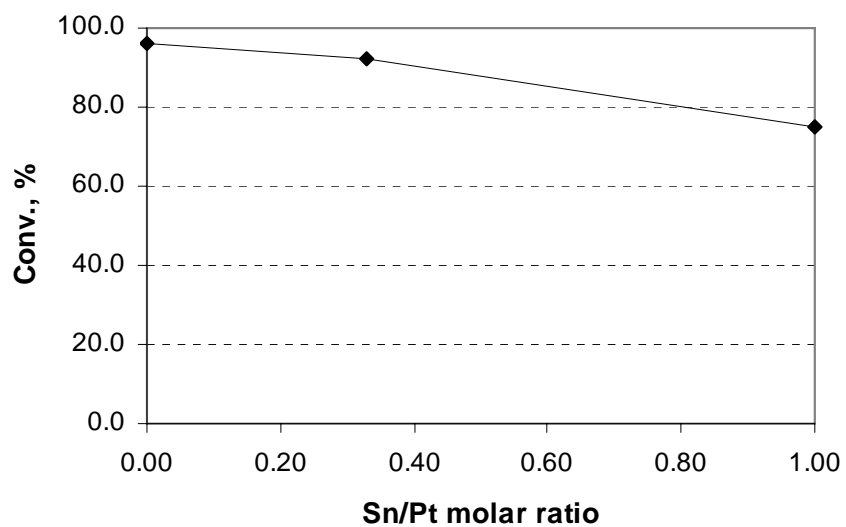


**Figure III-16.** Effect of Sn/Pt molar ratio on cyclohexane dehydrogenation. Reaction condition: 320 °C, space time=20 kg cat h/kmol, H<sub>2</sub>/cyclohexane=3.

### III.3.4 The Dehydrogenation of Decalin

#### III.3.4.1 Definition of Conversions and Selectivities

Conversion of trans-decalin (TDC)

$$X_{\text{TDC}} = \frac{\text{moles of TDC in} - \text{moles of TDC out}}{\text{moles of TDC in}} \times 100$$

Conversion of cis-decalin (CDC)

$$X_{\text{CDC}} = \frac{\text{moles of CDC in} - \text{moles of CDC out}}{\text{moles of CDC in}} \times 100$$

Conversion of decalin to tetralin (TT)

$$X_{\text{TT}} = \frac{\text{moles of TT out}}{\text{moles of DC in}} \times 100$$

(III-21)

Conversion of TDC and CDC to naphthalene (NP)

$$X_{\text{NP}} = \frac{\text{moles of NP out}}{\text{moles of DC in}} \times 100$$

Selectivity for products

$$\text{Selectivity} = \frac{\text{moles of product } i \text{ formed}}{\text{moles of DC converted}} \times 100 \quad i \text{ refers to TT or NP}$$

### III.3.4.2 Effect of Temperature

Decalin used in the dehydrogenation consists of 24% cis- and 76% trans- isomers. The dehydrogenation of decalin was performed in a temperature range 250 - 350 °C, space time of 60 g cat h/mol, hydrogen to decalin molar ratio of 1 and atmospheric pressure. It is shown in Figure III-17 that the conversion of cis-decalin is much higher than that of trans-isomer. For example, the conversions of cis- and trans- decalin at 300 °C are 66.8 and 98.0%, respectively. Two factors may contribute to this. First, cis-isomer is more active in the dehydrogenation reaction. Second, there exists isomerization of decalin isomers over the acid sites of  $\gamma$ -alumina, and the reaction rate for the isomerization of cis- to trans-isomer is much faster than the reverse reaction. The conversions of both decalin isomers increase with temperature. The selectivity for naphthalene is much higher than that of tetralin. With the increase of the temperature from 250 °C to 350 °C, the selectivity for naphthalene increases from 93.6% to 99.7%, whereas, the selectivity for tetralin decreases from 6.4 to 0.3%. The dehydrogenation of decalin is a consecutive reaction. The intermediate product, tetralin, can be further dehydrogenated to produce more hydrogen at higher temperature.



### **III.3.4.3 Catalyst Stability**

The stability of 0.8 wt%Pt-0.3wt% Sn/ $\gamma$ -alumina catalyst in decalin dehydrogenation was tested in the absence and presence of hydrogen at 340 °C and space time 80 kg cat h/kmol. As shown in Figure III-18, the conversion decreases from the original 98.8 % to 95.4% after 40 h, whereas, the conversion shows no apparent decrease after 30 h when hydrogen was co-fed.

The gravimetric hydrogen content in decalin is higher than that in cyclohexane and, the dehydrogenated product, naphthalene, is environmentally favorable. These advantages make decalin a good candidate as a hydrogen carrier. Next, a rigorous Hougen-Watson type kinetic model will be built for the dehydrogenation of decalin. It will be a valid tool for the process design and the guide of the operation.

## **III.3.5 Kinetic Study of the Dehydrogenation of Decalin**

### **III.3.5.1 Experimental Results**

#### **III.3.5.1.1 Effect of Space Time**

The kinetic study of the dehydrogenation of decalin over Pt/ $\gamma$ -alumina catalyst was performed in a temperature range 275-345 °C at atmospheric pressure. Holding constant temperature and H<sub>2</sub>/decalin molar ratio of 1, the feed rate of decalin was varied to check the effect of the space time on the conversion. Figure III-19 shows an example of the conversions of cis-, trans- decalin, tetralin and naphthalene as a function of space time at 325 °C. It is shown that the conversions of cis -, trans- decalin and naphthalene increase

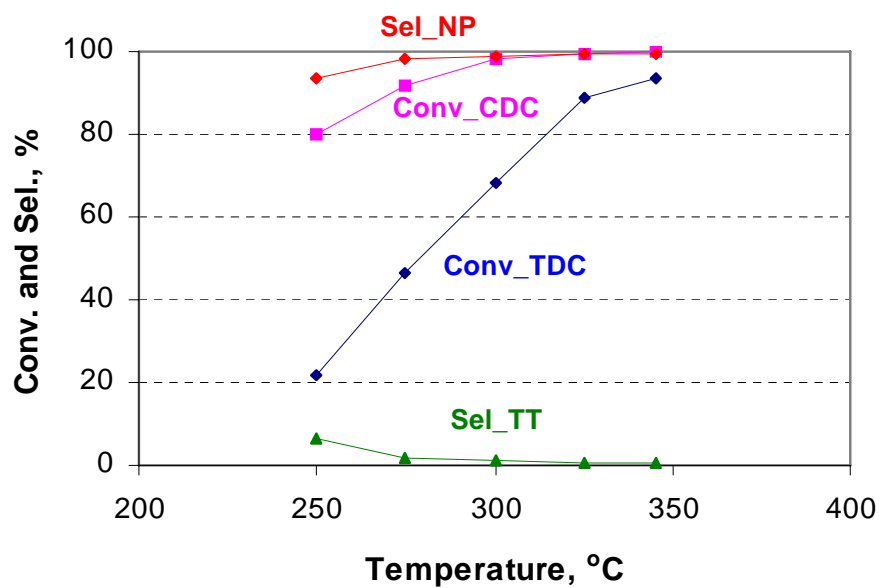


**Figure III-17.** Effect of temperature on decalin dehydrogenation. Reaction condition: 0.8 wt% Pt/ $\gamma$ -Alumina, space time=60 kg cat h/kmol,  $H_2$ /cyclohexane=1.

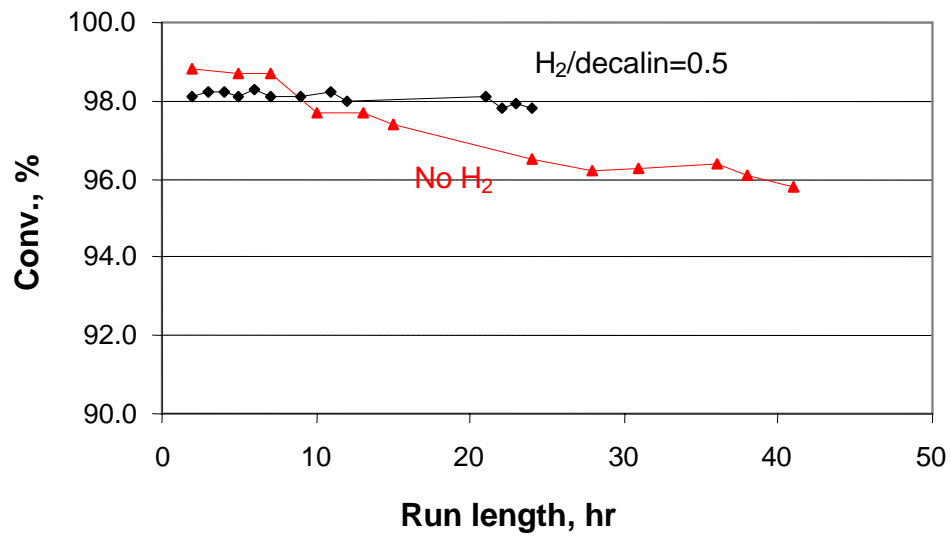


**Figure III-18.** The stability of catalyst in decalin dehydrogenation at 340 °C and space time=80 kg cat h/kmol.

with the space time. The conversion to tetralin is below 2.0%. Then, similar experiments were carried out at 345, 300, and 275 °C.

#### **III.3.5.1.2 Effect of H<sub>2</sub>/Decalin Molar Ratio**

The dehydrogenation of decalin is a reversible reaction. While the co-feed of hydrogen will inhibit the deactivation of the catalyst, it may also decrease the conversion of the dehydrogenation reaction. Holding the space time and temperature constant, the H<sub>2</sub> to decalin molar ratio was varied from 1 to 7 to check the effect of H<sub>2</sub> on the conversion. Figure III-20 shows the conversions as a function of H<sub>2</sub> to decalin molar ratio at 325 °C and space time 60 g cat hr/mol. The conversions of cis-, trans- decalins and naphthalene decrease with the increase of H<sub>2</sub> to decalin molar ratio. But, the conversion to tetralin increases with the H<sub>2</sub> to decalin molar ratio. Tetralin is the intermediate product in decalin dehydrogenation. The co-feed of H<sub>2</sub> may inhibit the dehydrogenation reactions, which results in the buildup of the intermediate product, tetralin.

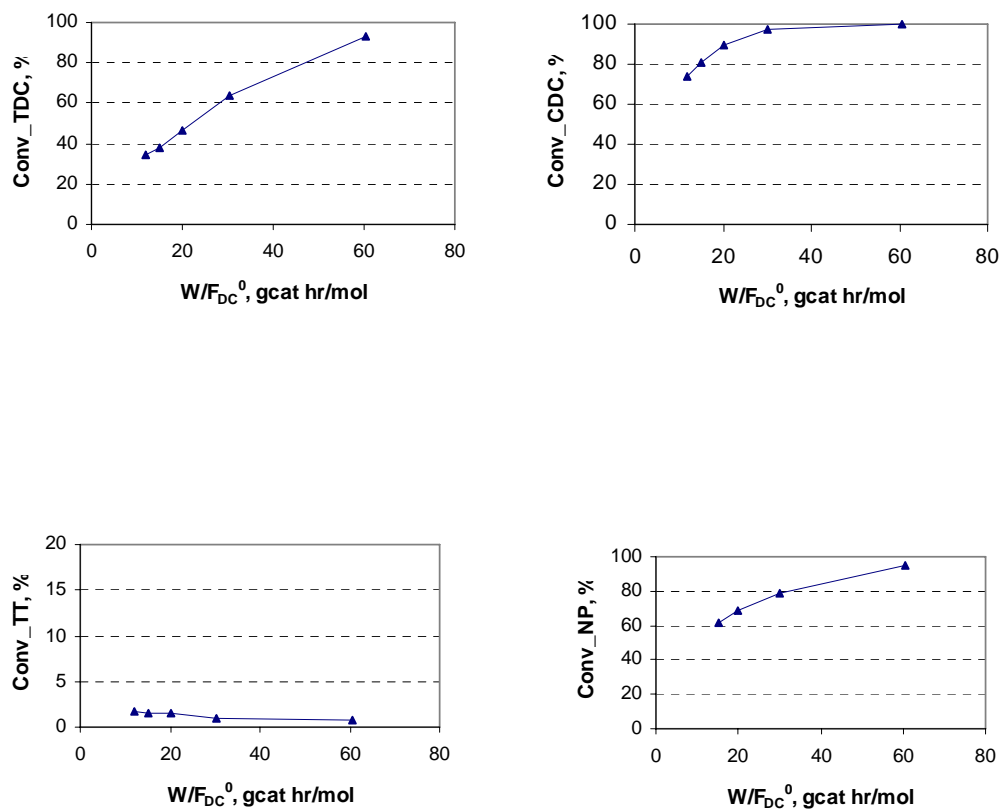


**Figure III-19.** Conversions as a function of space time in the dehydrogenation of decalin at 325 °C and  $H_2$ /decalin molar ratio of 1.

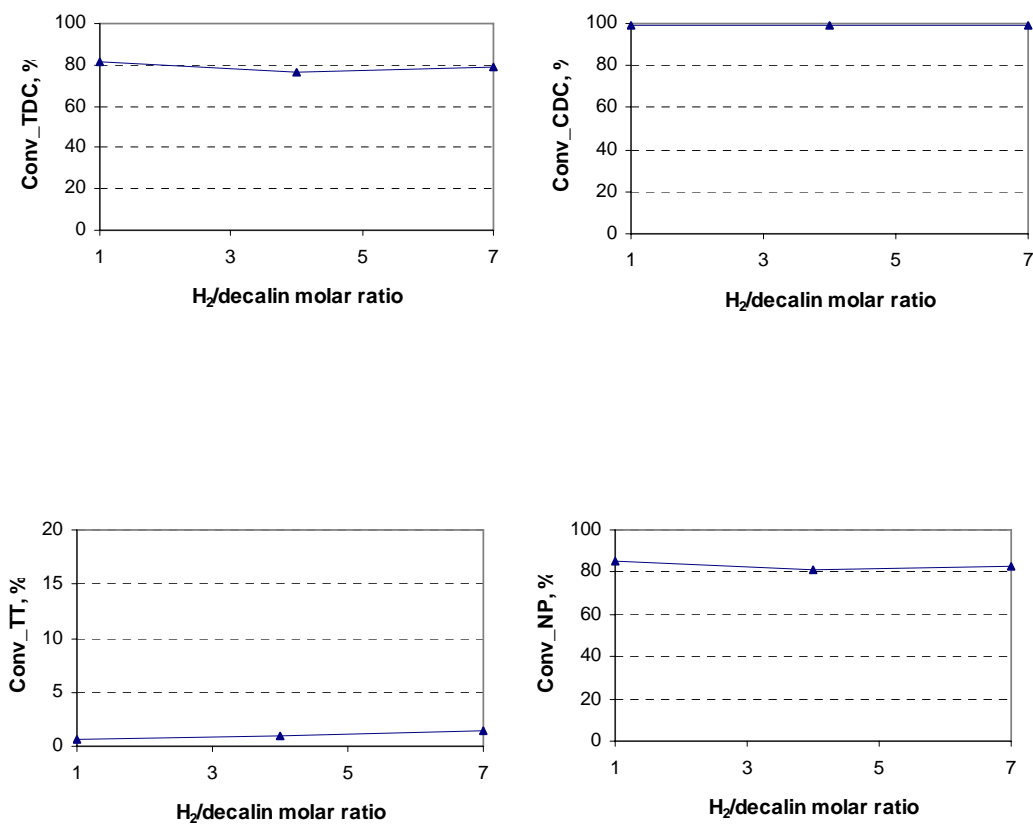


**Figure III-20.** Conversions as a function of H<sub>2</sub>/decalin molar ratio in the dehydrogenation of decalin at 325 °C and space time of 60 kg cat h/mol.

### III.3.5.2 Thermodynamic Aspects of Decalin Dehydrogenation

Thermodynamic calculation of the equilibrium constant of a reaction can provide the information on the limit of the conversion, thus tell the possible reactions that can occur in a complex reaction system. The equilibrium constant of each possible reaction in the dehydrogenation of decalin was calculated (Figure III-21). Four possible reactions are involved in the dehydrogenation of decalin. Both cis- and trans- decalin can be dehydrogenated to form the intermediate product tetralin. Tetralin can be consecutively dehydrogenated to form the final product naphthalene. The equilibrium constant at 325 °C for the isomerization of cis- decalin to trans- and the reverse reaction are 7.4 and 0.1, respectively. Therefore, the rate of the isomerization of cis- to trans- decalin will be much faster than that of the reverse reaction. The equilibrium constants at 325 °C for the dehydrogenation reactions of cis-decalin to tetralin, trans-decalin to tetralin, and tetralin to naphthalene are 441.8, 3268.8, and 28.5, respectively. All these equilibrium constants are not so big that the reverse reaction could be neglected. All these reactions should be considered as reversible. Furthermore, the equilibrium constants of all the dehydrogenation reactions increase with the temperature, whereas, the equilibrium constant of cis- to trans- isomerization decreases with temperature. Thus, high temperature will favor dehydrogenation, and low temperature will be favorable for the isomerization of cis- to trans- decalin.

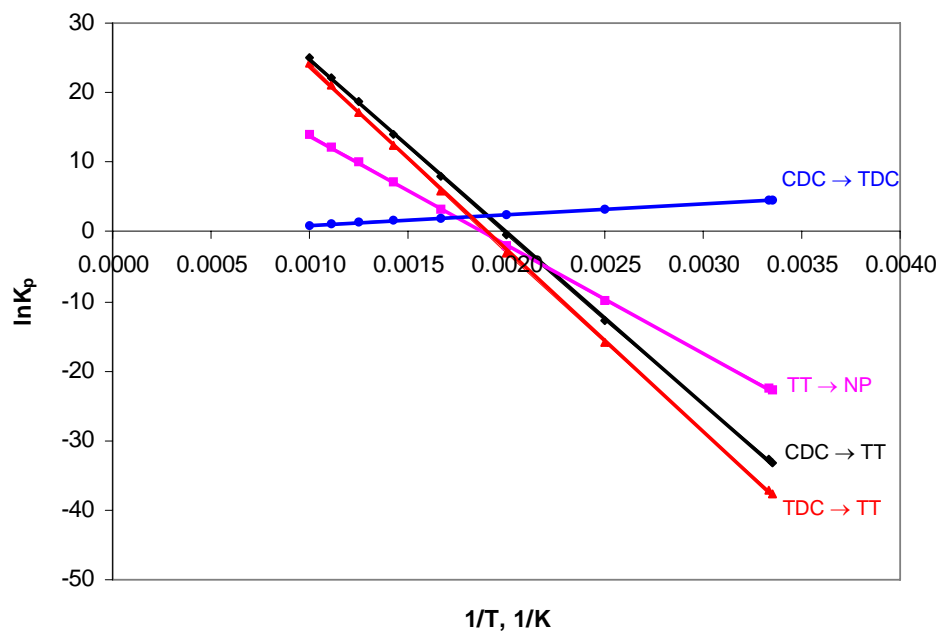
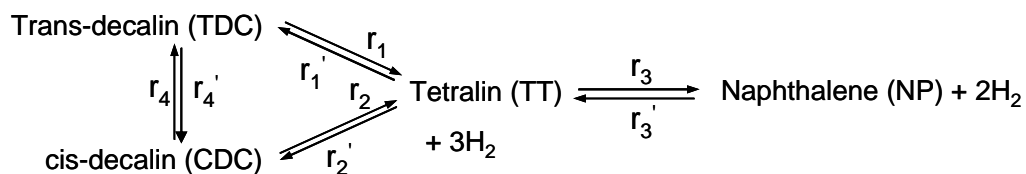


**Figure III-21.** Calculation of the equilibrium constants of the reactions involved in the dehydrogenation of decalin.



### III.3.5.3 Derivation of the Kinetic Model

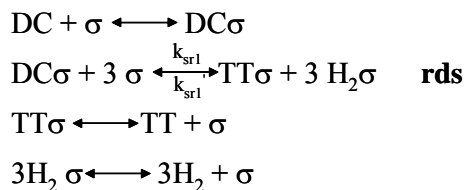
In the dehydrogenation of decalin over Pt/ $\gamma$ -Al<sub>2</sub>O<sub>3</sub> catalyst, two kinds of active sites, i.e. metal sites and acid sites, are involved. The metal sites catalyze dehydrogenation reactions, but the acid sites from the  $\gamma$ -alumina catalyze the isomerization of two decalin isomers. Based on thermodynamic calculations, the possible reaction scheme in the dehydrogenation of decalin is shown in scheme III-1. Both cis- and trans-decalin can be dehydrogenated to form tetralin and H<sub>2</sub>. Tetralin can be further dehydrogenated to form the final product, naphthalene, to generate more H<sub>2</sub>. At the same time, the isomerization between two decalin isomers will occur over the acid active site. All these reactions are reversible.



Scheme III-1. Reaction scheme of the dehydrogenation of decalin.

Reaction rate equations can be derived based on the assumption of different rate determining steps. When the surface reactions of the adsorbed decalins and naphthalene are the rate determining steps, the dehydrogenation rates on Pt sites can be written for the following two cases.

### III.3.5.3.1 Case I



In case I, the surface reaction, in which three hydrogens are removed simultaneously, is assumed to be the rate determining step. The dehydrogenation rate on Pt sites can be written

$$\begin{aligned}
 r_1 &= k_{sr1} K_{TDC} P_{TDC} / \Delta^4 \\
 r_2 &= k_{sr2} K_{CDC} P_{CDC} / \Delta^4 \\
 r_3 &= k_{sr3} K_{TT} P_{TT} / \Delta^3
 \end{aligned} \tag{III-22}$$

The reverse hydrogenation rates on Pt sites can be written

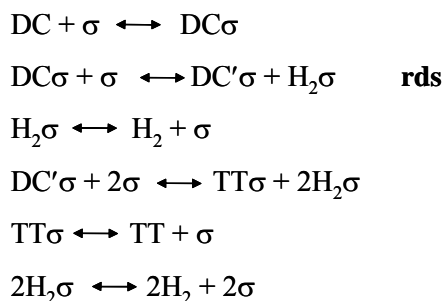
$$\begin{aligned}
 r_1' &= k_{sr1}' K_{TT} K_{H_2} P_{TT} P_{H_2}^3 / \Delta^4 \\
 r_2' &= k_{sr2}' K_{TT} K_{H_2} P_{TT} P_{H_2}^3 / \Delta^4 \\
 r_3' &= k_{sr3}' K_{NP} K_{H_2} P_{NP} P_{H_2}^2 / \Delta^3
 \end{aligned} \tag{III-23}$$

The  $\Delta$  appearing in the denominator in the above reaction rates is

$$1 + K_{CDC} P_{CDC} + K_{TDC} P_{TDC} + K_{TT} P_{TT} + K_{H_2} P_{H_2} + K_{NP} P_{NP} \tag{III-24}$$

As the active sites involved in the rate determining steps of the dehydrogenations of TDC, CDC and TT are 4, 4 and 3, the exponents appearing in the denominator of rate equations  $r_1$ ,  $r_2$  and  $r_3$  should be 4, 4 and 3, respectively. It is the same for the reverse reactions  $r_1'$ ,  $r_2'$  and  $r_3'$ .

### III.3.5.3.2 Case II



In case II, the removal of the first hydrogen is assumed to be the rate determining step. The partially dehydrogenated species are then subject to further dehydrogenation to remove the remaining hydrogen. In this case the dehydrogenation rate on Pt sites can be written

$$\begin{aligned}
 r_1 &= k_{sr1} K_{\text{TDC}} P_{\text{TDC}} / \Delta^2 \\
 r_2 &= k_{sr2} K_{\text{CDC}} P_{\text{CDC}} / \Delta^2 \\
 r_3 &= k_{sr3} K_{\text{TT}} P_{\text{TT}} / \Delta^2
 \end{aligned} \tag{III-25}$$

The reverse hydrogenation rates on Pt sites can be written

$$\begin{aligned}
 r_1' &= k_{sr1}' K_{\text{TT}} K_{\text{H}_2} P_{\text{TT}} P_{\text{H}_2}^3 / \Delta^2 \\
 r_2' &= k_{sr2}' K_{\text{TT}} K_{\text{H}_2} P_{\text{TT}} P_{\text{H}_2}^3 / \Delta^2 \\
 r_3' &= k_{sr3}' K_{\text{NP}} K_{\text{H}_2} P_{\text{NP}} P_{\text{H}_2}^2 / \Delta^2
 \end{aligned} \tag{III-26}$$

The  $\Delta$  appearing in the denominator in the above reaction rates are

$$\Delta = 1 + K_{CDC}P_{CDC} + K_{TDC}P_{TDC} + K_{TT}P_{TT} + K_{H_2}P_{H_2} + K_{NP}P_{NP} + K_{TT}P_{TT}K_{H_2}^2P_{H_2}^2/K_{DC}' + K_{NP}P_{NP}K_{H_2}P_{H_2}/K_{TT}' \quad (III-27)$$

for the removal of the remaining two hydrogen simultaneously. And

$$\Delta = 1 + K_{CDC}P_{CDC} + K_{TDC}P_{TDC} + K_{TT}P_{TT} + K_{H_2}P_{H_2} + K_{NP}P_{NP} + K_{TT}P_{TT}K_{H_2}^2P_{H_2}^2/(K_{DC}'K_{DC}'') + K_{TT}P_{TT}K_{H_2}P_{H_2}/K_{DC}'' + K_{NP}P_{NP}K_{H_2}P_{H_2}/K_{TT}' \quad (III-28)$$

for the removal of the remaining two hydrogens in two steps. But, given the selection of the rate determining steps, the partially dehydrogenated species are present in very low concentrations so that they can be neglected in the denominator. The denominator can be written

$$1 + K_{CDC}P_{CDC} + K_{TDC}P_{TDC} + K_{TT}P_{TT} + K_{H_2}P_{H_2} + K_{NP}P_{NP} \quad (III-29)$$

As the active sites involved in the rate determining steps of the dehydrogenations of TDC, CDC and TT are 2, 2 and 2, the exponents appearing in the denominator of rate equations  $r_1$ ,  $r_2$  and  $r_3$  should all be 2. It is the same for the reverse reactions  $r_1'$ ,  $r_2'$  and  $r_4'$ .

The acid sites of  $\gamma$ -alumina are responsible for the isomerization of cis- and trans-decalin isomers. The reaction rate for the formation of trans- isomer from cis-decalin is:

$$r_4 = k_{sr4}K_{CDC}'P_{CDC}/\omega \quad (III-30)$$

The rate of the reverse reaction is

$$r_4' = k_{sr4}'K_{TDC}'P_{TDC}/\omega \quad (III-31)$$

The denominator  $\omega$  in the above reaction rates is

$$1 + K_{TDC}'P_{TDC} + K_{CDC}'P_{CDC} \quad (III-32)$$

In Scheme III-1, the equations defining the net rate of formation for the various components are

$$\begin{aligned}
 R_{TDC} &= r_1 - r_1' + r_4 - r_4' \\
 R_{CDC} &= r_2 - r_2' + r_4 - r_4' \\
 R_{TT} &= r_1 - r_1' + r_2 - r_2' + r_3' - r_3 \\
 R_{NP} &= r_3 - r_3'
 \end{aligned}
 \tag{III-33}$$

The set of steady state continuity equations for the reacting components in a plug flow reactor can be written

$$\frac{dX_i}{dW/F_i^0} = R_i \quad i = 1, \dots, 4 \tag{III-34}$$

$X_1$ ,  $X_2$ ,  $X_3$  and  $X_4$  represent conversions of TDC, CDC, TT and NP, respectively.  $F_i^0$  represents feed rate of TDC for  $i = 1$ , CDC for  $i = 2$ , and total feed rate of TDC+CDC in the case of  $i = 3$  and 4.

#### III.3.5.4 Parameter Estimation

The integral method was used for the kinetic analysis. The above set of differential equations was numerically integrated by a fourth-order-Runge-Kutta method. Values for the model parameters are estimated by means of regression methods. When the experimental errors are normally distributed with zero mean, the parameters are estimated by the minimization of the following multiresponse objective function.

$$S = \sum_{j=1}^m \sum_{l=1}^m w_{jl} \sum_{i=1}^n (y_{ij} - y_{ij})(y_{il} - y_{il}) \tag{III-35}$$

where  $m$  = number of responses,  $n$  = number of experiments, and  $w_{ji}$  = elements of the inverse of the covariance matrix of the experimental errors on the response  $y$ . As the equations are nonlinear in the parameters, the parameter estimates were obtained by minimizing the objective function by the Marquardt algorithm for multiple responses. The number of parameters in the above model is 22. The parameter estimation was performed on all data simultaneously at all temperatures by directly substituting the temperature dependence of all the parameters into the corresponding continuity equations.

$$\text{Rate constant } k_i = A_i \exp(-E_i/RT) \quad (\text{III-36})$$

$$\text{Adsorption constant } K_i = A_i \exp(H_i/RT) \quad (\text{III-37})$$

Based on the desorption of tetralin as the rate determining step, another model was also formulated. However, this model fits the experimental data poorly. It is not listed here for brevity. The discrimination between rival models was based on the requirement for all parameters to be positive and statistically significant, and on the residual sum of squares as a test for the fit of the data. The sums of squares of residues for the model with the simultaneous removal of three hydrogens as the rate determining step and the model with the removal of the first hydrogen as the rate determining step are 0.10 and 0.47, respectively. Furthermore, as shown in Tables III-2 and III-3, the calculated  $F$  and  $t$  values for the model of case I are much larger than that for the model of case II. Finally, the model of case I, i.e. derived based on surface reaction as the rate determining step with the removal of three hydrogens simultaneously, was retained. Tables III-2 and III-3 are the list of the 22 parameter estimates generated by Marquardt for the models of case

I and case II, respectively. Figures III-22 and III-23 are the Arrhenius and Van't Hoff plots of rate coefficients and adsorption coefficients in the retained model, respectively. The rate coefficients increase with temperature, whereas, the adsorption coefficients decrease with the increase of temperature. Figures III-24 through III-30 compare the experimental conversions vs. space time and experimental conversions vs.  $H_2$ /decalin molar ratio at different temperatures with the values calculated using the retained model.

### **III.3.6 The Dehydrogenation of Jet A**

#### **III.3.6.1 The Dehydrogenation of Jet A Surrogate on Pt/ $\gamma$ - $Al_2O_3$ Catalyst**

The Jet A surrogate blend used in this experiment has an molar average formula of  $C_{10}H_{19}$ . It consists of six components in weight percentage as follows: 30% decane, 35% dodecane, 14% methylcyclohexane, 6% decalin, 10% t-butyl benzene, and 5% 1-methyl naphthalene. Figure III-31 shows the hydrogen production yield in Jet A surrogate dehydrogenation as a function of temperature. The hydrogen yield, defined as hydrogen produced per total hydrogen content in the fuel, increases with the temperature until 480 °C, then starts to decrease. The maximum yield obtained at 480 °C is 11.6%. This yield is lower than that obtained in the dehydrogenation of pure cyclohexane and decalin, which are calculated by the same definition as 47.5 and 52.0%, respectively. From a comparison of the chromatograms of the feed and reforming product, it follows that the conversions of paraffins are low. As in industrial naphtha reforming, if paraffins, which account for 60% in molar percentage in Jet fuel, can be dehydro-aromatized., the yield of  $H_2$  will be greatly increased.

Table III-2. Estimates of frequency factors A, activation energy E and enthalpies of activation  $\Delta H$  for the model of case I by the Levenberg-Marquardt algorithm

Name of Parameter	Estimate	STANDARD	95%-CONFIDENCE LIMITS		t-VALUE
		DEVIATION	LOWER	UPPER	
A_TDC	2.75620D+00	8.20297D-03	2.73979D+00	2.77260D+00	3.36000D+02
A_CDC	1.94694D+01	4.06669D-02	1.93880D+01	1.95507D+01	4.78753D+02
A_TT	2.07370D+02	9.24493D-01	2.05521D+02	2.09219D+02	2.24307D+02
A_NP	5.05188D+00	1.30750D-02	5.02573D+00	5.07803D+00	3.86377D+02
A_H	7.20591D-01	2.27083D-03	7.16049D-01	7.25133D-01	3.17326D+02
A_TDC'	9.41793D+01	2.19826D-01	9.37396D+01	9.46189D+01	4.28426D+02
A_CDC'	1.88592D+00	6.73058D-03	1.87246D+00	1.89938D+00	2.80201D+02
A_TDC_TT	1.24477D+03	5.80256D+00	1.23317D+03	1.25638D+03	2.14521D+02
A_CDC_TT	3.44675D+02	1.45690D+00	3.41761D+02	3.47589D+02	2.36581D+02
A_TT_NP	3.19363D+02	1.58139D+00	3.16201D+02	3.22526D+02	2.01951D+02
A_CDC_TDC	9.90831D+00	4.77090D-02	9.81289D+00	1.00037D+01	2.07682D+02
$-\Delta H_{TDC}$	9.46250D+03	3.97098D+01	9.38308D+03	9.54192D+03	2.38291D+02
$-\Delta H_{CDC}$	1.14421D+04	5.33529D+01	1.13354D+04	1.15488D+04	2.14460D+02
$-\Delta H_{TT}$	7.61700D+03	2.31711D+01	7.57066D+03	7.66334D+03	3.28729D+02
$-\Delta H_{NP}$	1.24701D+04	4.21098D+01	1.23859D+04	1.25544D+04	2.96134D+02
$-\Delta H_H$	8.81563D+03	2.16738D+01	8.77228D+03	8.85898D+03	4.06740D+02
$-\Delta H_{TDC}'$	1.10568D+04	4.43685D+01	1.09680D+04	1.11455D+04	2.49203D+02
$-\Delta H_{CDC}'$	6.25504D+03	2.29984D+01	6.20904D+03	6.30104D+03	2.71977D+02
E_TDC_TT	1.21456D+04	4.00310D+01	1.20655D+04	1.22256D+04	3.03404D+02
E_CDC_TT	1.06321D+04	3.24516D+01	1.05672D+04	1.06970D+04	3.27629D+02
E_TT_NP	5.30952D+03	1.34883D+01	5.28254D+03	5.33650D+03	3.93638D+02
E_CDC_TDC	1.46495D+04	6.49495D+01	1.45196D+04	1.47794D+04	2.25553D+02

$$F = \frac{\text{Regression sum of squares}}{\text{Residual sum of squares}}$$

$$= \frac{\sum_{j=1}^m \sum_{i=1}^m w_{ji} \sum_{i=1}^n \hat{y}_{ij} \hat{y}_{il} / p}{\sum_{j=1}^m \sum_{i=1}^m w_{ji} \sum_{i=1}^n (y_{ij} - \hat{y}_{ij})(y_{il} - \hat{y}_{il}) / (mn-p)} = 2049.74$$

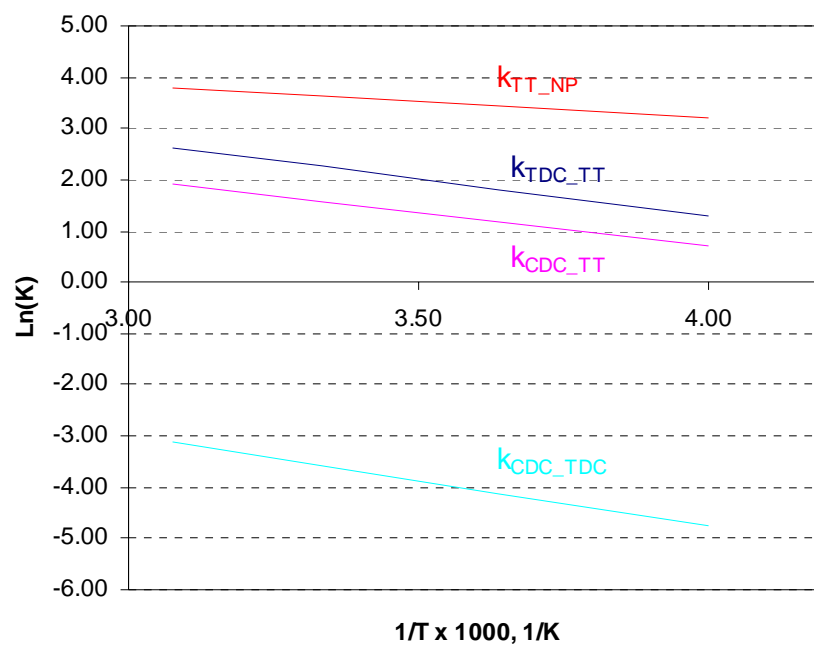


Table III-3. Estimates of frequency factors A, activation energy E and enthalpies of activation  $\Delta H$  for the model of case II by the Levenberg-Marquardt algorithm

Name of Parameter	ESTIMATE	STANDARD	95%-CONFIDENCE LIMITS		t-VALUE
		DEVIATION	LOWER	UPPER	
A_TDC	7.09952D+00	5.06542D-01	6.08644D+00	8.11261D+00	1.40157D+01
A_CDC	5.86274D+00	3.29724D-01	5.20329D+00	6.52219D+00	1.77808D+01
A_TT	5.51894D+01	4.61043D+00	4.59685D+01	6.44103D+01	1.19705D+01
A_NP	3.22731D+00	2.62533D-01	2.70225D+00	3.75238D+00	1.22930D+01
A_H	4.83629D-01	2.20577D-02	4.39513D-01	5.27744D-01	2.19256D+01
A_TDC'	7.85633D+00	4.18247D-01	7.01984D+00	8.69283D+00	1.87840D+01
A_CDC'	1.05837D+01	4.80358D-01	9.62299D+00	1.15444D+01	2.20330D+01
A_TDC_TT	3.97068D+00	1.80076D-01	3.61053D+00	4.33084D+00	2.20500D+01
A_CDC_TT	3.40492D+00	1.69390D-01	3.06614D+00	3.74370D+00	2.01011D+01
A_TT_NP	6.06927D+01	1.03048D+00	5.86317D+01	6.27536D+01	5.88974D+01
A_CDC_TDC	1.46912D+01	4.71354D-01	1.37485D+01	1.56339D+01	3.11681D+01
$-\Delta H_{TDC}$	1.12936D+04	6.10755D+02	1.00721D+04	1.25151D+04	1.84913D+01
$-\Delta H_{CDC}$	9.11006D+03	3.48862D+02	8.41234D+03	9.80779D+03	2.61136D+01
$-\Delta H_{TT}$	1.97523D+04	6.50034D+02	1.84523D+04	2.10524D+04	3.03866D+01
$-\Delta H_{NP}$	1.39794D+04	5.99206D+02	1.27810D+04	1.51778D+04	2.33298D+01
$-\Delta H_H$	3.62703D+03	2.34724D+02	3.15758D+03	4.09647D+03	1.54523D+01
$-\Delta H_{TDC}'$	7.90498D+03	6.06223D+02	6.69253D+03	9.11742D+03	1.30397D+01
$-\Delta H_{CDC}'$	1.36410D+04	1.30829D+03	1.10244D+04	1.62576D+04	1.04266D+01
E_TDC_TT	9.85450D+03	2.80018D+02	9.29446D+03	1.04145D+04	3.51924D+01
E_CDC_TT	6.88942D+03	3.07466D+02	6.27448D+03	7.50435D+03	2.24071D+01
E_TT_NP	1.03841D+04	6.35116D+02	9.11386D+03	1.16543D+04	1.63499D+01
E_CDC_TDC	1.28361D+03	1.02551D+02	1.07851D+03	1.48871D+03	1.25169D+01

$$F = \frac{\text{Regression sum of squares}}{\text{Residual sum of squares}}$$

$$= \frac{\sum_{j=1}^m \sum_{i=1}^m w_{ji} \sum_{i=1}^n \hat{y}_{ij} \hat{y}_{il} / p}{\sum_{j=1}^m \sum_{i=1}^m w_{ji} \sum_{i=1}^n (y_{ij} - \hat{y}_{ij})(y_{il} - \hat{y}_{il}) / (mn-p)} = 444.32$$



**Figure III-22.** Arrhenius plot of rate coefficients.

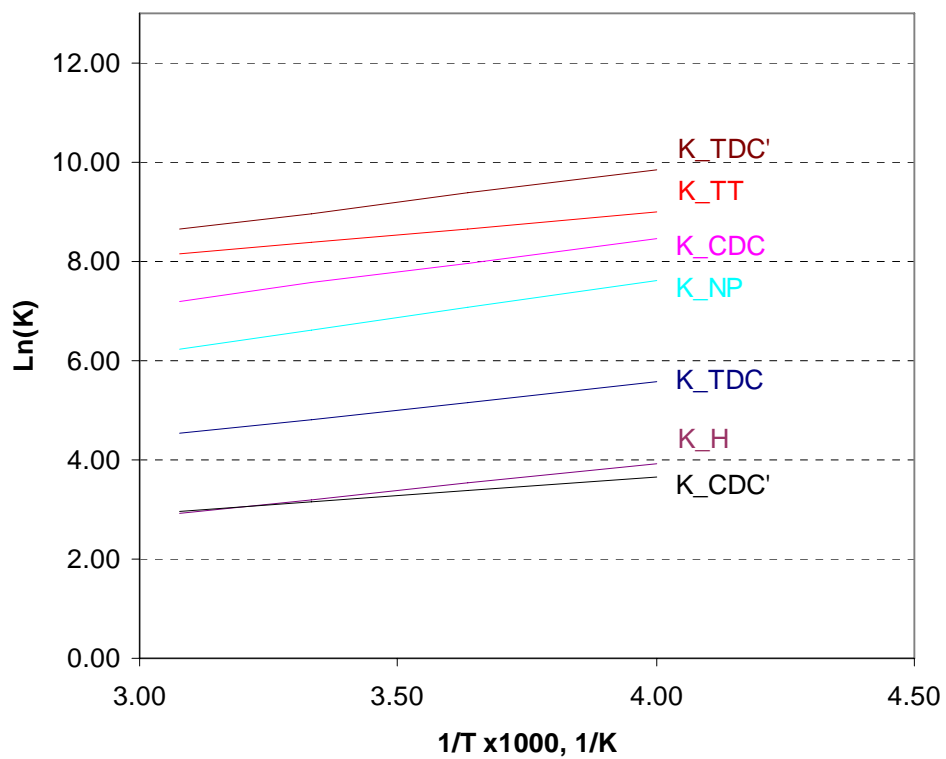


**Figure III-23.** Van't Hoff plot of adsorption coefficients.

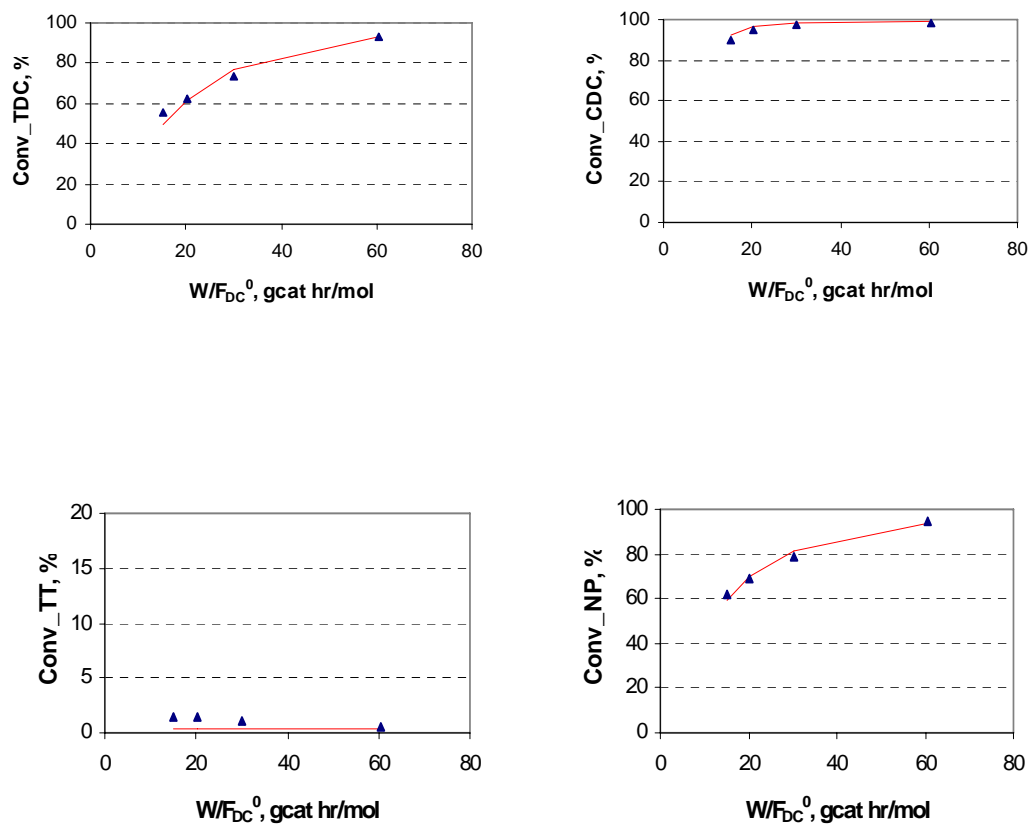


**Figure III-24.** Comparison of experimental and calculated conversions as a function of space time at 345 °C ( $\Delta$ : EXP; Solid line: CAL).

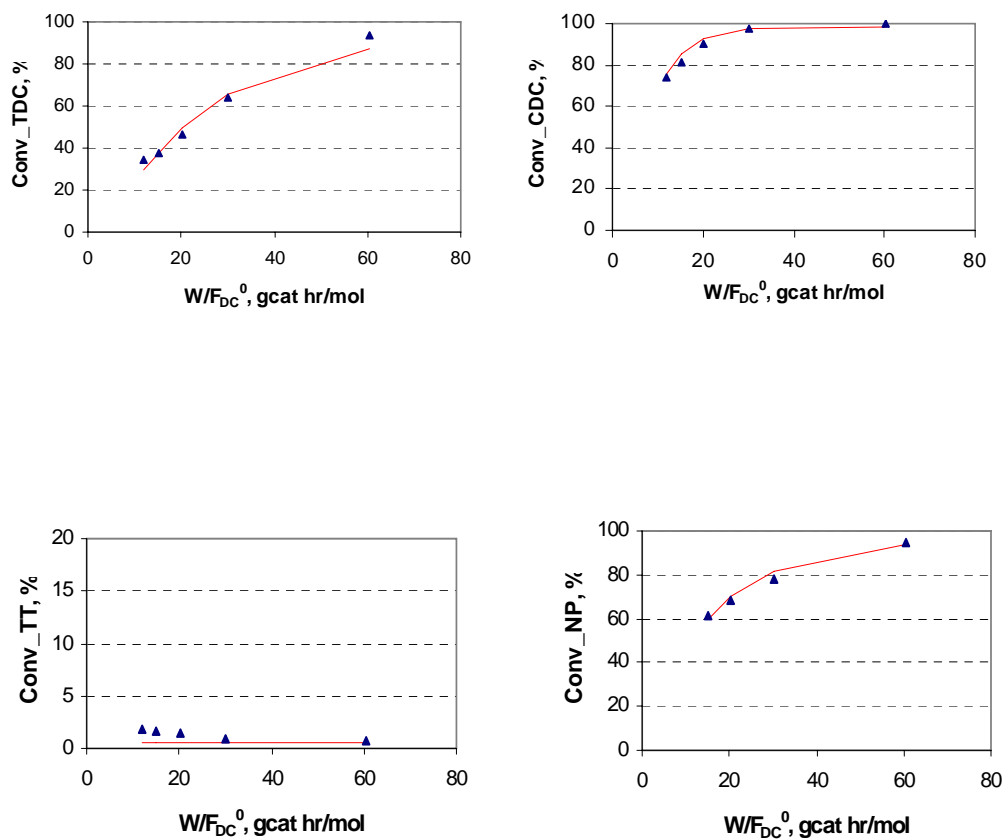


**Figure III-25.** Comparison of experimental and calculated conversions as a function of space time at 325 °C ( $\Delta$ : EXP; Solid line: CAL).

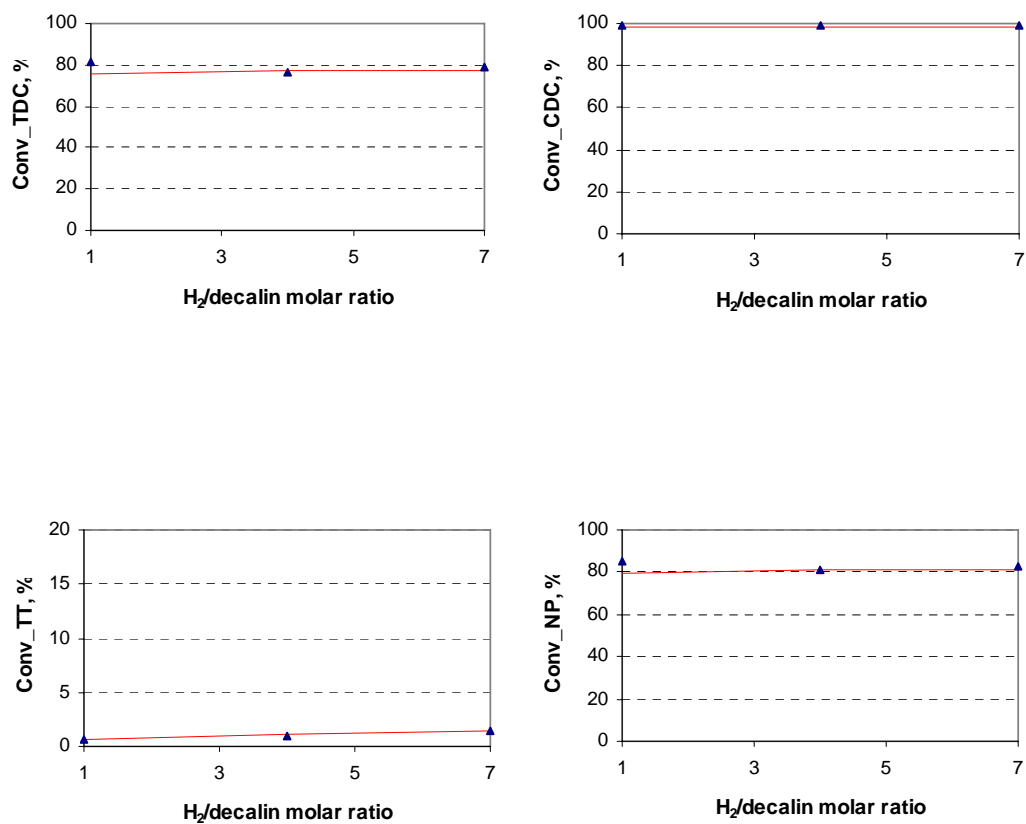


**Figure III-26.** Comparison of experimental and calculated conversions as a function of H<sub>2</sub>/decalin molar ratio at 325 °C and space time of 40 kg cat/h/ kmol ( $\Delta$ : EXP; Solid line: CAL).

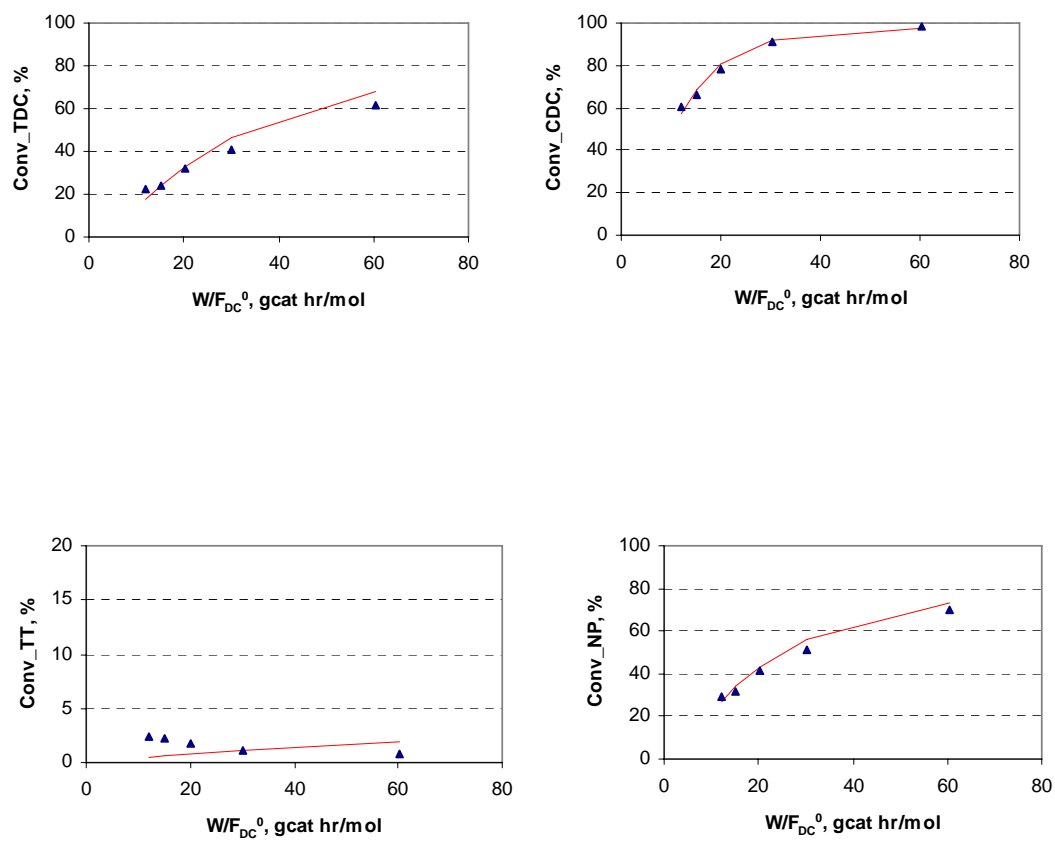


**Figure III-27.** Comparison of experimental and calculated conversions as a function of space time at 300 °C ( $\Delta$ : EXP; Solid line: CAL).

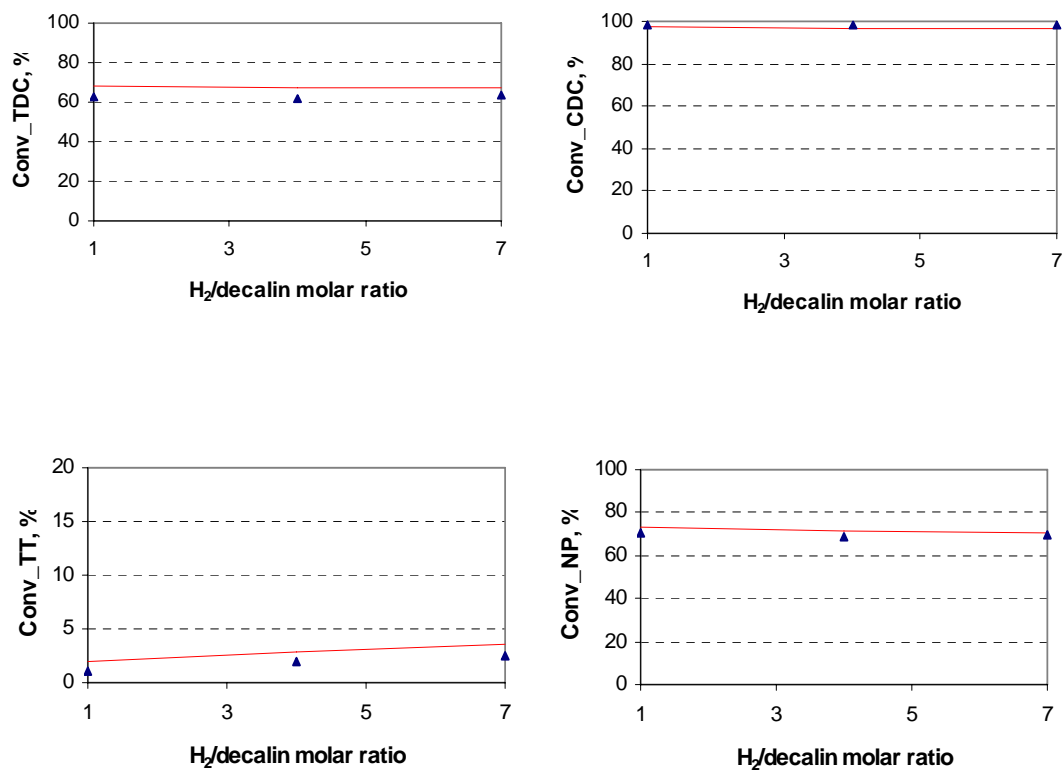


**Figure III-28.** Comparison of experimental and calculated conversions as a function of H<sub>2</sub>/decalin molar ratio at 300 °C and space time of 60 kg cat/h/ kmol ( $\Delta$ : EXP; Solid line: CAL).



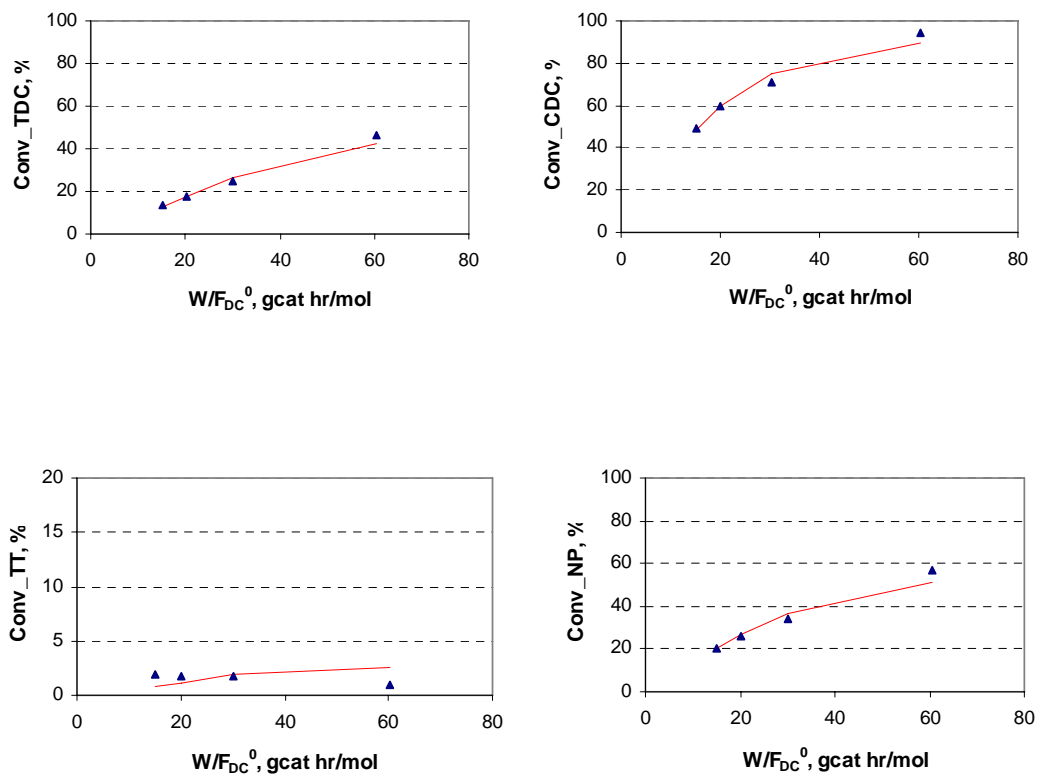


**Figure III-29.** Comparison of experimental and calculated conversions as a function of space time at 275 °C ( $\Delta$ : EXP; Solid line: CAL).

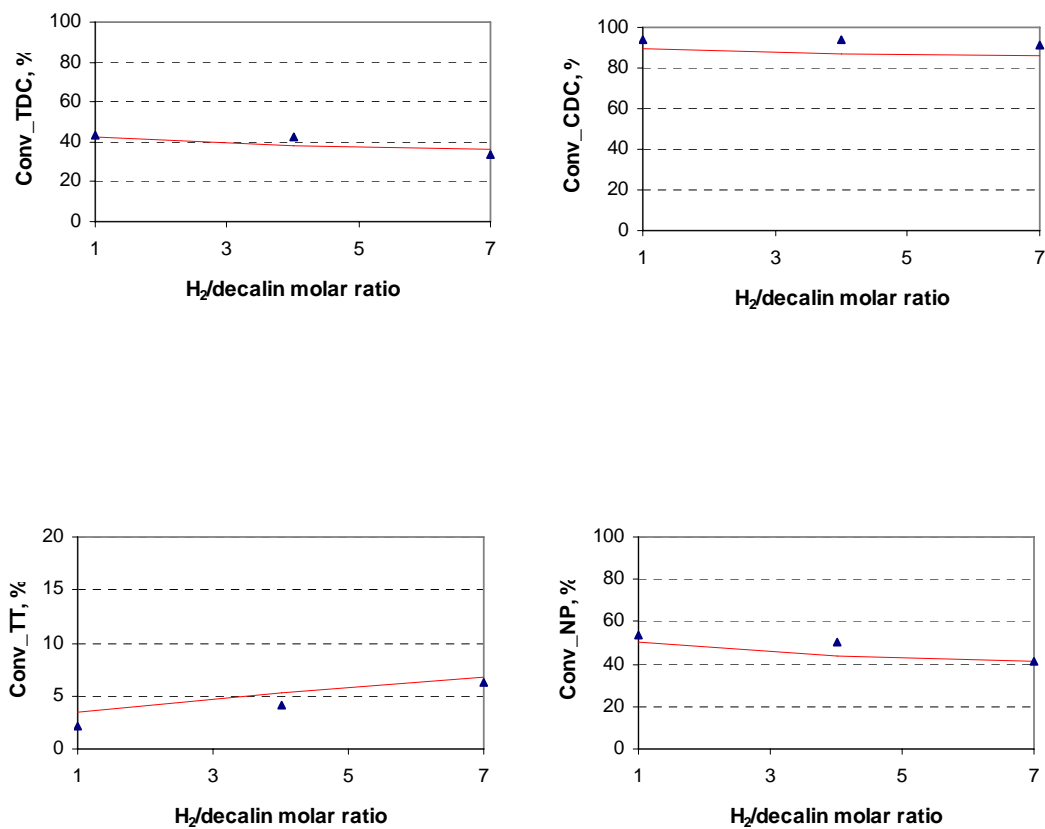


**Figure III-30.** Comparison of experimental and calculated conversions as a function of H<sub>2</sub>/decalin molar ratio at 275 °C and space time of 60 kg cat/h/ kmol ( $\Delta$ : EXP; Solid line: CAL).

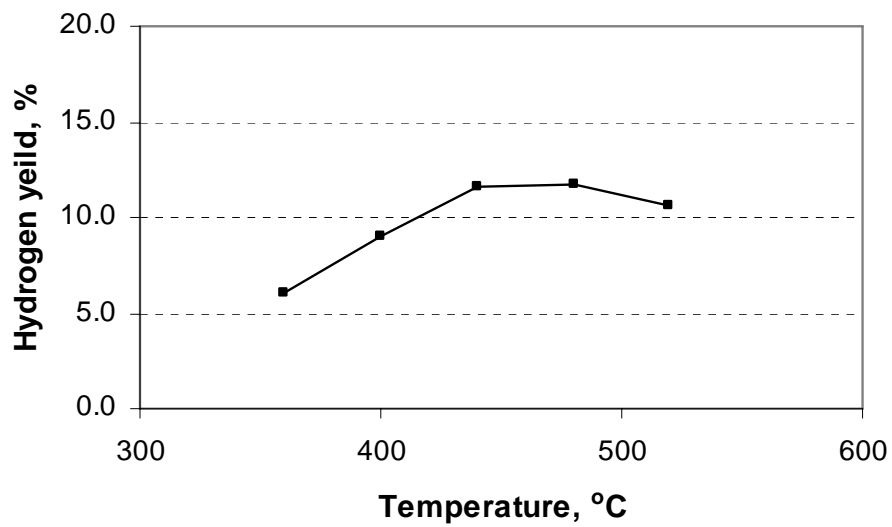


**Figure III-31.** The hydrogen production yield as a function of reaction temperature in the dehydrogenation of Jet A surrogate on Pt/ $\gamma$ -alumina catalyst. Feed of Jet A surrogate =10ml/min, H<sub>2</sub>=10ml/min, N<sub>2</sub>=40 ml/min.

### III.3.6.2 The Dehydrogenation of Jet A on Various Catalysts

#### III.3.6.2.1 Pt/ $\gamma$ -alumina Catalyst

The Jet A used in this experiment consists of 18% aromatics, 20% naphthenes, 60% paraffins, 2% olefins. Figure III-32 shows the hydrogen production yield as a function of reaction temperature on a 0.8 wt% Pt-0.3 wt% Sn/alumina catalyst. The maximum yield obtained at 500 °C is 12.8%. The low yield indicates that paraffins in Jet A are not dehydro-aromatized. This is probably because the acidity of  $\gamma$ - alumina is not sufficiently strong for this reaction to occur. Also, the catalyst is prone to deactivation in Jet A dehydrogenation. The hydrogen yield, defined as hydrogen produced per total hydrogen content in Jet A, decreases from 12.0% to 7.2% after 180 min (Figure III-33). To suppress the deactivation of the catalyst, the H<sub>2</sub>/Jet A molar ratio was increased to 10, and the yield of Jet A decreases much slower from 11.2% to 9.2% after 180 min. Next, USY zeolite with acidity stronger than alumina was used to prepare the supported Pt catalyst.

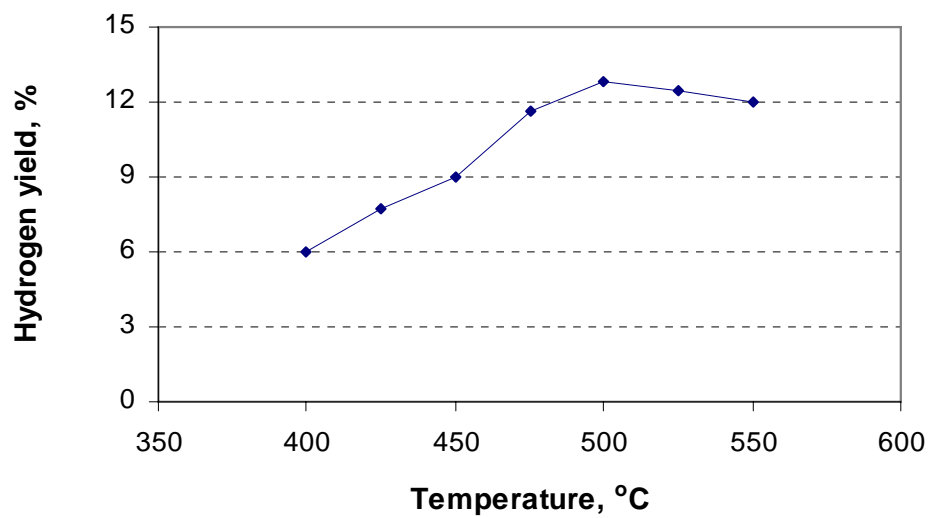


**Figure III-32.** The hydrogen production yield as a function of temperature in the dehydrogenation of Jet A on Pt/ $\gamma$ -alumina catalyst. Jet A=10ml/min, H<sub>2</sub>=10ml/min, N<sub>2</sub>=40 ml/min.

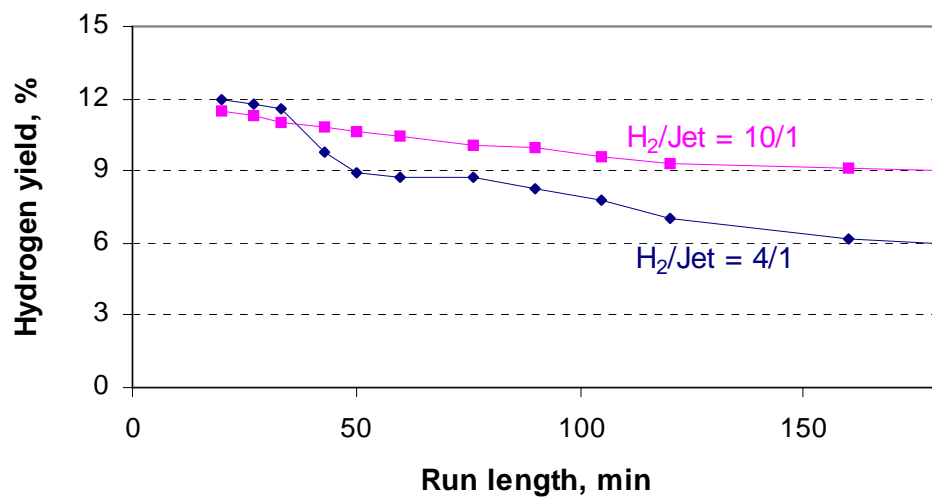


**Figure III-33.** The effect of H<sub>2</sub>/Jet A molar ratio on the dehydrogenation Jet A. Temperature= 500 °C, Feed of Jet A =10ml/min, H<sub>2</sub>=10ml/min, N<sub>2</sub>=40 ml/min.

### III.3.6.2.2 Pt/USY Catalyst

Figure III-34 compares the dehydrogenation of Jet A over different catalysts. In industry, bifunctional catalysts with both metal and acid active sites are employed in catalytic reforming to convert paraffins to aromatic compounds and produce H<sub>2</sub> as a by product. In this process the metal sites are responsible for the dehydrogenation of paraffins. The acid sites are essential to transform these dehydrogenated long chain hydrocarbon intermediates to cycloalkanes. Acid sites may also crack the paraffins to generate H<sub>2</sub>. The acidity of USY is stronger than that of  $\gamma$ -Al<sub>2</sub>O<sub>3</sub>. The H<sub>2</sub> production yield over Pt/USY at 425 °C is 2% higher than that on Pt/ $\gamma$ -Al<sub>2</sub>O<sub>3</sub> catalyst. However, due to the relatively small pore openings of USY, it deactivates much faster.

### III.3.6.2.3 Pt-Sn/ $\gamma$ -Al<sub>2</sub>O<sub>3</sub>-ZrO<sub>2</sub>/SO<sub>4</sub><sup>2-</sup> Hybrid Catalysts

Sulfated zirconia is a well known superacid catalyst and can be added into Pt/ $\gamma$ -alumina catalyst to increase its acidity. Pt-Sn/ $\gamma$ -alumina-ZrO<sub>2</sub>/SO<sub>4</sub><sup>2-</sup> hybrid catalysts were prepared by calcining a physical mixture of the two components in Pt-Sn/ $\gamma$ -Al<sub>2</sub>O<sub>3</sub> to ZrO<sub>2</sub>/SO<sub>4</sub><sup>2-</sup> mass ratio of 6 to 4 at 550 °C for 12 hr. The hydrogen production yield over this hybrid catalyst is 5% higher than that of Pt/ $\gamma$ -alumina at same operating conditions. As a strong acidic component, the addition of sulfated zirconia may promote the cracking ability of Pt-Sn/ $\gamma$ -Al<sub>2</sub>O<sub>3</sub>. It may also interact with Pt-Sn/ $\gamma$ -Al<sub>2</sub>O<sub>3</sub> to promote the transforming of paraffins to aromatics, leading to the increase of the hydrogen production yield.

#### III.3.6.2.4 Catalyst Regeneration

The catalysts in the dehydrogenation of Jet A are prone to deactivation. The hybrid catalyst was regenerated by two means, as shown in Figure III-35: 1) regeneration by oxidation in air at 500 °C, then reduction in H<sub>2</sub> at 300 °C, 2) regeneration by oxidation in air at 300 °C, then reduction in H<sub>2</sub> at 300 °C. It is shown in Figure III-35 that oxidation at 500 °C is essential to burn the coke deposited on the catalyst so as to fully recover the catalyst activity. Oxidation at 300 °C can only partially recover the catalyst activity.

Pt-Sn/ $\gamma$ -Al<sub>2</sub>O<sub>3</sub> is a good catalyst for the dehydrogenation of naphthene components in Jet A, but it needs stronger acidity to extract hydrogen from paraffin components. The strong acidic sites could be obtained by physically combining Pt-Sn/ $\gamma$ -Al<sub>2</sub>O<sub>3</sub> and sulfated zirconia components in hybrid catalysts. The deactivation of the catalyst due to coking reaction is a problem in this application. However, the deactivated catalyst can be regenerated by oxidative regeneration at 500 °C.



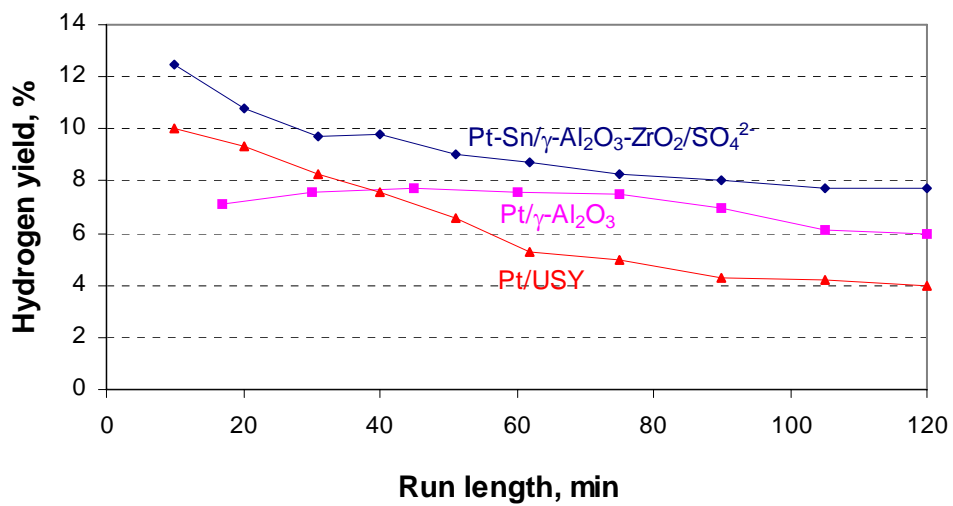


**Figure III-34.** The dehydrogenation of Jet A over different catalysts. Temperature= 425 °C, Jet A=10 ml/min, H<sub>2</sub>=10 ml/min, N<sub>2</sub>=40 m/min.

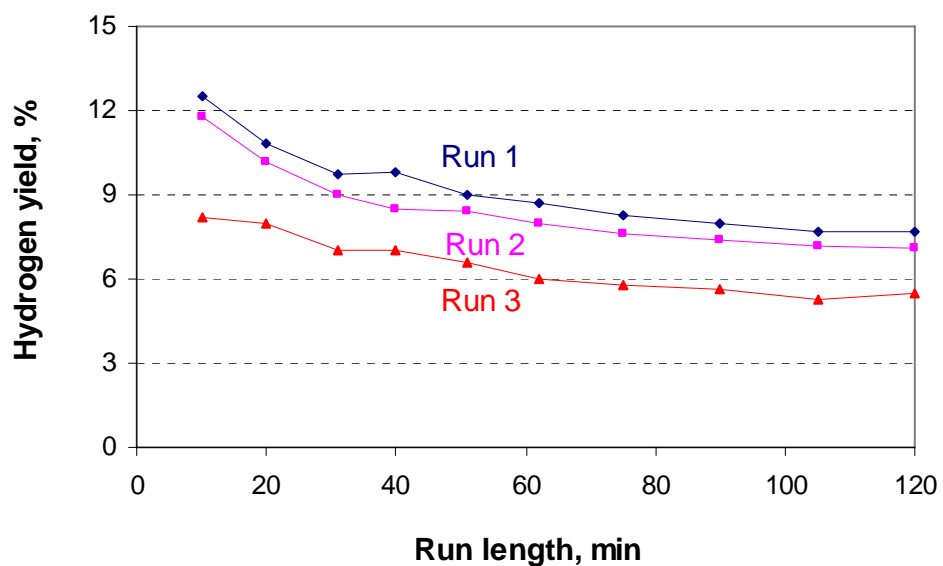


**Figure III-35.** The regeneration of Pt-Sn/ $\gamma$ -Al<sub>2</sub>O<sub>3</sub>-ZrO<sub>2</sub>/SO<sub>4</sub><sup>2-</sup> hybrid catalysts in the dehydrogenation of Jet A by oxidation in air at different temperatures. Run 1: fresh catalyst; Run 2: oxidation at 500 °C in air, then reduction at 300 °C in H<sub>2</sub>; Run 3: oxidation at 500 °C in air, then reduction at 300 °C in H<sub>2</sub>.

## CHAPTER IV

### CONCLUSIONS

Applications of hydrogenation and dehydrogenation on noble metal catalysts were investigated in this work. The hydrotreating of  $C_3$  cut from a cracking unit is of industrial importance to produce pure propylene. A detailed reaction scheme was found to be necessary for the description of essential features of the gas phase selective hydrogenation of the  $C_3$  cut from a thermal cracking unit. It considered the hydrogenation reactions on metal sites but also oligomerization on acid sites leading to green oil, i.e. oligomers with varying C-number. The kinetic model explicitly accounted for the adsorption of MA, PD, propylene, propane and green oil components and also for the deactivation of the catalyst, by linking the activity to the true deactivating agent, instead of just time. Such an approach requires a reaction scheme and a rate equation for the formation of the deactivating agent. Because  $C_6$ - $C_{12}$  oligomers eluted from the reactor higher oligomers with a carbon number of 15 or higher were taken to be responsible for the deactivation through irreversible adsorption on the acid sites.

The kinetic model was plugged into a pseudo-homogeneous reactor model to simulate the industrial adiabatic reactor at a given point in time. For a commercial process this can not be done without accounting for the history of the plant. The effect of both catalyst deactivation and feeding CO at the start of the run had to be included to produce a good fit of the industrial data. The simulation also revealed certain

consequences of the choices made in the design stage of the reactor, associated with the deactivation of the catalyst and a policy of long operating cycles between catalyst regeneration.

Hydrogen as a fuel for fuel cells in energy and transportation applications will dominate in the hydrogen economy. Onboard hydrogen storage is the main obstacle in the transportation application of fuel cells. This work considered the production of hydrogen via the dehydrogenation of hydrocarbons. Cyclohexane and decalin were investigated for this application. It differs from the steam reforming of hydrocarbons to produce hydrogen in that the product is free of CO, thus superior for PEM fuel cell application. Supported Pt catalysts can achieve about 98% conversion with over 99.9% selectivity for the dehydrogenation reaction, and the cracking reactions only occur at high temperature. The catalyst has a long longevity in the dehydrogenation of cyclohexane. In the dehydrogenation of decalin, slight deactivation of the catalyst was observed, but, the deactivation of the catalyst can be inhibited by co-feeding of hydrogen. Benzene, the final product in cyclohexane dehydrogenation, is toxic. The gravimetric hydrogen content in decalin is higher than that in cyclohexane and the dehydrogenated product, naphthalene, is environmentally favorable. These advantages make decalin a good candidate for the use as H<sub>2</sub> carrier. One problem with this method of onboard hydrogen production is that other than the fuel tank, there is a need for the storage of the dehydrogenated hydrocarbons, which will occupy limited space and increase the weight of a vehicle. The reaction network in the dehydrogenation of decalin was derived. It took into account consecutive dehydrogenation of decalin on Pt active sites and also the

isomerization of decalin isomers on acid sites. Rates equations were written in terms of Hougen-Watson equations which accounted for the adsorption of various species. The model gave a good fit of the experimental data and will be a valid tool for the design and operation of a dehydrogenation reactor.

Jet A can be another source for the production of hydrogen for fuel cell application. In the dehydrogenation of Jet A on Pt/ $\gamma$ -Al<sub>2</sub>O<sub>3</sub>, the conversions of paraffins, the major component in Jet A are low, more likely because the acidity of  $\gamma$ - alumina is not sufficient. Bifunctional catalysts with both metal and acid active sites are essential to increase the hydrogen yield for this application. The acidity can be increased by the addition of the strong acid component, sulfated zirconia, or using a strong acid support to prepare the Pt catalyst. The strong acid sites may promote the cracking ability of Pt-Sn/ $\gamma$ -Al<sub>2</sub>O<sub>3</sub>. It may also interact with Pt-Sn/ $\gamma$ -Al<sub>2</sub>O<sub>3</sub> to promote the transformation of paraffins to aromatics, leading to the increase of the hydrogen production yield. The strong acidity may also promote coke formation and thus lead to the fast deactivation of the catalyst. The deactivated catalyst can be regenerated by oxidative regeneration at 500 °C.

**NOMENCLATURE**

MA: methylacetylene

PD: propadiene

PP: propylene

PN: propane

GO: green oil

TDC: trans-decalin

CDC: cis-decalin

TT: Tetralin

NP: naphthalene

$A_i$ : frequency factor for elementary reaction step  $i$ , kmol/kg cat. hr

$A_C$ : frequency factor for formation of the deactivating agent, kmol/kg cat. bar<sup>4</sup> hr

$c_{pi}$ : specific heat of fluid  $i$ , kJ/kg K

$C_i$ : molar concentration of component  $i$ , kmol/m<sup>3</sup>

$C_C$ : deactivating agent content of the catalyst, kg  $C_C$ /kg cat.

$d_t$ : internal tube diameter, m<sub>r</sub>

$d_p$ : particle diameter, m<sub>p</sub>

$W/F^0_{MAPD}$ : space time in terms of MAPD feed, kg cat. hr/kmol

$W/F^0_{DC}$ : space time in terms of decalin feed, kg cat. hr/kmol

$E_i$ : activation energy for elementary reaction step  $i$ , kJ/kmol

$E_C$ : activation energy for formation of the deactivating agent, kJ/kmol

$F_{MAPD}^0$ : molar feed rate of reactants MA and PD, kmol/hr

$F_{DC}^0$ : molar feed rate of reactants decalin, kmol/hr

$F_i$ : molar feed rate of reactant i, kmol/hr

$F_t$ : total molar feed rate, kmol/hr

$-\Delta H$ : heat of reaction, kJ/kmol

$k_i$ : reaction rate coefficient, kmol/kg cat. hr

$K_i$ : adsorption equilibrium constant, bar<sup>-1</sup>

$L$ : reactor length, m<sub>r</sub>

$M_m$ : mean molecular mass, kg/kmol

$r_i^0$ : rate of elementary reaction step i at zero deactivation, kmol/kg cat. hr

$r_i$ : rate of elementary reaction step i in the presence of deactivation, kmol/kg cat. hr

$r_C^0$ : rate of formation of the deactivating agent at zero deactivation, kg C<sub>C</sub>/kg cat. hr

$r_C$ : rate of formation of the deactivating agent in the presence of deactivation, kg C<sub>C</sub> /kg cat. hr

$R_i$ : net rate of formation for the component i, kmol/kg cat. hr

$T$ : temperature, K or C

$T_m$ : mean temperature, K

$R$ : gas constant, kJ/kmol K

$X_{MA}$ ,  $X_{PD}$ : conversion of MA and PD, respectively

$X_{PP}$ ,  $X_{PN}$ ,  $X_{GO}$ : conversion of MA and PD into propylene, propane and green oil, respectively

$X_{TDC}$ ,  $X_{CDC}$ : conversion of TDC and CDC, respectively

$X_{TT}$ ,  $X_{NP}$ : conversion of DC into TT and NP, respectively

$Z$ : axial reactor coordinate,  $m_r$

*Greek Letters*

$\alpha_i$ : deactivation constant for main reaction  $i$

$\alpha_C$ : deactivation constant for formation of deactivating agent

$\gamma_{CO}$ : constant for CO effect

$\varepsilon$ : void fraction of bed,  $m_f^3/m_r^3$

$\rho_g$ : gas density,  $kg/m_G^3$

$\rho_B$ : catalyst bulk density,  $kg\ cat./m_r^3$

$\Omega$ : cross section of reactor,  $m_r^2$

$\Phi_i$ : deactivation function for main reaction  $i$

$\Phi_C$ : deactivation function for formation of deactivating agent



**LITERATURE CITED**

- (1) Goossens, A.G.; Dente, M.; Ranzi, E. Improve steam cracker operation. *Hydrocarbon Process.* **1978**, 57(9), 227.
- (2) Schnetzler, H.; Dittmann, H.; Wernicle, H.J. Pyrolysis of hydroconverter products for olefins production. *Chem. Eng. Prog.* **1980**, 76(7), 54.
- (3) Wang, X.Q.; Chen, Z.; Jiang, F.K; Comparison of FCC processes for light olefin production from heavy oils. *Lianyou Sheji* **1995**, 25(6), 15.
- (4) Golden, s.; Kowalczyk, D.; Compagna, B. Increase FCC propylene production and recovery. *World Refining* **2000**, 10(8), 16.
- (5) Golden, S.; Pulley, R.; Dean, C.F. Catalyst changes, downstream improvements increase FCC propylene yields. *Oil Gas J.* **2004**, 102(37), 44.
- (6) Laugier, J.P. Metathesis. An enhanced propylene production. In *Proceedings of the 12th Ethylene Producers Conference*, Atlanta, GA, 2000, 9, 123.
- (7) Weiss, A.H. Manufacture of propylene, In *Advances in Chemistry Series*, American Chemical Society: Washington, DC, 1970.
- (8) Caldwell, D.; Lichtenstein, I. *Kirk-Othmer Encyclopedia of Chemical Technology*; John Wiley & Sons: New York, 1965.
- (9) Derrien, M.L. Selective hydrogenation applied to the refining of petrochemical raw materials produced by steam cracking. *Stud. Surf. Sci. Catal.* **1986**, 27, 613.
- (10) Derrien, M.L.; Andrews, J.W.; Bonnifay, P.; Leonard, J.; The IFP selective hydrogenation process. *Chem. Eng. Prog.* **1974**, 70, 1.
- (11) Kronig, W.; Meckelburg, A.; Schlepplinghoff, B.; Sharfe, G., U.S. Pat. 3,075,917, **1963**.
- (12) Xie, W.Q.; Application of C<sub>2</sub> hydrogenation process and novel catalyst in China. *Yixi Gongye* **2006**, 18(3), 55.

- (13) Huang, W.; McCormick, J.R.; Lobo, R.F.; Chen, J.G. Selective hydrogenation of acetylene in the presence of ethylene on zeolite-supported bimetallic catalysts. *J. Catal.* **2007**, 40, 24691.
- (14) Khan, N.A.; Shaikhutdinov, S.; Freund, H.J. Acetylene and ethylene hydrogenation on alumina supported Pd-Ag model catalysts. *Catal. Lett.* **2006**, 108(3-4), 159.
- (15) Vincent, M.J.; Gonzalez, R.D. A Langmuir-Hinshelwood model for a hydrogen transfer mechanism in the selective hydrogenation of acetylene over a Pd/ $\gamma$ -Al<sub>2</sub>O<sub>3</sub> catalyst prepared by the sol-gel method. *Appl. Catal., A* **2001**, 217, 143.
- (16) Zhao, H.B.; Koel, B.E. Hydrogenation of 1,3-butadiene on two ordered Sn/Pt(111) surface alloys. *J. Catal.* **2005**, 234, 24.
- (17) Sarkany, A.; Revay, Z. Some features of acetylene and 1,3-butadiene hydrogenation on Ag/SiO<sub>2</sub> and Ag/TiO<sub>2</sub> catalysts. *Appl. Catal., A* **2003**, 243, 347.
- (18) Lambert, C.K.; Gonzalez, R.D. Activity and selectivity of a Pd/ $\gamma$ -Al<sub>2</sub>O<sub>3</sub> catalytic membrane in the partial hydrogenation reactions of acetylene and 1,3-butadiene. *Catal. Lett.* **1999**, 57, 1.
- (19) Benner, L.S.; Suzuki, T.; Meguro, K.; Tanaka, S. Precious Metals: Science and Technology, The International Precious Metals Institute, Allentown, PA, 1991.
- (20) J. Anderson, S.H. McAllister, E.L. Derr and W.H. Peterson, Diolefins in alkylation feedstocks conversion to monolefins by selective hydrogenation *Ind. Eng; Chem.* **1948**, 40, 2295.
- (21) Hoffmann, E.J.; Lewis, E.W.; Wadley, E.F. Set conditions for hydrogen testing, *Petrol. Refiner.* **1957**, 36(6), 179.
- (22) Kang, M; Song, M.W.; Kim, T.W.; Kim, K.L.  $\gamma$ -alumina supported Cu-Ni bimetallic catalysts: characterization and selective hydrogenation of 1,3-butadiene. *Can. J. Chem. Eng.* **2003**, 80(1), 63.
- (23) Bond, G.C; Philipson, J.J.; Wells, P.b.; Winterbottom, J.M. Hydrogenation of olefins. III. Reactions of ethylene and propylene with deuterium over alumina-supported palladium and rhodium. *Trans. Faraday Soc.* **1966**, 62(518), 443.
- (24) Bond, G.C.; Winterbottom, J.M. Hydrogenation of olefins. VI. Reaction of n-butenes with hydrogen and with deuterium over alumina-supported palladium. *Trans. Faraday Soc.* **1969**, 65(10), 2779.

- (25) Tai, J., Haraki, K., Kondo, J.N., Domen, K., and Tamaru, K. Selective hydrogenation of acetylene over Au/Al<sub>2</sub>O<sub>3</sub>. *J. Phys. Chem., B* **2000**, 104, 11153.
- (26) Bond, G.C., Webb, G., Wells, P.B., and Winterbottom, J.M. Patterns of behavior in catalysis by metals. *J. Catal.* **1962**, 1, 74.
- (27) Palczewska, W., Ratajczykowa, I., Szymerska, I., Krawcayk, M. Lead and carbon monoxide as additives modifying the selectivity of palladium catalysts in partial hydrogenation of acetylenes, In *Proceedings of the 8th International Congress on Catalysis*, Berlin, 1984, 4, 173.
- (28) Palczewska, W.; Jablonski, A.; Kaszukur, Z. Study on lead additives in modified palladium catalysts. *J. Mol. Catal.* **1984**, 25, 307.
- (29) Tamaki, J., Yamamura, M., Imanaka, T. The effect of the heat treatment of Pd thin film alloy on the hydrogenation of olefins. *Bull. Chem. Soc. Jpn.* **1988**, 61(5), 1725.
- (30) Schay, Z., Sarkany, A., Gucci, L., Weiss, A.H., Nair, V. Selective hydrogenation of trace acetylene in ethylene over Pd-Cu/Al<sub>2</sub>O<sub>3</sub> catalysts. In *Proceedings of the 5th International Symposium on Heterogeneous Catalysis*, Varna, 1983, 1, 315.
- (31) Sarkany, A.; Gucci, L.; Weiss, A.H. On the aging phenomenon in palladium catalysed acetylene hydrogenation. *Appl. Catal.* **1984**, 10, 369.
- (32) Clarke, J., Selectivity in catalysis by alloys. *Chem. Rev.* **1975**, 75(3), 291.
- (33) Dowden, D., Haining, I., Irving, J., Whan, D., Hydrogen spillover on alumina-supported platinum-rhenium catalysts. *J. Chem. Soc., Chem. Commun.* **1977**, 18, 631.
- (34) Palczewska, W., Jablonski, A., Kaszukur, Z. The role of tin in bimetallic Ir-Sn/Al<sub>2</sub>O<sub>3</sub> catalysts. *J. Mol. Catal.* **1984**, 25, 173.
- (35) Abon, M.; Massardier, J.; Tardy, B.; Bertolini, J. C. Platinum-nickel(111) alloy and platinum(111): Chemisorptive properties for acetylene and ethylene and catalytic behavior for the acetylene selective hydrogenation. *Surf. Sci.* **1987**, 189, 880.
- (36) Hancock, F.E.; Booth, J.S. A mechanistic study of the deactivation by hydrocarbon fouling of front end acetylene hydrogenation catalysts and the effect of carbon monoxide incorporation. In *Proceedings of the 6th Ethylene Producers Conference*, Atlanta, GA, 1994, 3, 698.
- (37) Miller, S. Acetylene, its properties, manufacture and uses; Academic Press: New York, 1965

- (38) Didillion, B.; Sarrazin, P.; Boitiaux, J.P.; Advanced catalyst design for high ethylene production and maximized cycle lengths, Presented at *the AIChE Spring Meeting*, Session 43, Houston, TX, 1995.
- (39) Jun, L.Y.; Jing, Z. and Ru, M.X.; Study on the formation of polymers during the hydrogenation of acetylene in an ethylene-ethane fractions, In *Proceedings of the Joint Meeting of Chemical Engineering; Chemical Industry and Engineering Society of China, American Institute of Chemical Engineers, BeiJing, China*, 1982, 2, 688.
- (40) Süb-Chemie Technical Bulletin on C<sub>2</sub>-tail end hydrogenation. (Information not available to public, Süb-Chemie, Munich)
- (41) Moses, J.M.; Weiss, A.H.; Matussek, K.; Guzzi, L. The effect of catalyst treatment on the selective hydrogenation of acetylene over palladium/alumina. *J. Catal.* **1984**, 86(2), 417.
- (42) Almanza, L.O.; Martinez, O.I. Regeneration of supported palladium catalyst for selective hydrogenation of acetylene. *Stud. Surf. Sci. Catal.* **2001**, 139, 311.
- (43) Liu, R.J.; Crozier, P.A.; Smith, C.M.; Hucul, D.A.; Blackson, J.; Salaita, G. Metal sintering mechanisms and regeneration of palladium/alumina hydrogenation catalysts. *Appl. Catal., A* **2005**, 282, 111.
- (44) Boitiaux, J., Cosyns, J., Martino, G. Metal-support and metal-additive effects in catalysis; Elsevier Scientific: Amsterdam, 1982.
- (45) McGown, W., Kemball, C., Whan, D., Scurrel, M., Hydrogenation of acetylene in excess ethylene on an alumina supported palladium catalyst in a static system. *J. Chem. Soc., Faraday Trans. 1*, **1977**, 73, 632.
- (46) McGown, W., Kemball, C., Whan, D. Hydrogenation of acetylene in excess ethylene on an alumina-supported palladium catalyst at atmospheric pressure in a spinning basket reactor. *J. Catal.* **1978**, 51, 173.
- (47) Al-Ammar, A., Webb, G., Hydrogenation of acetylene over supported metal catalysts. Part 3.—[<sup>14</sup>C] tracer studies of the effects of added ethylene and carbon monoxide on the reaction catalysed by silica-supported palladium, rhodium and iridium. *J. Chem. Soc., Faraday Trans. 1*, **1979**, 75, 1900.
- (48) Joaquin, S.A.; Rupprechte, G.; Freund, H.J. Atmospheric pressure studies of selective 1,3-butadiene hydrogenation on Pd single crystals: effect of CO addition. *J. Catal.* **2005**, 235(1), 52.

- (49) LeViness, S., Weiss, A.H., Schay, Z., Guzzi, L., J. Acetylene hydrogenation selectivity control on Pd-Cu/Al<sub>2</sub>O<sub>3</sub> catalysts. *J. Mol. Catal.* **1984**, 25, 131.
- (50) Weiss, A.H., LeViness, S., Nair, V., Guzzi, L., Sarkany, A., Schay, Z., The effect of Pd dispersion in acetylene selective hydrogenation. In *Proceedings of the 8th International Congress on Catalysis*, Berlin, 1984, 5, 591.
- (51) Armor, J.N. Membrane catalysis: where is it now, what needs to be done? *Catal. Today.* **1995**, 25, 99.
- (52) Gryzanov, V.M.; Slin'ko, M.G. Selectivity in catalysis by hydrogen-porous membranes. *Faraday Discuss.* **1982**, 72, 73.
- (53) Itoh, N.; Xu, W.C.; Sather, A.M. Capability of permeate hydrogen through palladium-based membranes for acetylene hydrogenation. *Ind. Eng. Chem. Res.* **1993**, 32, 2614.
- (54) Wang, B.; Froment, G.F. Kinetic modeling and simulation of the selective hydrogenation of C<sub>3</sub>-cut of a thermal cracking unit. *Ind. Eng. Chem. Res.* **2005**, 44(26), 9860
- (55) Fajardo, J.C.; Godines, C.; Cabanes, A.L.; Villora, G. Kinetic analysis of rate data for propylene and methylacetylene hydrogenation. *Chem. Eng. Sci.* **1996**, 35, 203.
- (56) Godinez, C; Cabanes, A.L.; Villora, G. Experimental study of the front-end selective hydrogenation of steam-cracking C<sub>2</sub>-C<sub>3</sub> mixture. *Chem. Eng. Proc.* **1995**, 34, 459.
- (57) Uygur, H.; Atalay, S.; Savasci, T. Kinetics of liquid phase selective hydrogenation of methylacetylene and propadiene in C<sub>3</sub> streams. *J. Chem. Eng. Jpn.* **1998**, 31(2), 178.
- (58) Froment, G.F.; Bischoff, K.B. Chemical reactor analysis and design, 2<sup>nd</sup> ed.; John Wiley & Sons: New York, 1992.
- (59) Froment, G.F. Coke formation in catalytic processes: kinetics and catalyst deactivation. *Stud. Surf. Sci. Catal.* **1997**, 111, 53.
- (60) Froment, G.F. Modeling of catalyst deactivation. *Appl. Catal., A* **2001**, 212, 117
- (61) Winter, C.J. Into the hydrogen energy economy-milestones. *Int. J. Hydrogen Energy* **2005**, 30(7), 681.
- (62) Kammen, D.M.; Lipman, T.E. Assessing the future hydrogen economy. *Science* **2003**, 302(5643), 226.

- (63) Zegers, P. Fuel cell commercialization: The key to a hydrogen economy. *J. Power Sources* **2006**, 154, 497.
- (64) Hellman, H.L.; Hoed, R.V.D.; Characterising fuel cell technology: Challenges of the commercialization process. *Int. J. Hydrogen Energy* **2007**, 32, 305.
- (65) Wee, J.H.; Lee, K.Y.; Overview of the development of CO-tolerant anode electrocatalysts for proton-exchange membrane fuel cells. *J. Power Sources* **2006**, 157, 128.
- (66) Demirci, U.B. Direct liquid-feed fuel cells: Thermodynamic and environmental concerns. *J. Power Sources* **2007**, 169, 239.
- (67) Farooque, M.; Maru, H.C. Carbonate fuel cells: Milliwatts to megawatts. *J. Power Sources* **2006**, 160, 827.
- (68) Scott, K.; Taama, W.; Cruickshank, J. Performance and modeling of a direct methanol solid polymer electrolyte fuel cell. *J. Power Sources* **1997**, 65, 159.
- (69) Litster, S.; Mclean, G. PEM fuel cell electrodes. *J. Power Sources* **2004**, 130, 61.
- (70) Acres, G.J. Recent advances in fuel cell technology and its applications. *J. Power Sources* **2001**, 100, 60.
- (71) Yamamoto, O. Solid oxide fuel cells: fundamental aspects and prospects. *Electrochimica Acta*. **2000**, 45, 2423.
- (72) Berry, G.D.; Aceves, S.M. Onboard storage alternatives for hydrogen vehicles. *Energy Fuels* **1998**, 12(1), 49.
- (73) Ewald, R. Requirements for advanced mobile storage systems. Hydrogen Energy Progress XI. In *Proceedings of the 11th World Hydrogen Energy Conference*, Stuttgart, June 23-28, 1996, 2, 1029.
- (74) Aceves, S.M.; Berry, G.; Weisberg, A.H. Lightweight cryogenic compatible pressure vessels for vehicular fuel storage. U.S. Patent 6,708,502, **2004**.
- (75) Tang, S.H.; Zhang, L.F.; Yu, Z.L. Advances in research on hydrogen storage in carbon nanotubes. *Huaxue Tongbao* **2003**, 66(10), 687.
- (76) Mpourmpakis, G.; Froudakis, G.E.; Lithoxoos, G.P.; Samios, J. SiC nanotubes: a novel material for hydrogen storage. *Nano Lett.* **2006**, 6(8), 1581.

- (77) Sun, D.L.; Srinivasan, S.S.; Chen, G.R.; Jensen, C.M. Rehydrogenation and cycling studies of dehydrogenated NaAlH<sub>4</sub>. *J. Alloys Compd.* **2004**, 373(1-2), 265.
- (78) Zuttel, A.; Wenger, P.; Rentsch, S.; Sudan, P.; Emmenegger, C. LiBH<sub>4</sub> a new hydrogen storage material. *J. Power Sources* **2003**, 118, 1.
- (79) Ichikawa, T.; Hanada, N.; Isobe, S.; Fujii, H. Hydrogen storage properties in Ti catalyzed Li-N-H system. *J. Alloys Compd.* **2005**, 404-406, 435.
- (80) Shang, Y.; Chen, R. Hydrogen storage via the hydrolysis of NaBH<sub>4</sub> basic solution: optimization of NaBH<sub>4</sub> concentration. *Energy Fuels* **2006**, 20, 2142.
- (81) Ortega, J.V.; Wu, Y.; Amendola, S.; Kelly, M.T.; Process for synthesizing alkali metal borohydride compounds, U.S. Patent 6,586,563, **2003**.
- (82) Grosjean, M.H.; Zidoune, M.; Roue, L.; Huot, J.Y. Hydrogen production via hydrolysis reaction from ball-milled Mg-based materials, *Int. J. Hydrogen Energy* **2006**, 31(1), 109.
- (83) Ross, J.R.H. Natural gas reforming and CO<sub>2</sub> mitigation, *Catal. Today*, 2005, 100, 151. 24-Ming, Q.; Healey, T.; Allen, L.; Irving, P. Steam reforming of hydrocarbon fuels. *Catal. Today* **2002**, 77, 51.
- (84) Wang, X.; Gorte, R.J. A study of steam reforming of hydrocarbon fuels on Pd/ceria. *Appl. Catal., A* **2002**, 224, 209.
- (85) Rosen, M.A. Thermodynamic investigation of hydrogen production by steam-methane reforming. *Int. J. Hydrogen Energy* **1991**, 16(3), 207.
- (86) Bharadwaj, S.S.; Schmidt, L.D. Catalytic partial oxidation of natural gas to syngas. *Fuel Process. Technol* **1995**, 42(2-3), 109.
- (87) Groote, A.M.D.; Froment, G.F. Simulation of the catalytic partial oxidation of methane to synthesis gas. *Appl. Catal., A* **1996**, 138, 245.
- (88) Semelsberger, T.; Brown, L.F.; Borup, R.L.; Inbody, M.A.M. Equilibrium products from autothermal processes for generating hydrogen-rich fuel-cell feeds. *Int. J. Hydrogen Energy* **2004**, 29, 1047.
- (89) Meyers, R.A. Handbook of petroleum refining processes, 3rd ed.; McGraw-Hill: New York, 2004.
- (90) Wiessner, F.G. Basics and industrial applications of pressure swing adsorption(PSA), the modern way to separate gas. *Gas Sep. Purif.* **1988**, 2(3), 115.

- (91) Socker, J.; Whysall, M.; Miller G.Q.; 30 years of PSA technology for hydrogen purification, UOP website, **1998**.
- (92) Henderson, M.; Gandhi, M. Consider cryogenic methods to improve ammonia production. *Hydrocarbon Process.* **2001**, 80(10), 97.
- (93) Park, Y.K.; Ribeiro, F.H.; Somorjai, G.A. The effect of potassium and tin on the hydrogenation of ethylene and dehydrogenation of cyclohexane over Pt(111). *J. Catal.* **1998**, 178, 66.
- (94) Biniwale, R.B.; Kariya, N.; Ichikawa, M. Dehydrogenation of cyclohexane over Ni based catalysts supported on activated carbon using spray-pulsed reactor and enhancement in activity by addition of a small amount of Pt, *Catal. Lett.* **2005**, 105(1-2), 83.
- (95) Kariya, N.; Fukuoka, A.; Utagawa, T.; Ichikawa, M. Efficient hydrogen production using cyclohexane and decalin by pulse spray mode reactor with Pt catalysts. *Appl. Catal., A* **2003**, 247, 247.
- (96) Hodoshima, S.; Arai, H.; Saito, Y. Liquid-film-type catalytic decalin dehydrogenation for long-term storage and long-distance transportation of hydrogen. *Int. J. Hydrogen. Energy* **2003**, 28, 197.
- (97) Okada, Y.; Sasaki, E.; Watanabe, E.; Hyodo, S.; Nishijima, H. Development of dehydrogenation catalyst for hydrogen generation in organic chemical hydride method. *Int. J. Hydrogen. Energy* **2006**, 31, 1348.
- (98) Wang, Y.G.; Shah, N.; Huffman, G.P. Pure hydrogen production by partial dehydrogenation of cyclohexane and methylcyclohexane over nanotube-supported Pt and Pd catalysts, *Energy Fuels.* **2004**, 18, 1429.
- (99) Lechuga, F.T.; Hill, C.G.; Anderson, M.A. Effect of dilution in the experimental dehydrogenation of cyclohexane in hybrid membrane reactors. *J. Membr. Sci.* **1996**, 118, 85.
- (100) Kokugan, T.; Trianto, A.; Takeda, H. Dehydrogenation of pure cyclohexane in the membrane reactor and prediction of conversion by pseudo equilibrium model, *J. Chem. Eng. Jpn.* **1998**, 31(4), 596.
- (101) Mile, B.; Morton, L.; Sewell, P.A. Equilibrium displacement in a chromatographic reactor. *J. Chromatogr.* **1981**, 204, 35.



- (102) Trimpont, P.A.V.; Marin, G.B.; Froment, G.F. Kinetics of methylcyclohexane dehydrogenation on sulfided commercial platinum/alumina and platinum-rhenium/alumina catalysts. *Ind. Eng. Chem. Fundam.* **1986**, 25, 544.
- (103) Ibarreta, A.F.; Sung, C.J. Optimization of Jet-A fuel reforming for aerospace applications. *Int. J. Hydrogen Energy* **2006**, 31, 1066.
- (104) Lenz, B.; Aicher, T. Catalytic autothermal reforming of Jet fuel. *J. Power Sources* **2005**, 149, 44.
- (105) Benitez, V.M.; Yori, J.C.; Grau, J.M.; Pieck, C.L.; Vera, C.R. Hydroisomerization and cracking of n-octane and n-hexadecane over zirconia catalysts. *Energy Fuels* **2006**, 20, 422.
- (106) Berlowitz, P.J.; Peden, C.H.F.; Goodman, D.W. Kinetics of CO oxidation on single-crystal Pd, Pt, and Ir. *J. Phys. Chem.* **1988**, 92, 5213.

## VITA

Bo Wang was born in Hanzhong, P.R. China. In 1993 he received a Bachelor of Science degree in petrochemical engineering from Dalian University of Technology. He continued his graduate study and received a Master of Science degree in chemical engineering from the same university in 1996. In the same year, he joined Sinopec Liaoyang Petrochemical Company and worked as a process engineer in the refinery for three years. In 1999 he continued his Ph.D. study in the field of solid acid catalysis in Dalian University of Technology and Korea Research Institute of Chemical Technology, South Korea, and received a Doctor of Philosophy degree in 2002. Upon graduation, he came to the United States to conduct research at Texas A&M University as a postdoctoral research associate with Prof. Gilbert F. Froment and Prof. Rayford G. Anthony. In 2005 he enrolled in the graduate program at Texas A&M University and began research in the field of reaction engineering under the guidance of Professor Gilbert F. Froment and Professor D. Wayne Goodman. He received his Ph.D. in chemical engineering from Texas A&M University in August 2007.

He can be reached at the following address:

Nanjiao St. 44-4-47, Liaoyang 111000, Liaoning Province, P.R.China